

**Changes in Human Horizontal Angular VOR
After the SpaceLab SL-1 Mission**

by

John Theodore Liefeld

B.E.Sc. (Mechanical), University of Western Ontario, 1991

Submitted to the department of Aeronautics and Astronautics
in Partial Fulfillment of
the Requirements for the Degree of

MASTER OF SCIENCE
in

AERONAUTICS AND ASTRONAUTICS
at the

MASSACHUSETTS INSTITUTE OF TECHNOLOGY

Cambridge, Massachusetts
May 10, 1993

© Massachusetts Institute of Technology 1993. All rights reserved.

Signature of Author _____
Department of Aeronautics and Astronautics
May 12, 1993

Certified by _____
Dr. Charles M. Oman
Thesis Supervisor; Senior Research Engineer

Accepted by _____
Professor Harold Y. Wachman
Chairman, Department Graduate Committee

MASSACHUSETTS INSTITUTE
OF TECHNOLOGY

JUN 08 1993

Aero

Changes in Human Horizontal Angular VOR After the SpaceLab SL-1 Mission

By John Theodore Liefeld

Submitted to the Department of Aeronautics and Astronautics
on May 10, 1993 in partial fulfillment of the
requirements for the Degree of Master of Science in
Aeronautics and Astronautics

ABSTRACT

The human horizontal vestibulo ocular reflex (VOR) was studied in four crew members of the Space Lab SL-1 mission (1983). Five testing sessions were performed over the four months prior to flight, and three testing sessions were performed in the first four days after landing. Subjects were seated upright over the axis of rotation of a rotating chair. The chair was rotated in the dark at a constant velocity of ± 120 °/s for one minute then stopped. After stop, the subjects remained seated head upright for half the runs, and tilted their heads down 90° from $t=5$ to 10 seconds after stop for the other half. Eye movements were recorded throughout the spin, and for 60 seconds after chair stop via EOG.

A automated software package was developed to perform data analysis. Slow Phase eye velocity (SPV) was calculated using order statistic filtering. Statistical methods were used to remove outliers, and the data was fit to several VOR models. A first order exponential (1OE) and Raphan Cohen derived three parameter model (3P) were used to analyze the data, while a new model using a fractional adaptation operator ($s^k, 0 < k < 1$) and velocity storage was developed and tested against the other models. A new data acquisition and chair control software package was developed for use with future experiments. New methods were developed to improve the statistical robustness of the model fitting procedure.

Due to poor data quality, one subject's data could not be reliably analyzed individually. Post flight changes in model parameters were different between subjects. Two subjects exhibited increased 3P normalized model gain post flight ($p=.01, p=.06$) while one showed a decrease ($p=.001$). All three subjects showed a decrease in 3P indirect pathway gain (not significant). One subject showed an increase in 1OE gain ($p < 0.1$) and one showed a decrease ($p < 0.1$). 1OE apparent time constant decreased in all three subjects. A correlation was noted between reported space motion sickness intensity for the subjects, and the magnitude and direction of post flight changes. All three subjects showed significant changes when Σt^2 statistics were used to compare ensemble averaged pre and post flight data.

Comparison to previous analysis of this data set (Kulbaski, 1988), indicates that the new methods of data filtering and analysis are more effective. Some conclusions from the previous analysis have been overturned while others have been reinforced. Data filtering in the new methods has allowed reliable analysis of individual runs through model fitting.

Individual model fit results have confirmed the variability in individual preflight responses noted by Balkwill (1992) and Oman and Calkins (1993). This may have implications in the clinical testing of the VOR. Average parameters of individual fits show similar changes as the parameters of averaged fits.

The new s^k model was found capable of fitting the data well, but was ill suited to this data set. Analysis of s^k model parameters showed no significant changes post flight. Suggested improvements in this model could improve its effectiveness at measuring post flight changes. Comparison of the s^k model with the 3P and 1OE models showed that for analysis of individual run data, better fits to the data were obtained with higher order models (3-4 parameter), than with low order models (2 parameters). However when higher order models are used to fit individual runs, the model fitting routines may also exploit the additional degrees of freedom in an attempt to fit artifacts in the data. This increases the variance of the resulting model parameters.

Thesis Supervisor: Dr. Charles M. Oman
Title: Director
Man-Vehicle Laboratory
Senior Research Engineer
Department of Aeronautics and Astronautics

Acknowledgments

There are many people that have helped me reach the end of this thesis, but I would first like to thank Jim Costello, for teaching me more than I ever wanted to know about electronics and life. Also thanks go to Dave Balkwill for all the help, even long after he graduated, and being the pathfinder.

For technical help, I would like to thank Nick Groleau for teaching me LabView, Alan Natapoff for helping me with the statistics, and Chuck Oman for the physiology, controls and all the little things that tied it together. Also thanks to Scott Stevenson, and Dan Merfeld for all the helpful discussions of the contents.

Thanks are especially out to Rick Paxon, Mark Schafer and Dave again for showing me that there is life after thesis. Also, Matt Butler, Beave, Pax, Scott, Mark and the rest for reminding me that there is life after midnight, but only across the river. Thanks to all the MVL lunch crowd; the conversations were the comic relief that kept me (almost) sane.

Thanks to Bev, Sherry, Kim, and Christian for keeping the world spinning despite the Gods.

For getting me through all those cold winter weekends, I must thank Dynamic, Salomon, and Tyrolia.

To my family, Mom, Dad, Oma, Jen, and by now Tony, I would like to thank you for all the support you gave me over the telephone. Even on the darkest days you seemed to find some sliver of light.

To Carolyn, I would like to thank you for putting up with me, especially at the end of this thing. Words alone will never suffice...

Thanks also to NASA Contract NAS 9-16523, for supporting this work, and especially for paying my tuition for the last two years.

Table of Contents

Abstract	3
Acknowledgments	4
Table of Contents	5
List of Figures	8
List of Tables	9
1. Introduction	10
1.1 Thesis Organization	12
2.0 Background	13
2.1 The Vestibular system	13
2.2 The Vestibulo-Ocular Reflex	15
2.3 Duration of Nystagmus	17
2.4 Testing of Human VOR using Velocity Pulse Stimulation	18
2.5 Velocity Storage Tilt Suppression (Dumping)	19
2.6 Vestibular Models	20
2.7 Effects of Altered GIF	26
2.8 Previous Analysis of SL-1 Data	29
2.8.1 Preliminary Processing	30
2.8.2 Statistical Analysis	31
2.9 Justification for Reanalysis	32
3.0 Experimental Methods	33
3.1 Equipment	33
3.2 Subjects	35
3.3 Experimental Protocol	35
4.0 Data Analysis	38
4.1 New Algorithms for Data Reanalysis	38
4.2 Calibration Procedure	38
4.3 Order Statistic Filtering	39
4.3.1 Predictive FIR Median Hybrid Filter	39
4.3.2 Calculation of SPV using Adaptive Asymmetrical Trimmed Mean (OS) Filter	40
4.4 Tachometer Analysis	41
4.5 Outlier Removal and Decimation	42
4.6 Run Rejection	45

4.7 Individual Model Fits	46
4.7.1 First Order Model Fits	47
4.7.2 Three Parameter Model Fits	47
4.7.3 S^k Model Fits	48
4.8 Dumping Model Fits	48
4.9 Residual Analysis	49
4.10 Mean Model Fits	49
4.10.1 Statistical Comparison of Mean SPV Curves	50
5.0 Results	53
5.1 Calibration	53
5.2 Rejected Runs	55
5.3 Individual Model Fitting	56
5.3.1 Assessment of Model Gain Results	57
5.3.2 Three Parameter Model Directional Asymmetry Analysis	59
5.3.3 Normalization of Data	60
5.3.4 Comparison of Preflight and Post Flight Response	60
5.3.5 Evaluation of s^k Model	66
5.3.5.1 Comparison of s^k and Three Parameter Models	67
5.3.5.2 Comparison Using Synthetic Data	67
5.3.5.3 Fitting Both Models to real Data	69
5.3.6 Miscellaneous	72
5.4 Analysis of Dumping Runs	73
5.5 Analysis of Ensemble Averaged Responses	78
6.0 New Hardware and Software	85
6.1 Data Analysis Scripts	85
6.1.1 New Algorithms	85
6.1.2 Batch Analysis Scripts	87
6.2 EOG Amplification	89
6.3 LabView Data Acquisition and Chair Control	90
7.0 Conclusions	92
7.1 Trends in Data and Interpretation	92
7.2 Analysis of New Methods	97
7.3 Suggestions for Future Work	101
References	102
Appendix A. Data	105
Appendix B. LabView Routines User's Manual	117

Appendix C. MatLab External C Codes	126
Appendix D. Batch Analysis Scripts	136
Appendix E. New Algorithm Scripts	145

List of Figures

Figure 2.1	Membranous Labyrinth of the right ear, and schematic diagram of one semi-circular canal.	14
Figure 2.2	Physiology of the otolith organ.	15
Figure 2.3	Theoretical relative slow phase velocity response to a step in angular velocity.	19
Figure 2.4	Robinson Model for VOR-OKN interaction for rotations in the dark.	21
Figure 2.5	Raphan-Cohen model of OKN, OKAN, and Vestibular Nystagmus.	22
Figure 2.6	Five parameter modified Laplace Transfer Function Model for rotation in the dark without left-right asymmetries.	22
Figure 2.7	Simple first order model (1OE) for nystagmus decay	23
Figure 2.8	SpaceLab SL-1 grouped mean post-rotatory SPV	27
Figure 2.9	SpaceLab D-1 grouped mean post-rotatory SPV	28
Figure 3.1	Experimental set-up	33
Figure 5.1a	Normalized Three Parameter Model gain, K , for all subjects, both CW and CCW, per and post rotatory.	61
Figure 5.1b	Normalized Three Parameter Model h_0 , for all subjects, both CW and CCW, per and post rotatory..	61
Figure 5.1c	Normalized Three Parameter Model g_0 , for all subjects, both CW and CCW, per and post rotatory.	62
Figure 5.2a	Normalized first order model gain, K , for all subjects, both directions, per and post rotatory.	62
Figure 5.2b	Normalized first order model time constant, T , for all subjects, both directions, per and post rotatory.	63
Figure 5.3	Comparison of s^k and three parameter models	68
Figure 5.4	s^k and three parameter model fits to the C203 post-rotatory data	70
Figure 5.5	Residuals of C203 post-rotatory model fits between s^k model and data, between three parameter model and data, and between models	70
Figure 5.6,	C304 log-linear fits to before dumping region, dumping region, and after dumping regions	74
Figure 5.7	C205 log-linear fits to pre-dumping region, dumping region, and post-dumping regions	75
Figure 5.8a	Subject B, Mean dumping model slopes	76
Figure 5.8b	Subject C, Mean dumping model slopes	76
Figure 5.8c	Subject D, Mean dumping model slopes	77
Figure 5.9	Subject B ensemble averaged preflight versus post flight	79
Figure 5.10	Subject C ensemble averaged preflight versus post flight	79
Figure 5.11	Subject D ensemble averaged preflight versus post flight	80
Figure B1	<i>DAM/DQM.L-mod6</i> front panel	124
Figure B2	Run/Cal front panel.	125
Figure D1	Batch_analysis flow chart	138

List of Tables

Table 5.1a	Run rejection status for subject A	55
Table 5.1b	Run rejection status for subject B	55
Table 5.1c	Run rejection status for subject C	56
Table 5.1d	Run rejection status for subject D	56
Table 5.2	Summary of directional asymmetry t-test results	59
Table 5.3	All subjects three parameter model mean normalized model parameters	65
Table 5.4	All subjects first order model mean normalized model parameters	65
Table 5.5	All subjects two-tailed t-test results	66
Table 5.6	Synthetic data generation parameters and model fit parameters from figure 5.1	68
Table 5.7	Model fit parameters for s^k and three parameter models to C203 post-rotatory data	69
Table 5.8	Ensemble averaged model fit parameters for each subject	81
Table 5.9	χ^2 results for pre and post flight head up ensemble averaged SPV curves	82
Table 5.10	s^k model fit parameters to ensemble averaged data	83
Table 5.11	Two parameter s^k model fits to ensemble averaged data	84
Table 7.1	Apparent time constant for ensemble averaged runs as found previously (Kulbaski, 1988).	94
Table 7.2	Apparent time constant for ensemble averaged runs as found in this study.	94
Table A.1a	Horizontal calibration factors for subject A	106
Table A.1b	Horizontal calibration factors for subject B	106
Table A.1c	Horizontal calibration factors for subject C	106
Table A.1d	Horizontal calibration factors for subject D	106
Table A.2.1	Subject B per-rotatory model fit parameters	107
Table A.2.2	Subject B post-rotatory model fit parameters	108
Table A.3.1	Subject C per-rotatory model fit parameters	109
Table A.3.2	Subject C post-rotatory model fit parameters	110
Table A.4.1	Subject D per-rotatory model fit parameters	111
Table A.4.2	Subject D post-rotatory model fit parameters	111
Table A.5a	Dumping log-linear model fits for subject B.	112
Table A.5b	Dumping log-linear model fits for subject C.	112
Table A.5c	Dumping log-linear model fits for subject D.	113
Table A.6.a	Per rotatory s^k model fit parameters for subject B.	113
Table A.6.b	Post rotatory s^k model fit parameters for subject B.	114
Table A.7.a	Per rotatory s^k model fit parameters for subject C.	114
Table A.7.b	Post rotatory s^k model fit parameters for subject C.	115
Table A.8.a	Per rotatory s^k model fit parameters for subject D.	115
Table A.8.b	Post rotatory s^k model fit parameters for subject D.	116

1. Introduction

As spacecraft have grown larger, from the small Mercury and Gemini vehicles, to the larger Sky-Lab and Space Shuttle in the US fleet, most astronauts have begun to experience a physical discomfort upon entry into the micro gravity environment, known as space motion sickness (SMS). First reported by cosmonaut G. Titov in 1961, approximately 60% of both American and Soviet crews experience some symptoms of SMS while in micro gravity. The symptoms of SMS are similar to motion sickness on earth; pallor, sweating, lethargy, nausea and vomiting. The symptoms experienced by any individual vary, but generally decrease and disappear over the course of two to five days. Due to the great expense of space flights, the lost productivity of crew members due to SMS is of considerable concern, as are long term adaptation effects which could impact on longer space flights, such as the proposed manned Mars mission.

On the earth, The human body is subjected to a constant gravito-inertial force (GIF) caused by Earth's gravitational field, equaling 9.81 m/s^2 . The human brain processes information from its sensory systems (vestibular, proprioceptive, and visual) with knowledge of this 1-G bias in order to determine position and orientation. When the body is subjected to a GIF different from that to which it is accustomed, the body is forced to adapt the sensori-motor systems for the new environment. Adaptive change in the CNS processing of sensori-motor systems can result in symptoms similar to SMS . This has been seen in centrifuge studies (Guedry and Benson, 1978) and parabolic flight (Lackner and Graybiel, 1984) where the GIF acting on the body is changed.

The sensory conflict theory of SMS states that when conflicting information is passed to the central nervous system (CNS) by the sensory systems, the CNS is unable to convert the sensory information into a recognizable body orientation, resulting in physical

discomfort and illusions. If the unusual gravitational force persists, the CNS is able to adapt by creating new internal models with which to interpret body position. Thus, symptoms decrease and disappear eventually as the unusual conditions persist.

In order to study this phenomenon, a set of experiments have been designed and performed in a series of space shuttle SpaceLab flights including the SL-1 (1983), D-1 (1985) and SLS-1 (1991) missions and the upcoming SLS-2 mission (1993). This thesis work is a re-analysis of one of these experiments from the SL-1 mission, the use of a rotating chair to identify the dynamics of the horizontal angular vestibulo-ocular reflex (VOR). Experiments were performed on five crew members preflight and four crew members post flight, after micro-gravity adaptation had occurred. Analysis of the D-1 data and previous analysis of the SL-1 data (Kulbaski, 1986; Oman and Wiegl, 1989) has shown some changes in how the CNS interprets sensory information after adaptation. However, new methods in data filtering and analysis, and the use of more complex models justifies re-analysis of the SL-1 data (see section 4.2).

The SL-1 data was compared against two mathematical models of the vestibular system to quantitatively determine the changes in the CNS after adaptation. A third VOR model was developed and compared to the existing models to assess its strengths and weaknesses. A new data acquisition and chair control system was developed, and the existing analysis algorithms were automated, and, in some cases improved, to allow rapid, on-site data processing and preliminary analysis on future missions.

1.1 Thesis Organization

Chapter 2 presents the physiology and previous research into the human vestibular system. Various models of the vestibular system are discussed.

Chapter 3 describes the experiment protocol and data acquisition.

Chapter 4 describes algorithms used in previous analysis of the SL-1 data, provides justification for reanalysis and describes the new algorithms developed.

Chapter 5 presents the results of the data analysis.

Chapter 6 introduces new software and hardware developed for future missions.

Chapter 7 is a discussion of the implications, and conclusions based on the data analysis. Also, recommendations for future work are included.

2.0 Background

The basis of human orientation is reflexive, and seldom is it consciously noted or controlled. Orientation is determined through CNS processing of the various sensory inputs available to it. This information is used to maintain balance, as well as awareness of the relative positions of limb and body. Visual and vestibular cues are used to stabilize vision in the presence of head movements. Vestibular information is used to stabilize vision during rapid head movements, while retinal slip helps to stabilize vision during slow head movements, or steady state.

2.1 The Vestibular System

For a complete reference on the vestibular system, refer to Wilson and Jones, 1979.

The vestibular labyrinth is the location of the body's sensors of angular motion, linear motion, and gravity. Angular motions are sensed by the semi-circular canals while linear motions are sensed by the otolith organs. Each labyrinth comprises three canals, lying approximately orthogonal to each other, and two otoliths oriented horizontally (utricle otolith) and vertically (sacculus otolith). The canals are arranged such that they are tilted approximately 20° back from the horizontal. The canal which lies closest to the horizontal plane is referred to as the horizontal semi-circular canal.

Each semicircular canal is composed of a semicircular duct, filled with endolymph fluid. In each duct, there is a diaphragm composed of gelatinous tissue which is attached to the ampulla much like a drum skin. When the head is rotated in the plane of the semicircular canal, the inertia of the endolymph causes it to lag behind the head. This gives a relative motion between the endolymph and the head, which causes the cupula to deform, and a corresponding deflection of cilia of the sensory cells which are attached to the cupula. The deformation in the cilia causes a change from the resting firing rate of the sensory

cells. The change in the firing rate is proportional to cupula deflection and therefore head angular velocity, and is direction dependent. For large stimuli, the firing rate can saturate. The tension in the cupula and ampulla causes a restoring force which accelerates the endolymph, and returns the cupula to the resting position. The cupular motion can be approximated by a highly damped torsional pendulum.

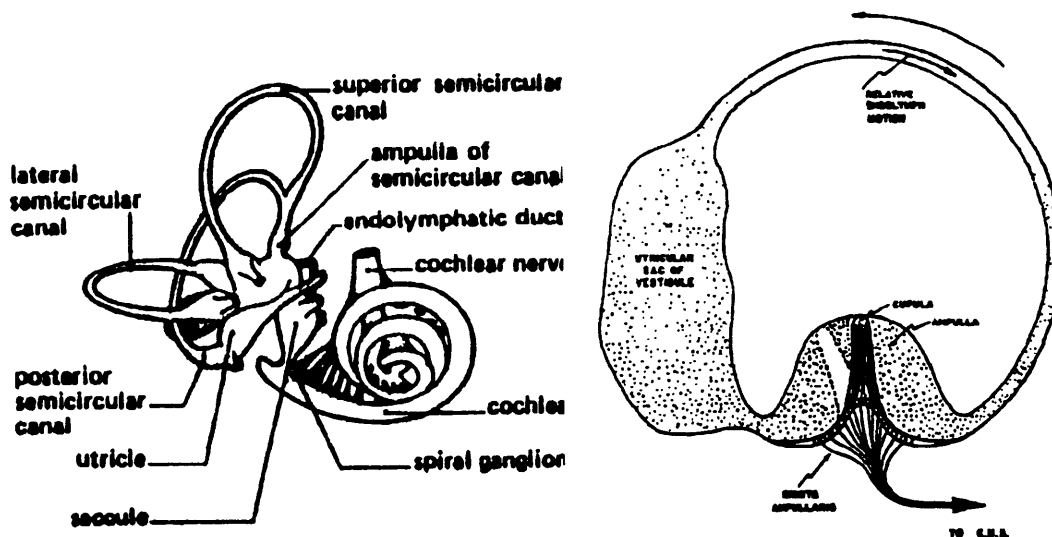


Figure 2.1, Membranous Labyrinth of the right ear, and schematic diagram of one semi-circular canal showing the relationship between head rotation and cupula deflection. Actual deflections are very small. [from Laurence Urdang, 1982, and Benson 1967]

Within the vestibule lie two large membranous sacks, part of the labyrinth, known as the utricle and saccule. Within each of these cavities lie the body's linear accelerometers, the otoliths. The sensory part of the cavities is called the macula. This consists of ciliated sensory cells covered by the otolithic membrane, and a calcium carbonate deposition in the membrane. These calcium crystals have a density approximately three times that of the surrounding endolymph, so when the head is subjected to a linear acceleration, the crystals lag behind the surrounding endolymph, shearing the crystals relative to the macula, bending the cilia and thereby causing the sensory cells to change their firing rates (Fernandez and Goldberg, 1976). Due to the equivalency of gravitational force and acceleration (Einstein equivalence principle), the otoliths respond to changes in the

orientation and magnitude of the GIF as well as to linear accelerations and head rotations. Since the macula of the saccule lies in a predominantly vertical plane, gravity induces a bias in the resting position of the saccular macula. During exposure to micro gravity, the saccular otoconia are unloaded, removing the 1-G bias, and changing the resting firing rate of this macula. Pitch and roll head rotations in micro gravity will no longer cause the otoliths to sense a changing GIF, while centripetal forces due to head rotations and linear accelerations will still stimulate the otoliths normally. Thus, the otoliths will no longer give information on the orientation of the head to an external reference (i.e.

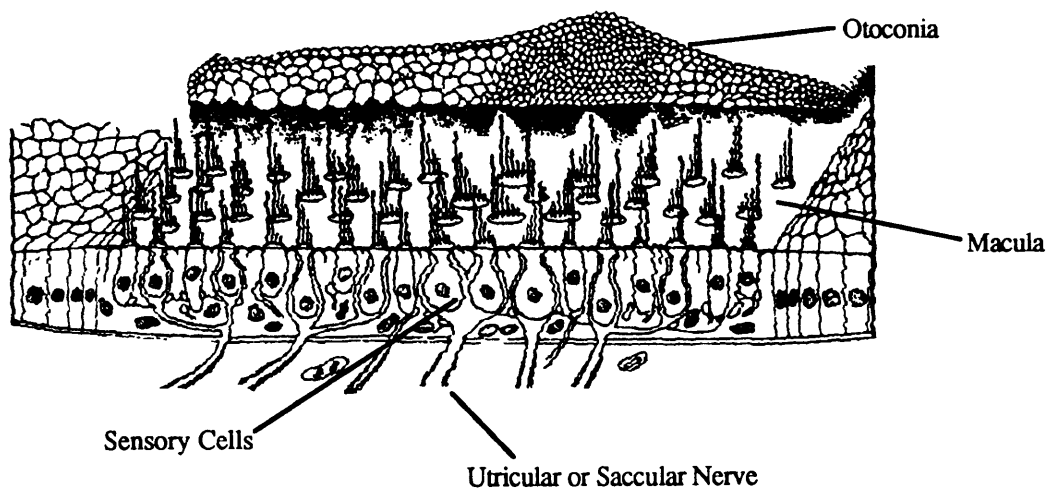


Figure 2.2, Physiology of the otolith organ. [from Wilson and Melvill Jones, 1979]

gravity) and the CNS must adapt to the absence of this signal.

2.2 The Vestibulo-Ocular Reflex

When you are looking at some target, and make a head movement, your eye must compensate by rotating the opposite direction to maintain a stable image on the retina.

For steady state gaze, and slow head movements image stabilization can be accomplished by the CNS by minimizing retinal slip. For fast head movements, the visual processing of retinal slip is too slow (about 70 msec) to stabilize the image, and the vestibular system is used to generate the requisite compensatory eye movements. This is called the vestibulo-ocular reflex (VOR). The VOR relies on the semicircular canals and otoliths to provide information on how the head is moving, and uses this to rapidly (about 10 msec latency (Robinson, 1975)) generate compensatory eye movements to prevent retinal slip, while retinal processing is used to correct small error remnants.

When head rotations are large or continuous, the magnitude of the required compensatory eye movements exceeds the physical limitations of eye rotation. When this happens, the eye will make a fast jump in the direction of motion, known as a saccade, and then continue tracking from this new position. For very long or continuous rotations, the eyes will saccade forward after they have counter rotated back past the center position, maintaining eye position biased towards the direction of rotation. A series of these saccades with reflexive slow tracking between is known as optokinetic nystagmus (Komatsuzaki et al, 1969). During nystagmus, the saccades are generally referred to as fast phases, while the tracking portion is referred to as the slow phase. The eye velocity of the slow phases (SPV) is equal to the velocity of the visual scene relative to the head, when a visual scene is presented to the subject. During rotations in darkness however, there is no longer a retinal slip signal from the eyes to fine-tune the eye movements, and the CNS relies entirely on vestibular information. Thus the eye movements are only due to the VOR. For long or continuous rotations in darkness, the nystagmus that is generated is known as vestibular nystagmus.

VOR is capable of being consciously modified by subjects rotating in the dark (Barr et al, 1976). When subjects were asked to imagine and stare at a point rotating with them in

front of their faces, they are able to partially suppress the VOR. Provided with a real point to fixate on, subjects can almost totally suppress the VOR. Level of mental alertness also affects VOR (Collins, 1962). Low levels of alertness also cause partial suppression of the VOR. Thus it is very important to properly and instruct subjects prior to testing.

2.3 Duration of Nystagmus

Through direct single unit neuron recordings in monkeys (Raphan et al, 1979), it has been seen that the firing rate of the sensory canal neurons during continuous rotation in the dark returns to the resting rate before nystagmus ceases. The deviation from the resting firing rate follows an approximately exponential decay with a time constant of approximately 5 seconds, while nystagmus decay follows a time course with a decay time constant closer to 20 seconds. From this, it has been hypothesized that there exists an element in the CNS that stores the sensory information from the canal afferents to prolong nystagmus. This is commonly referred to as velocity storage. From an evolutionary standpoint the existence of velocity storage would serve to aid the CNS in properly evaluating rotations that persist longer than the time constant of the cupula, when the vestibular system equilibrates and indicates no motion when in fact a steady state rotation has been achieved. Studies in optokinetic after nystagmus (OKAN) also support the theory of a velocity storage element. OKAN occurs when an immobile subject is exposed to a moving visual field which induces nystagmus. After the scene is stopped, nystagmus persists, which indicates the presence of a storage element.

Current theory holds that the source of velocity storage mechanisms in the brain is in the flocculus of the cerebellum, where vestibular, visual and proprioceptive cues are integrated. However, to date anatomists have been unable to determine the location of the velocity storage element, although recordings in the vestibular nucleus have found both

the afferent neuron signals from the vestibular system as well as units with signals corresponding to canal signals modified by the additional velocity storage element.

2.4 Testing of Horizontal VOR using Velocity Pulse Stimulation

Several tests of the human horizontal VOR have been developed. While various sorts of rotational stimuli are commonly used, only velocity pulse stimuli will be discussed here.

To test the human horizontal VOR, the subject is seated upright in a rotating chair, and rotated about the vertical axis. In order to isolate the VOR, sensory cues other than from the VOR are masked out by rotating in the dark with auditory and proprioceptive cues removed through the use of earphones and long clothing to eliminate wind cues.

Subjects are subjected to a step in horizontal angular velocity . At the beginning of the stimulus, the VOR drives a rapid rise in SPV to a maximum usually between 0.5 and 0.8 of the stimulus velocity in the opposite direction to compensate. The cupula returns to its initial position rapidly, and the primary afferents return to their resting firing rate due to the absence of any angular acceleration at the constant rotation. Velocity storage prolongs the SPV of the eye movements which decay approximately exponentially to zero after 40 seconds. In humans and animals, often the SPV decay will "overshoot", briefly reversing nystagmus, giving SPV in the same direction as the stimulus with low magnitude. This is thought to be a result of neural adaptation, and has a time constant on the order of approximately 80 seconds. When the rotation is then stopped, an equal but opposite angular acceleration is induced in the canals causing nystagmus in the opposite direction with equal magnitude. The subject subjectively interprets this period as a rotation in the opposite direction although they are immobile. Figure 2.3 shows a typical SPV response to a velocity step input, calculated using a five parameter model (section 2.7).

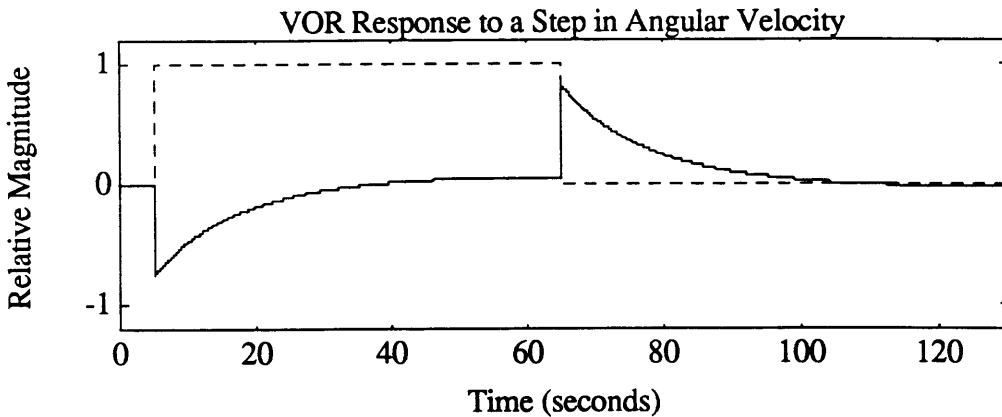


Figure 2.3 Theoretical relative slow phase velocity response to a step in angular velocity. Solid line is SPV response. Dashed line is stimulus. Calculated using a five parameter model (Balkwill, 1992)

2.5 Velocity Storage Tilt Suppression (Dumping)

If, immediately following the cessation of rotation of a velocity step, the head is pitched forward, the CNS will receive conflicting information from the otoliths and canals. Following chair stop, the canal afferents signal the CNS that they are rotating in yaw. After the head is pitched, this is translated to an apparent rotation in roll in body axes coordinates. Meanwhile, the otoliths are recording a steady GIF, whereas if the head were rolling, the GIF would be changing relative to the otoliths. Other senses, such as the proprioceptors also indicate that no roll is taking place. This conflict persists until the cupula returns to its steady state position. The SPV response during this period has a characteristically faster decay approximating that of the canal time constant alone. It is theorized that in the presence of the conflicting information coming from the canals and otoliths, the CNS suppresses, or dumps the information in the velocity storage element. Presumably, the CNS realizes that it no longer has a reasonable estimate of body orientation, and is attempting to develop a new estimate from "scratch". Information from the velocity storage element is suppressed, not lost, for if the subject returns to the upright, the SPV time course will sometimes return to the appropriate velocity as if the head had remained upright continuously (Kulbaski, 1986).

An alternative theory of what happens during "dumping" is called axis shifting. As the head rotates forward, the CNS keeps track of the eye movements in global coordinates. While the head is pitched down, the CNS calculates the axis of rotation between the original vertical axis and the new horizontal axis. Eye movements are shifted accordingly, reducing horizontal nystagmus while beginning torsional nystagmus. Experiments in monkeys have shown some evidence of axis shift during passive head movements (Merfeld, 1990), however recent experimentation in humans has shown no evidence of axis shift following active head movements (Fetter et al, 1992 in progress).

2.6 Vestibular Models

As this thesis is primarily concerned with modeling the human horizontal angular VOR, the inputs and outputs of each model are chosen to be the rotational velocity stimulus, and the eye SPV respectively. The following models have several differences between them, but there are several areas in which they are in agreement. The dynamics of the semicircular canals are modeled in each case as a low pass filter on head angular acceleration, giving head velocity as output over a mid-frequency range. All three models assume implicitly at least, that the brain uses an internal model of SCC dynamics. It is this model that generates the brain's best estimate of head velocity based upon the most recent sensory inputs. In the absence of new information, such as during prolonged rotation, the model continues to update the estimate of body rotation based upon its model of the dynamics.

The characteristics of the VOR are commonly modeled using engineering controls methods designed for linear systems. In general, Laplace transform methods will be used here to describe the models.

The Robinson model (Robinson, 1971) is based on the idea that the sole purpose of the VOR-OKN system is to provide a signal proportional to head velocity for low frequencies where the canals are ineffective (see figure 2.4). The positive feedback loop of eye velocity command (upper feedback loop in figure 2.4) gives the system the high forward gain and long time constant to mimic velocity storage. In the dark, this will increase the main VOR time constant from T_c to T_{apparent} , the apparent time constant of the VOR.

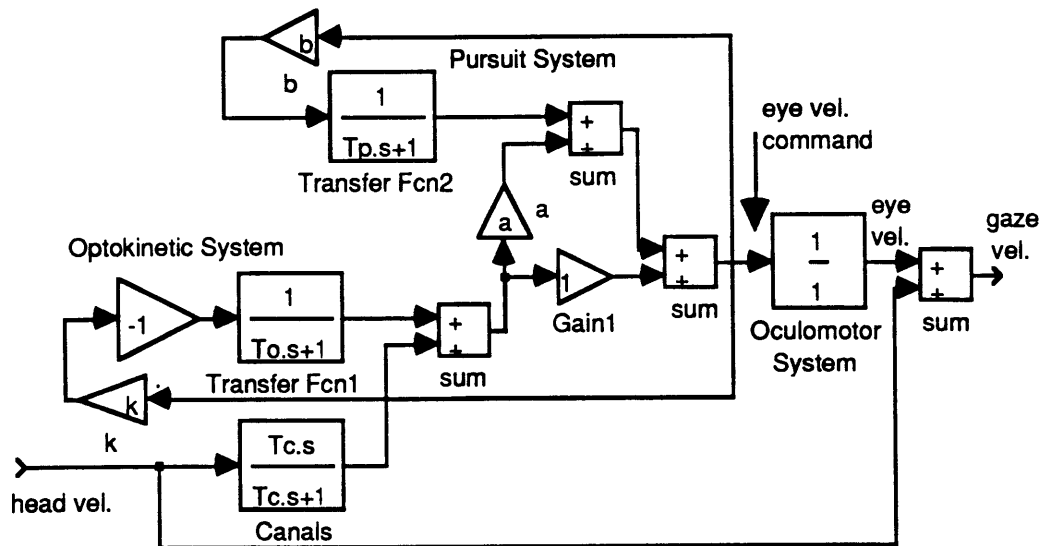


Figure 2.4, Robinson Model for VOR-OKN interaction for rotations in the dark (Robinson, 1977).

The Raphan-Cohen Model (Raphan et al, 1977) is shown in figure 2.5. This model takes into account all of the characteristics of the VOR mentioned above. The Raphan-Cohen model can be simplified and rendered into Laplace notation using some simplifying assumptions. First, rotation in the dark allows the neglect of the visual portion of the model. Second, we assume that the system is left-right symmetrical, allowing removal of the direction asymmetry terms. Next, cupula dynamics are assumed to be a simple exponential decay with a gain K , and time constant, T_c . Finally, adaptation effects are treated as another exponential decay in series with the cupula (Fernandez and Goldberg). This is here referred to as a five parameter modified Raphan-Cohen VOR

model or more simply, the five parameter model(Balkwill, 1992) (see figure 2.7). In this thesis, the five parameter model is used with T_a and T_c frozen at values of 80 and 6 seconds respectively. This is referred to as the three parameter (3P) model.

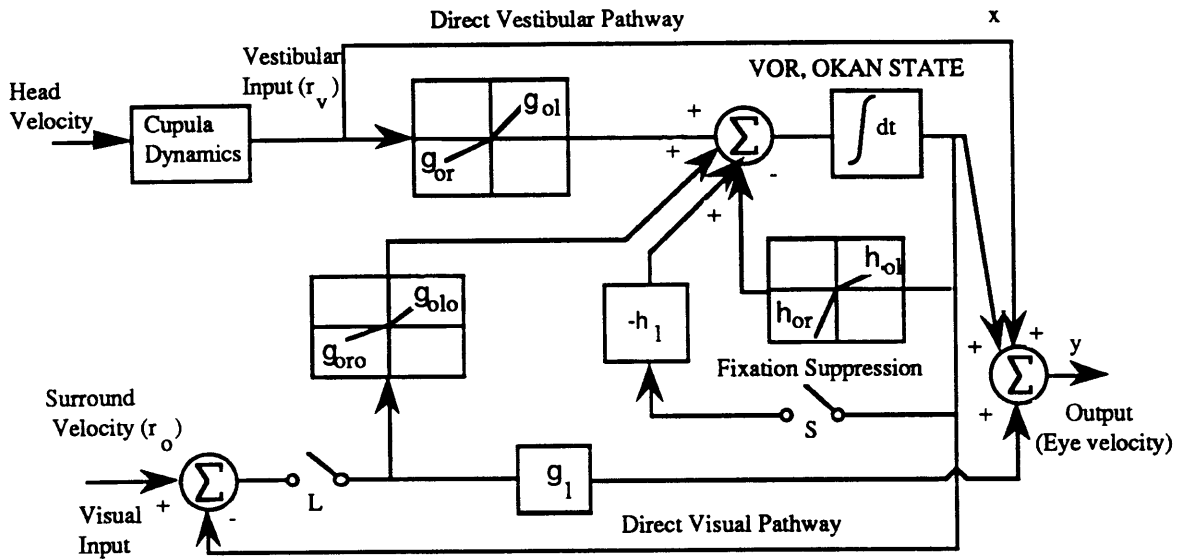


Figure 2.5, Raphan-Cohen model of OKN, OKAN, and vestibular nystagmus (From Raphan et al, 1979).

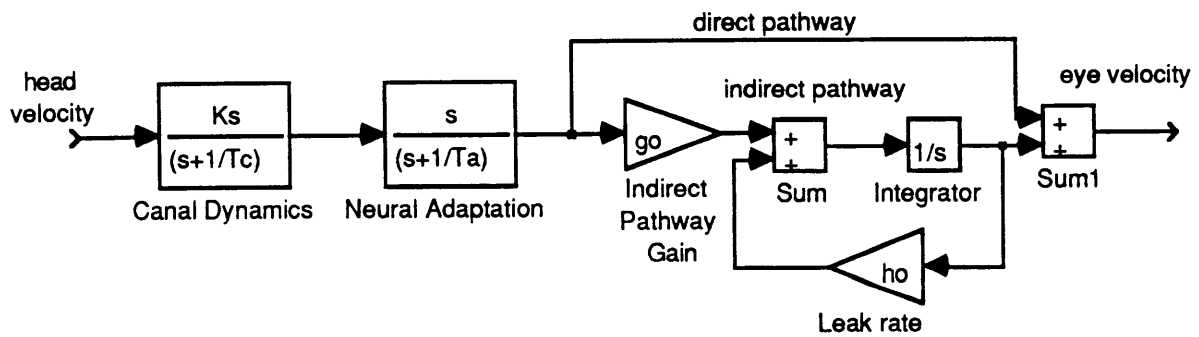


Figure 2.6, Five parameter modified R-C Laplace Transfer Function Model for rotation in the dark without left-right asymmetries.

In this model, the eye velocity signal is a sum of the activity in both the direct and indirect pathways. One major difference between this model, and the Robinson model, is that the storage effects of the system are modeled as efferent feedback in the Robinson model, whereas the modified Raphan-Cohen model assumes that the integrator

represents a separate state of the system, and models this using feed forward. A significant feature of the modified Raphan-Cohen model, is that the zero associated with the indirect pathway is believed to cancel the canal pole. Thus, as with the Robinson model, the response can be approximated by a single apparent time constant that lies between the adaptation and indirect pathway time constants.

Both the Robinson and modified Raphan-Cohen models can be simplified to a simple first order model representation (1OE model). This consists of a first order lag, with a gain and time constant to describe the decay of horizontal nystagmus in the dark (see figure 2.7). The time constant can be likened to the apparent time constants of the previous models. An apparent time constant is the time constant of a first order equivalent system to a higher order VOR model. It does not represent the dominant time constant of the higher order model, but is influenced by both time constants.

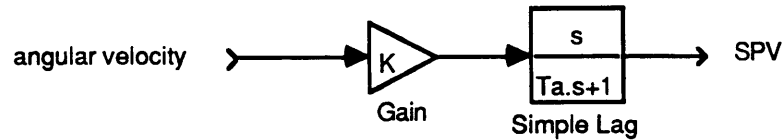


Figure 2.7, Simple first order model (1OE) of nystagmus decay.

An alternative model is based upon work carried on the semicircular canal afferent fibers of the pigeon (Landolt and Correia, 1980). This model, here referred to as the s^k model, uses a different method to express the effects of canal adaptation. Canal afferent response to accelerations can be modeled with a transfer function of the form,

$$H(s) = Gs^k \frac{1}{(\tau_L s + 1)} \frac{1}{(\tau_S s + 1)}$$

Here, the parameter G represents the system gain, k is an adaptation constant ($0 < k < 1$), and τ_L and τ_S are the long and short time constants of the torsion pendulum model of the cupula. The term s^k can be decomposed into a series of polynomials in s of the form;

$$s^k = C \sum_1^{\infty} \frac{J_i \tau_i s}{\tau_i s + 1}$$

A single term equivalent to this expansion, $C' J_i \tau_i s / (\tau_i s + 1)$ is similar to the neural adaptation term found in the five parameter model above. The C' term is a magnitude adjustment for reducing the infinite sum to a single term. The J_i term is the value of a probability density function, $J(\tau)$, evaluated at $\tau = \tau_L$. The Probability density function (Thorsen and Biederman-Thorsen, 1974) has the form;

$$J(\tau) = \frac{1}{\tau_L^{k+1}}$$

for all $\tau > 0$

This has the effect of amplifying fast acting time constants the most, and long time constants very little. As the fractional Laplace operator (s^k) was originally developed for use with visco-elastic materials, there is an analog to these we can use (Gross, 1953). For a fast acting force/response, the material behaves elastically like a spring. For slower force/response, the material relaxes, or creeps. One significant feature of this relaxation spectrum for vestibular modeling, is that for the longer time constants, the J_i term is much smaller than for shorter time constants, and thus faster time constants are more heavily weighted in the overall response.

Due to its small effect on the response (two orders of magnitude below the $(\tau_L s + 1)^{-1}$ for the frequency range concerned here), the $(\tau_s s + 1)^{-1}$ term was ignored in this model, simplifying it to;

$$H(s) = G s^k \frac{1}{(\tau_L s + 1)}$$

Given an input acceleration impulse stimulus of $\alpha_m^\circ/\text{second}$ the model response in the time domain becomes;

$$r(t) = (G \frac{\alpha_m}{t^k}) [\gamma^*(-k, -t/\tau_L) e^{-t/\tau_L}]$$

Where,

$$\gamma^*(a, x) = e^x \frac{x^{-a}}{\Gamma(a)} \int_0^{\infty} t^{a-1} e^{-t} dt$$

is the incomplete gamma function (which is single valued and finite in terms of a and t) and $\Gamma(a)$ is the complete gamma function evaluated at a . At negative values of t , for $-1 < a < 1$, the incomplete gamma function can be evaluated using the following series;

$$\gamma^*(a, x) = \frac{1}{\Gamma(1+a)} \left[1 + a \sum_{n=1}^{\infty} \frac{y^n}{(n+a)n!} \right]$$

where $y = |x|$

To change this from a canal model to a VOR model, velocity storage terms, using the same notation as for the five parameter model, were added. This gives the VOR model transfer function as;

$$H(s) = G s^k s \left\{ \frac{A}{\tau_L s + 1} + \frac{B}{s + h_o} \right\}$$

$$A = \frac{1 - \tau_L(g_o + h_o)}{1/\tau_L - h_o}$$

$$B = \frac{g_o}{1/\tau_L - h_o}$$

The time response of this system to an acceleration impulse may then be written as

$$r(t) = \left(\frac{G}{t^k}\right) [A \gamma^*(-k, -t/\tau_L) e^{-t/\tau_L} + B \gamma^*(-k, -h_o t) e^{-h_o t}]$$

This model will be referred to as the s^k model although it also incorporates VOR velocity storage effects.

Motivation for the use of this model arises from Correia, et al (1992). Correia found that following 14 days of space flight, two Rhesus monkeys showed increased gain and adaptation in SCC afferents. This suggested that one or more components of the vestibular end organ was transiently modified following space flight, and that the sites of

plasticity of vestibular responses may not be exclusively within the CNS. The modified Raphan-Cohen models do not predict gain changes due to changes in peripheral neuron adaptation. The s^k model accounts for neural response changes through the k parameter, which affects both gain and apparent time constant.

2.7 Effects of Altered GIF

Early tests of VOR response in centrifuge have shown, that the magnitude and duration of nystagmus was shorter when the head was reclined during a GIF greater than one. Later testing in parabolic flight (DiZio and Lackner, 1988) has shown that the apparent time constant of decay in both 0-G and 1.8-G is significantly shorter than it is in 1-G. Active head movement provoked velocity storage dumping was observed in both the 1-G and 1.8-G trials, but not in the 0-G trials. This implies that the presence of an altered GIF magnitude is equivalent to the dumping head movement, which alters the direction of the GIF, in provoking velocity dumping in humans.

Adaptation to altered GIF has been studied previously as part of the D-1 and SLS-1 SpaceLab missions. Also, there has been some previous examination of the SL-1 data presented here.

Previous analysis of the SL-1 data (Kulbaski, 1986) was confined to SPV responses averaged across all subjects and all five pre-flight data sessions versus the first two post-flight sessions (refer to section 3 for a description of the SL-1 experiment). A first order exponential model was fit to the first twenty seconds of averaged head up data, and $t=5$ to $t=10$ of dumping head movement data. This analysis found that while the head up time constant decreased significantly after exposure to micro-gravity (11.7 seconds pre-flight versus 9.3 seconds post-flight), the gain (0.60 pre-flight versus 0.59 seconds post-flight) and the dumping time constants (3.2 seconds pre-flight versus 3.4 seconds post-flight)

were unchanged . χ^2 analysis showed significant differences existed between the head up runs pre and post-flight from 6 to 20 sec after stop, and between the head up and dumping runs from 5 to 10 seconds after stop. SL-1 post-rotatory SPV averaged across subjects are shown in figure 2.9. It was believed that the change in pre-flight versus post flight responses, while there was no change in dumping responses, was due to two reasons; first, in the altered GIF environment of space, the CNS had partially suppressed the VOR velocity storage as a result of altered GIF, and second, over the time in flight, the CNS adapted to this altered GIF, and remained so for a short period post-flight. Because tilt suppression still occurred following exposure to micro gravity, there was no evidence that the otoliths were ignored by the CNS following exposure to micro

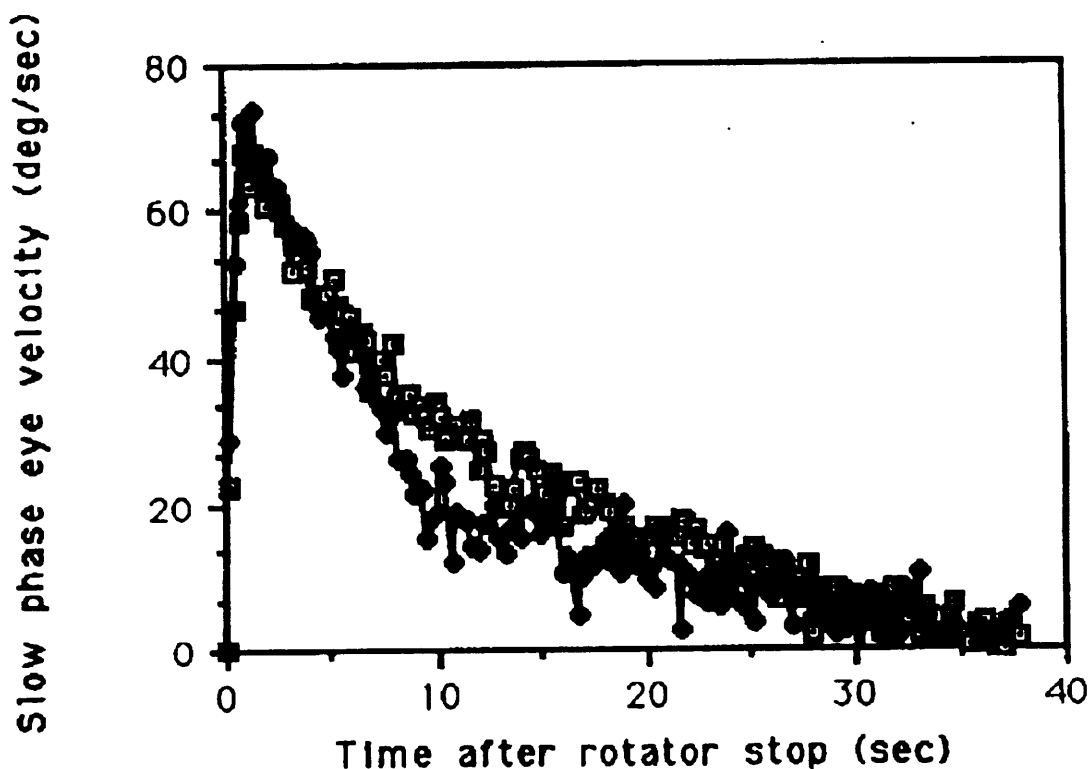


Figure 2.8 SpaceLab SL-1 grouped mean post-rotatory SPV pre-flight (squares) versus post-flight (circles).

gravity, and thus further tilt suppression beyond the adaptive tilt suppression was still possible.

On the D-1 mission, (Oman and Weigl, 1989), horizontal VOR was tested in five SpaceLab crew members 4 times pre-flight and five times post flight. Two of the subjects were directionally asymmetrical, while the other three subjects showed no change in VOR gain, and a more rapidly decaying SPV response post-flight than pre-flight. A χ^2 analysis showed a significant difference in the post-flight versus pre-flight at the $p < .001$ level. D-1 post-rotatory SPV averaged across subjects are shown in figure 2.8.

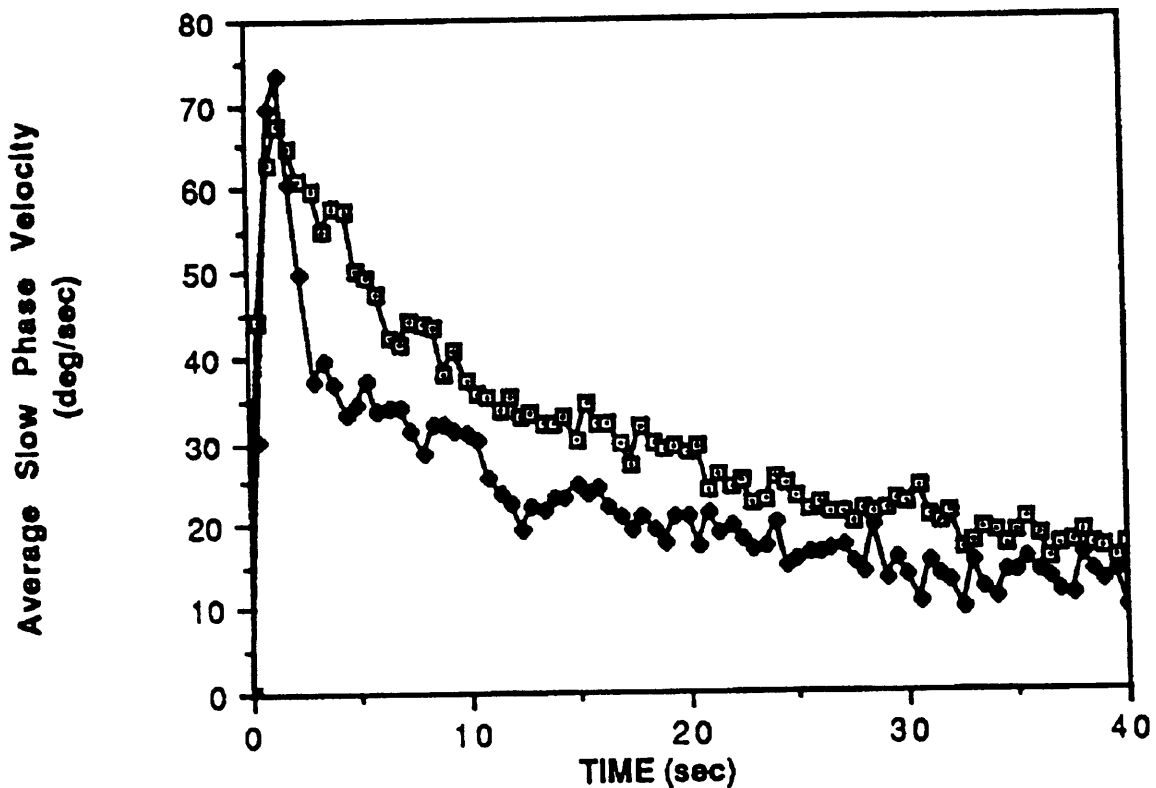


Figure 2.9, SpaceLab D-1 grouped mean post-rotatory SPV pre-flight (squares) versus post-flight (circles).

On the SLS-1 mission (Balkwill, 1992), four crew members were tested on four days pre-flight, and four days post-flight. The subjects were rotated at 120 °/second for sixty seconds while seated upright. The chair was stopped and the subjects remained upright for half the runs, and pitched their heads forward 90° after chair stop, for the other half. The dumping protocol was changed from the SL-1 and D-1 missions, in order for two reasons. First, this allowed a full sixty seconds of dumping data to be collected and modeled for changes, and second, as there is some uncertainty as to whether nystagmus suppression stops completely following return to the head erect position, analysis of post-dumping sections of previous data sets had been excessively complex. For SLS-1, the SPV was calculated, and fit to the five parameter modified Raphan-Cohen model (see section 2.6), and subjective duration of rotation was recorded. The apparent time constant of decay of the SPV was found to be lower post-flight than pre-flight, suggesting adaptation within the velocity storage mechanism. The change was believed to be a result of changes in indirect pathway gain on the model. Subjective responses were also found to be significantly shorter post-flight than pre-flight for three out of four subjects. For use on the SLS-1 and subsequent missions, new methods of analysis were developed including the use of order statistic filtering, automated dropout and outlier removal, iterative model fitting techniques, and Σ^2 testing (Balkwill, 1992).

2.8 Previous Analysis Methods used on SL-1 Data

Previous analysis of the SL-1 rotating chair data set was carried out in 1986 by Mark Kulbaski. Following digitization of the data, three data processing steps were carried out; SPV was determined, manual SPV editing was performed, and data was resampled at 4 Hz for statistical analysis.

2.8.1 Preliminary Processing

The SPV was calculated using the acceleration based Massoumnia algorithm (Massoumnia, 1983). The algorithm first differentiated the angular position signal to get angular eye acceleration. The algorithm then used a set of rules based on eye acceleration to classify each eye movement as either a fast phase or a slow phase of Nystagmus. Fast phase movements were replaced with a linear interpolation between adjacent slow phases. The Massoumnia algorithm occasionally failed to properly classify eye movements, and thus fast phases that were not removed had to be removed through manual editing.

Misclassification was due to several causes. One was that the low pass filters rounded out the peaks of high amplitude nystagmus preventing the algorithm from detecting the fast phase. A second cause was when the algorithm correctly determined a fast phase, but failed to accurately determine its beginning and end before interpolating across it. This was interpolated at an incorrect velocity as the interpolation would be between transition phases instead of slow phases. A third cause of errors was associated with transients in the EOG signal. There were two typical sources of transients: When the head tilted down during dumping runs, an electrode motion artifact occurred during each pitch movement. Also whenever the amplifier DC offset was manually adjusted to compensate for electrode drift, a transient was injected into the EOG. Finally, if the signal to noise ratio of the signal was low, the noise would confuse the algorithm, and it would completely fail to detect phases correctly.

Manual editing was performed on a PDP-11 using an interactive program known as SPARTA (Digital Equipment Corp., Maynard, MA). The program read the SPV file from the Massoumnia algorithm, and displayed the SPV on a CRT. Using potentiometers, the user positioned two cursors on the screen to mark the beginning and end of a fast phase. The data between the cursors was replaced with values linearly

interpolated between the values at the marked points. Following manual editing, the SPV files were resampled to 4 Hz before further processing.

Of the 145 runs analyzed, 21 of them were then discarded at this point on the following basis. If there was an abrupt change in the noise level in the EOG signal, this would suggest an electrode had lost contact. If an EOG signal had a low signal to noise ratio, the Massoumnia algorithm would fail to determine the SPV profile. If the SPV profile was markedly atypical the run would be discarded. If the SPV response lagged significantly behind chair motion, this indicated that the subject wasn't paying attention. In all of these cases, the runs were discarded. However, all criteria were only semi-quantitative.

2.8.2 Statistical Analysis

Two forms of statistical analysis were performed. The first was to conduct a χ^2 analysis to determine if two response curves were different. The second was to fit a simple exponential model to the data, and then to use ANOVA and t-tests to determine if the model gain and time constant were significantly different.

The CW and CCW responses were tested by χ^2 to determine if responses were directionally symmetrical. As no directional asymmetries were found, the CW and CCW runs were normalized for direction and averaged together. χ^2 analysis was performed to determine whether there was a trend across test days for all subjects. As no trend was determined, all pre-flight data was averaged together for each subject, and the first two post-flight sessions were averaged together for each subject. However this left the possibility of trends within individual subjects, which was not tested. Subsequently, Balkwill (1992) noted that Kulbaski had actually calculated the Σt^2 statistic and assumed that it followed the χ^2 distribution, which is not valid for small n.

Model fits were performed on averaged data sets for each subject using a simple exponential model. This was carried out through the use of a log-linear least squares fit to the data over the first twenty seconds of data for PRN and per-rotatory portions, and from 5-10 seconds after the chair stop for dumping runs.

Results from this analysis were reported in chapter 7.

2.9 Justification for Reanalysis

Previous analysis of SL-1 data had several weaknesses. First, the manual SPV editing was a potential source of error. Manual editing is always subject to variability due to human inconsistencies, and therefore standards for selection of edited portions on different runs may have varied. Also, the edited data was included in all subsequent processing even though the actual data had been replaced by an interpolated line. Thus interpolated points were inserted into the data at the interpolation regions that was then used for calculation of run statistics. Another weakness is the use of only semi-quantitative run exclusion criteria. A third weakness is that no individual runs were fit; all analysis was performed on data averaged over several trials. Analysis of individual runs would allow extraction of the variability of the responses. Individual and day to day variations were smoothed over by averaging. Through analysis of individual data, trends within subjects become much easier to see, where they are hidden by the averaging process and other analysis such as ANOVA become possible. A third weakness was the limitations of the model fit to the data. Only simple exponential models were fit to the data, and velocity storage was not modeled. New insight might be gained through re-analysis of this data using newer models such as the five parameter model and s^k models. Further justification for reanalysis is that new methods in EOG signal filtering have been developed (Balkwill, 1992) that can be used to improve the data quality.

3. Experimental Methods.

3.1 Equipment

The experimental apparatus was composed of the equipment used for the NASA Spacelab E072 F02 rotating chair experiment. This consisted of a motor driven rotating chair, and EOG data collection equipment.

The rotating chair (see figure 3.1) was constructed as an undergraduate thesis project by MIT students for use in the SL-1 and subsequent experiments (Johnson and Gidney, 1983). The chair was driven by a .75 hp, 27 ft-lbs torque DC motor, capable of smooth rotation of the chair at angular velocities up to 200°/sec. An Inland Motor Division TPA series motor controller and tachometer provided closed loop control of motor speed. The velocity control command was generated by a voltage across a potentiometer which was dialed by hand. Chair stop was initiated by grounding the velocity command using a toggle switch, which generated approximately a step velocity change.

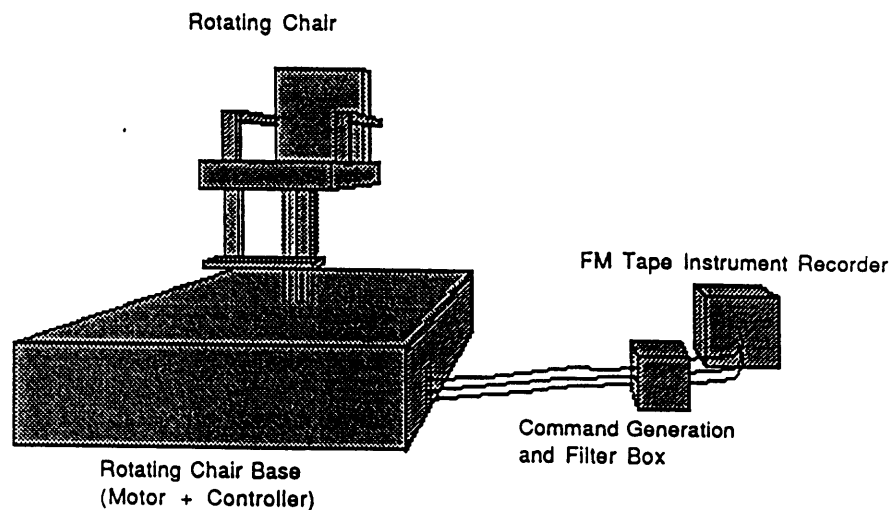


Figure 3.1, Experimental set-up

Data collection was accomplished through the use of electro-oculography (EOG). Five infant cardiac electrodes were placed above and below the right eye, on the left and right temples and either at the center of the forehead. The eye position was determined through measuring the relative voltage between pairs of electrodes. Since the eye has a dipolar magnetic field associated with its cornea (the corneo-retinal potential), movement of the eyes changes the induced voltages across electrode pairs, allowing eye position to be determined. The electrode pair at the temples monitored horizontal eye position, the electrode pair above and below the right eye monitored vertical eye position, while the fifth electrode was used as a reference ground for common mode rejection. Variability induced by inexact electrode placement and changing corneo-retinal potentials, was removed through calibration of the EOG using targets at known positions relative to the head. Electrode leads were connected to a differential amplifier (nominal gain 3000) mounted on the chair seat. Amplifier output was two voltage signals corresponding to horizontal and vertical eye position, with magnitudes between ± 15 volts. A manually controlled DC offset was added to these signals in the amplifier in order to keep the signals within ± 10 volts. The position voltage signals were passed through slip rings at the base of the chair shaft to the chair panel, and then through three cascaded first order analog low pass filters with corner frequencies at 30 Hz. Filtered EOG signals and the tachometer signal were recorded analog on FM tape using a calibrated Hewlett Packard 3964A Instrumentation Recorder.

The data was digitized in the MIT Man-Vehicle Laboratory (MVL) in two batches. The first batch consisted of all pre-flight runs, and post-flight runs for subjects A, C, and D. This was digitized from the FM tape using the same FM recorder playing into a Macintosh Mac II computer running the Labtech Notebook version 1.0.1 software package, sampling at 120 Hz. The output range of the recorder was limited to ± 3 volts, and for this batch of data, input range on the Mac II A/D board was set to ± 10 volts.

The second batch of data consisted of all subject B post-flight runs. This was digitized using the Labview version 2.1 software package sampling at 120 Hz. For this batch, A/D input range was ± 1 volt, with the recorder output being adjusted to ± 1 volt. Both batches were saved in identical binary form and all further processing was identical.

3.2 Subjects

Subjects used in this experiment were all members of the SL-1 crew team. Six subjects were tested preflight, including the four SL-1 payload specialists and two alternate payload specialists. Post flight testing was only conducted on the four payload specialists, as the alternate payload specialist did not fly on the mission. All subjects tested were male and all were free of any overt vestibular disease. To preserve confidentiality, flight subjects were assigned the code letters A, B, C and D and will be referred to as such herein.

Subjects were tested on five separate days before the flight. The pre-flight tests were performed on F-151, F-121, F-65, F-43, and F-10 days before launch. Post-flight testing was conducted on three days after recovery, R+1, R+2, and R+4 days after landing. All experiments were performed at the NASA Dryden Research Facility at Edward's Air Force base, California, by Dr. Oman.

3.3 Experimental Protocol

The same protocol was used for each subject on each test day. Deviations from this protocol are noted at the end of this section.

The subjects were seated upright in the rotating chair with their heads directly above the axis of rotation. Prior to electrode placement, the subjects skin was cleaned with alcohol. EOG surface electrodes were placed on the skin in the pattern previously

mentioned (section 3.1). Subjects were given a blindfold and stereo earphones in order to suppress visual and auditory signals. Subjects were asked to wear long sleeved shirts and pants to remove tactile wind cues, however, this was not consistently done by the subjects. Subjects were instructed to look straight ahead and keep their eyes open at all times during the runs.

The subjects performed two types of runs. The first was termed a post-rotatory nystagmus run (PRN). The second was termed a dumping run. For the PRN runs, the subject was subjected to a steep ramp in angular velocity up to 120 °/second, done by turning the dial on the velocity command potentiometer. This angular velocity was maintained for approximately 60 seconds, timed using a stopwatch, then the chair was stopped within one second. Eye movements were recorded for 45 seconds following chair stop as the subject remained upright. For a dumping run, the chair stimulus was identical to the PRN run, however following chair stop, the following protocol was observed. When the chair stopped, the operator would begin counting seconds aloud, '0-1-2-3-4- "down" -5-6-7-8-9- "up" '. As the operator called out "down", five seconds after stop, the subject would tilt their head down approximately 90 °, and remain so until the operator called out "up" at ten seconds after chair stop. Eye movements were recorded for 45 seconds following chair stop as with the PRN run.

Stimulus runs were performed in both clockwise (CW) and counter-clockwise (CCW) directions. Direction of runs was alternated between successive runs in order to prevent residual effects from the long time constant of neural adaptation from building up and biasing results. The nominal experimental protocol was as follows;

run #	1	EOG calibration
	2	CW PRN
	3	CCW PRN
	4	EOG calibration
	5	CW dumping
	6	CCW dumping
	7-9	additional sinusoidal runs, part of a separate investigation
	10	EOG calibration.

Not all data sessions were completed according to this pattern. For subject A, the non-standard sessions were; F-121, additional CCW dumping run performed. For subject B; F-121, additional CCW dumping performed; F-43 runs # 2 and 4 not done. For subject C; F-65, run #4 not done, F-43 runs # 2 and 4 not done. For subject D; F-121 additional CW and CCW dumping runs performed, F-65 runs #3,4,5 not done.

Each run was given a unique code, known as its run code, which were used to identify runs for the remainder of this work. The run code consists of the subject letter (A-D) followed by a one digit number representing the BDC session(1-8), followed by a two digit number representing the run # (1-11). Hence B304 would represent subject B, on the third BDC session (F-65) on the fourth run.

4.0 Data Analysis

4.1 New Algorithms for Data Reanalysis

All data analysis for the SL-1 data set was conducted in the MatLab 3.5 software package (The MathWorks Inc., Natick, MA). MatLab can be used as a fourth generation language for programming 'scripts', while it also allows execution of C language code from within the program as MatLab external (MEX) files. The analysis routines used a mixture of scripts and C code.

Prior to data analysis, all digitized data was resaved into MatLab format using a C language program, *batch_chair_convert*, a modification of *BDCF_convert* (Balkwill, 1992).

4.2 Calibration Procedure

Calibration of EOG potentials was carried out using the NysA Nystagmus Analysis package (Balkwill, 1992). The NysA *calibrate* script determines the calibration factors from A/D units to degrees of eye movement with a semi-automated procedure. The horizontal eye position of a calibration run is displayed. The user marks the regions of the signal where the subject is focused on the right and left calibration targets using the mouse. The calibration factor in degrees/unit is calculated as the ratio of the angular difference in calibration targets (20°) to the difference in the mean value of the A/D units over the selected regions.

Due to significant EOG drift, some calibration factors had to be calculated differently. Over a short time period (e.g., ten seconds), the EOG drift can be approximated as linear. When the user selects the fixation regions, a first order fit was made over each region, and these lines were projected to the midpoint between the two regions. The

calibration factor was then taken as the ratio of the angular difference in calibration targets (20°) to the difference in the projection of the linear fits onto the midpoint between the regions, in A/D units.

Calibration factors were calculated for each of the three calibration runs for each subject, for each BDC session. If calibrations were repeated within the run by the subject, the more consistent calibration was used to generate the calibration factor. Calibration factors for each stimulus run were then calculated by linearly interpolating between the calibration runs. If the middle calibration run was omitted, the calibration factors would be interpolated between the two known calibrations. If either the first or last calibration was missing, calibration factors were calculated by projecting the interpolated line from the other two calibrations over the stimulus runs.

4.3 Order Statistic Filtering

Prior to model fitting and data analysis, EOG data was filtered using two non-linear order statistic (OS) filters and one linear filter. This was to remove noise in the eye position signal, differentiate the position signal (linear filter), and remove saccades in the eye velocity signal. Filtering programs were originally written by Balkwill, 1992. Filter output corresponded to smoothed SPV profiles.

OS filters are a class of non-linear digital filters that operate on the local statistical properties of their input data streams. Since they are non-linear, they do not have a unique transfer function representation in the frequency domain.

4.3.1 Predictive FIR Median Hybrid Filter

Predictive FIR mean hybrid filters (PFMH) are a subtype of OS filters that work as follows (Heinonen and Nuevo, 1987). A sliding window of odd length moves along the

data. At each point, the data in the window is rank ordered, and the output corresponding to the middle of the window is assigned a value based on the statistics of the sorted data of the windowed samples. The first and last half window lengths of filter output are undefined, as there isn't a full window of data available. PFMH filters assume the existence of a root signal. As the filter is applied, it reduces the difference between the input data and the root signal. Repeated application of PFMH filters allows the filter output to asymptotically approach the root signal.

For this analysis, PFMH filters with a root signal corresponding to piecewise continuous polynomials are used. These filters use a window of length $2*N+1$. The first and last N samples are used to calculate first order polynomials (root signals), which then are used to estimate the value at the middle, $N+1^{st}$, point. Filter output is the median of the two predicted values, and the original value at the center of the window. Two filters were used, of lengths $N=6$, and $N=10$, and each filter made two passes on the data.

Since first order segments were used as the root signals, as the filters removed noise, they also tended to sharpen the corners of the nystagmus signals, which had previously been rounded off by the analog filtering prior to digitization.

4.3.2 Calculation of SPV using Adaptive Asymmetrical Trimmed Mean (OS) Filter

PFMH filtered eye position was differentiated to yield eye velocity using a linear nine point FIR velocity filter consisting of a three point differentiating filter convoluted with a seven point low pass filter with a 10 Hz cut off frequency (Massoumnia, 1983). The z-transform of the filter can be expressed as;

$$H(z) = \frac{-0.0332z^{-4} - 0.0715z^{-3} - 0.0678z^{-2} - 0.0522z^{-1} + 0.0678z^2 + 0.0715z^3 + 0.0332z^4}{Tz^{-4}}$$

where T is the sampling period, 1/120 seconds.

Using the eye velocity signal as input, an OS filter called the adaptive asymmetrically trimmed mean (AATM) filter was then used to calculate the SPV (Engelken and Stevens, 1990). The filter works on the assumption that the eye spends more time in the slow phase portion of nystagmus than the fast phase. With this assumption, a histogram of eye velocities would show a peak near the SPV, skewed off of the zero mean line, with a long tail or secondary peak at higher velocities representing the fast phase velocities. The filter takes a one second window of data and sorts the velocity values into ascending order. The ends of the sorted data are 'trimmed' asymmetrically, with more samples being removed from the high velocity tail of the histogram. The mean value of the remaining samples is taken as the filter output. It should be noted that the estimated SPV probably won't correspond to the actual eye velocity at any given point in time, as the SPV is estimated based on the velocity distribution of surrounding points rather than velocity at an individual point.

4.4 Tachometer Analysis

The tachometer signal was analyzed to determine the stimulus parameters. Since the chair velocity command was created by a hand controlled potentiometer, the ramps varied from run to run, as did the steady state chair speed. Also, due to inexact voice indicators used to mark the beginning and end of runs on the FM tape from which data was digitized, the beginning of the runs occurred at different points in time in the digitized data. Finally, due to stimulus duration being timed by the operator, stimulus duration's varied. To determine these parameters, a MatLab script, *tachan_MIT* was created by modifying an existing script, *tachan* (Balkwill, 1992).

In order to calibrate digitized chair velocity, a marker on the tachometer signal caused by a button push was used as a scale. The button caused a spike, equivalent to 50°/second,

to be superimposed on the tachometer signal. The value of the spike in A/D units was calculated, and the calibration ratio obtained.

The *tachan_MIT* script converted the sampled tachometer signal to degrees, then began searching from the beginning of the signal until it found the tachometer had climbed to 50% of its expected steady state rotation value. The delay from the beginning of data to chair start was recorded, and one second beyond the point of 50% chair velocity was recorded as chair start based on the assumption that the chair would accelerate to full speed in 2 seconds under ideal conditions. In some cases, due to low chair acceleration, the point marked as the chair start occurred before the chair had actually reached full speed. In these cases the triggering parameter was manually adjusted from 50% up to as much as 90% until the operator was satisfied that the indicated chair start corresponded to the chair's reaching its steady state velocity. In some cases, long chair acceleration times lead to loss of as much as 10 seconds of data.

The chair velocity was calculated as the mean value of velocity from five to fifteen seconds after chair start. Continuing from fifteen seconds, it continued to monitor the tachometer signal until it fell to less than 50% of its steady state value, it then recorded this as the end of chair rotation. For dumping runs an additional parameter was calculated. At the time of the head reaching ninety degrees pitch, the subject was to depress the previously mentioned button. The time of this button press was also recorded as the beginning of the five second head pitch movement.

4.5 Outlier Removal and Decimation

Outlier removal for this analysis was fully automated. A script called *stat_prep2*, modified from an existing script, *stat_prep* (Balkwill, 1992), performed this as well as other statistical preparation.

First, each SPV file was normalized in time to a uniform length of sixty seconds for each of the per and post-rotatory segments. This was done to facilitate comparisons between runs by having start and stop times occur at the same point in each run and identical run lengths. Per rotatory SPV data was retained from the calculated start time for sixty seconds. If chair stop occurred before sixty seconds had elapsed, the data was extrapolated to fill a full minute by adding points at the median value of the last five per-rotatory points to fill sixty seconds. If chair rotation persisted beyond sixty seconds, only the first sixty seconds were used. Post-rotational data was taken from chair stop for sixty seconds, and was truncated or extrapolated in the same manner as the per-rotatory data.

The algorithm for outlier detection was designed to remove artifacts in the EOG data. Artifacts are present at all times in EOG data from a variety of sources. One common source of artifacts in this data was subject alertness. A subject that shows a low level of alertness will also show a lower VOR gain. When SPV drops near zero due to low alertness, it is referred to as a dropout. High physical and mental demands on SpaceLab missions generally lead to fatigue, and resulted in dropouts in the SPV data. A second source of artifacts is caused by tugging on electrode leads. This could happen when the dumping maneuver was performed if the leads caught on the chair back. Other artifacts were the result of the subjects adjusting the goggles or touching the electrode leads. It should be noted that this list of artifacts is not all inclusive.

For short duration dropouts, the AATM algorithm would interpolate across the dropout due to its basis on the statistics of surrounding points. Dropouts of greater than about .25 second duration would cause AATM to reduce the SPV over that range, and of greater than one second would allow AATM to preserve the dropout. Due to intrinsic EOG noise

on the SPV of the order of $10^\circ/\text{second}$, dropouts in regions where SPV was at or below this level were indistinguishable from the baseline EOG SPV noise. The automated algorithm (Balkwill, 1992) considered only from $t=2$ to 20 seconds after start and stop for this reason. The natural logarithm of the data was taken, and a least squares log-linear fit was made to the data. The root mean square error (RMS) about the fit was calculated, and any points that were more than $3 \cdot \text{RMS}$ away from the curve, or below 7.4 deg/second were ignored as were any points within .5 second of one of these points in order to catch the beginning and end of any dropout. A new fit was calculated using the remaining points and all points were compared to this new fit. This would continue until the RMS of a fit converged to within 20% of the RMS of the previous iteration. The 'good' points of the last iteration were recorded for later use.

The data files were then decimated down to 4 Hz using *dec_30_new*. This was done in order to reduce the computational intensity and storage demands for subsequent analysis. Decimation was carried out by averaging points in $1/4$ second blocks. Points marked as bad by the outlier removal algorithm were omitted from this average. Each $1/4$ second segment was least squares fitted to a straight line to correct for the general trend of the curve. The variance of the points around the fitted lines was calculated and recorded, along with the number of good points in that section. Calculating variance with respect to the mean value in the window (as done by Balkwill, 1992) is equivalent to calculating the variance around a line of zero slope. However, since the curves were known to be changing with time, the least squares fit provided a local approximation to the curve over the window, and the variance was calculated relative to the estimated values generated by the line. This gave a better estimate of the variance than finding the variance about the mean value of the window (Balkwill, 1992), which gave elevated variance estimates due to the known trend in the curve. Due to intrinsic EOG SPV noise, and residual trends in the curve around the fitted straight line segments, the variance found in this way varied

greatly. Using such values of variance directly would compromise the robustness of the parameters estimated by the model fitting routine. Therefore, to make a robust estimate of the variance, a histogram for all the variances of decimated points was calculated, and divided into three sections of equal area. A mean variance was calculated for each area and each point in that area was replaced in the calculation with its sections average. This variance estimate was referred to as the assigned mean variance.

The weight given each decimated point was calculated as the number of contributing points, n_i divided by the assigned mean variance. The weights were used in the ensemble averaging process described in section 4.10.

Additional parameters were calculated at the time of decimation based on the number of good data points in the decimated regions. That number was used as a basis for deciding which runs were of sufficient quality to support a fit to the model. This number was used to help develop the rules for run rejection described below.

4.6 Run Rejection

Some runs were unsuitable for further processing due to the presence of artifacts as discussed in chapter 2. Some run segments were rejected after the model had been fitted.

Any run segment would be rejected if either;

1. *stat_prep* removed more than 10 seconds of data
2. It took more than 10 seconds for the chair to reach steady velocity.
3. The model fitting routine hit a constraint (i.e. chose a constraint as the best fit)
4. Peak SPV response was below 25 degrees/second.

The first rule was formulated to eliminate run segments which had a significant amount of data removed as outliers by the outlier detection algorithm. The second rule eliminated those runs for which SPV response would not approximately conform to response to a step function input. This was because the model fitting routine assumed a

step function input run through a low pass filter. The third rule eliminated runs for which the model fit was unable to find a physiologically reasonable set of parameters to fit the data. The fourth rule was devised to detect inattentive or sleepy subjects who would be expected to have reduced SPV response.

4.7 Individual Model Fits

MatLab scripts were written to fit the first order exponential, three parameter, and s^k VOR models to the individual runs. These are included in appendix M. The models were fitted by using a constrained optimization routine that searched the constrained variable space of the model in order to find the least squares best estimate parameters for the model. The optimization routine was a script called *CONSTR* from the MatLab optimization toolbox (Grace, 1990). As stated in Grace, 1990, '*CONSTR* uses a sequential quadratic programming method, which solves a quadratic programming sub problem at each iteration. An estimate of the Hessian of the Lagrangian is determined at each iteration and a line search is performed using a merit function and the quadratic programming sub problem is solved using an active set strategy.' Variable constraints were chosen on the basis of what was considered to be physiologically reasonable parameter values.

The per-rotatory and post-rotatory segments of each run were fit separately. This was done for two reasons. First, because some runs only had good quality data for either the per or post rotatory sections, but not both, this allowed runs where only half the data was good to have the good half uncorrupted by the inclusion of bad data. Second, this method allowed the separate halves of the data to reflect any asymmetries in the responses of subjects to the direction of the stimuli. This method had the disadvantage of providing data segments of only 60 seconds, which was too short to permit complete

observation of the adaptation time constant in the five parameter model, which is expected to be on the order of approximately 80 to 120 seconds.

4.7.1 First Order Exponential Model Fits

The simplest model that was fit to the data was the first order model of section 2.5. This model was fit to the data from 2 seconds following the start (or stop) to the full 60 seconds. The first two seconds were omitted to allow transients from the chair acceleration to damp out, and because, due to the same transients, outlier detection could not be reliably performed over this region. The constraints placed on the model were as follows;

$$.18 \leq K \leq 1.8$$

$$5 \leq T \leq 45$$

These constraints are believed to be physiologically reasonable, and were operationally satisfactory as no fits reached the parameter boundaries.

4.7.2 Three Parameter Model Fits

The three parameter model was also fit over the region of 2 to sixty seconds after chair start (or stop) for the same reasons noted in section 4.3.6.1.. Based on previous experience with this model (Balkwill, 1992), and expectations of what is physiologically reasonable, initial model constraints were chosen as follows;

$$.1 \leq K \leq 1.8$$

$$3 \leq 1/h_0 \leq 300$$

$$0 \leq g_0 \leq .45$$

$$T_a = 80 \text{ seconds} \quad (\text{fixed})$$

$$T_s = 6 \text{ seconds} \quad (\text{fixed})$$

The adaptation time constant was fixed because using a sixty second stretch of data, the time course of data was not long enough to accurately determine it. The cupula time

constant was fixed in order to assist convergence of the optimization. When fit to individual runs with the additional degrees of freedom available, the model fit can respond to atypical variations in individual run data. On three run segments, the fits of the model parameters reached one of the assigned boundaries, and were discarded (see section 4.6).

4.7.3 s^k Model Fits

For a subset of runs, the s^k parameter model was also fit over the region of 2 to sixty seconds after chair start (or stop). Based on experience with this model, and Correia's work, initial model constraints were chosen as follows;

$$0 \leq C \leq 15$$

$$0 \leq k \leq 1$$

$$5 \leq T_c \leq 15$$

$$3 \leq 1/h_0 \leq 300$$

$$0 \leq g_0 \leq .45$$

The results of the s^k model fits were used to evaluate the performance of the model, and were not used to analyze vestibular changes due to micro gravity. Not all runs were fit to this model due to slow computation.

4.8 Dumping Model Fits

Due to the brevity of the dumping head movement, the model fitting routines did not have enough data to fit only the dumping portion of a run, while the remainder of a run could not be used due to both possible contaminating effects from the dump movement, and the loss of the first 5-10 seconds of data due to the dumping head movement. This forced a different modeling approach for the dumping runs.

Due to the small amount of data, it was necessary to constrain the variation in the runs to as few parameters as possible. Thus, only a simple exponential was fitted. In order to minimize noise and computational speed, this was implemented as a log-linear least squares fit. The data was fit in three sections independently. From chair start to 0.25 seconds before indicated dump was referred to as the 'before' segment. From 0.25 seconds after indicated dump to 4.75 seconds after indicated dump was referred to as the 'dump' segment. From 5.75 seconds after indicated dump to 19.25 seconds after indicated dump (30 seconds after chair stop) was referred to as the 'after' segment.

4.9 Residual Analysis

Residuals of decimated SPV data around the three parameter model fitted values were calculated in order to better assess the quality of the model fits. They were visually scanned individually for possible systematic time trends, and the mean values of the residuals were calculated. For some of the runs, periodograms were calculated using the *Spectrum* function in MatLab in order to examine the frequency properties of the residuals.

4.10 Mean Model Fits

A selected group of decimated runs were averaged together. The mean SPV curve was calculated as a weighted average of the runs, using the weights calculated as described in section 4.5. This was done to give greater weight to runs that had low variance, and many contributing (pre-decimation) points. This would be expected to give a better estimate of SPV in the regions that included or lay adjacent to points that had been removed by *stat_prep* in any of the individual runs. In an individual run, due to the removal of some of the points, the estimate of the SPV created by *dec_30_new* would have larger variance due to the reduced number of data points contributing to the estimate. Therefore, when averaging runs together, this was taken into account through

the weights, which would allow each individual run to contribute proportionally to the mean relative to the number of good pre-decimation points divided by the variance of the good pre-decimated points. The variance of the mean SPV curve at each point in time was estimated as;

$$s^2 = \frac{\sum_1^n w_i [x_i(t) - \overline{x(t)}]^2}{\sum_1^n w_i} \frac{n_i}{(n_i - 1)}$$

where $x_i(t)$ is the value of the i^{th} run at time t , and $\overline{x(t)}$ is the value of the weighted mean value of all runs at time t . The multiplication by $\frac{n_i}{(n_i - 1)}$, where n was the number of

SPV curves contributing to the mean at each point in time, was in order to account for the lost degree of freedom.

The mean SPV curves were fit to the models in the same manner as the individual model fits (section 4.3.6), with one significant difference. The cost function for the optimization of the mean model fits was weighted at each point with a weight calculated in the same manner as the weight used for the averaging procedure. This was done in order to provide a maximum likelihood estimate fit to the data by placing higher weights on the points in time in the mean data with the lowest variance or most contributing points, and lower emphasis on points with higher variance, when fitting the models.

4.10.1 Statistical Comparison of Mean SPV Curves

Two forms of statistical analysis were performed on the mean SPV curves to determine if they were significantly different. The first test was the Σt^2 test, to determine if the two curves were different from each other. The second test was the students t test at each point along the line to determine where the curves were significantly different.

Both tests used the pooled variance of the two runs calculated at each point in time using the formula;

$$s_p^2(t) = \frac{((n_1(t)-1)s_1^2(t) + (n_2(t)-1)s_2^2(t))}{n_1(t) + n_2(t) - 2}$$

where, $n_i(t)$ = number of runs in i^{th} curve

$s_i^2(t)$ = i^{th} run's variance

$s_p^2(t)$ = pooled variance

The students t test (Balkwill, 1992), was conducted at every point in time

$$\tau(t) = \frac{x_1(t) - x_2(t)}{\left(s_p^2(t) \left(\frac{1}{n_1(t)} + \frac{1}{n_2(t)} \right) \right)^{1/2}}$$

and the sum of t-squares is just the summation of these values at every point of time;

$$\sum t^2 = \sum_t \frac{(\bar{x}_1(t) - \bar{x}_2(t))^2}{s_p^2(t) \left(\frac{1}{n_1(t)} + \frac{1}{n_2(t)} \right)}$$

This test statistic was also calculated in previous analysis of this data set (Kulbaski, 1988), and in analysis of the D-1 mission (Oman and Weigl, 1989). However it was compared to the χ^2 distribution. This is only valid if n_1 and n_2 (number of curves averaged together) are large. For cases with n_1 and n_2 small, this statistic should be compared to the Σt^2 distribution which depends on n_1 and n_2 instead of the $\chi^2 = \Sigma z^2$ distribution. Although the Σt^2 distribution was originally unknown, previously (Balkwill, 1992, Pouliot, 1991), a Monte Carlo simulation was run to determine Σt^2 probability values for profiles containing 100 points in time (100 degrees of freedom) for values of $2 < n_1 < 20$, and $1 < n_2 < 10$.

For degrees of freedom other than 100, tables of the Σt^2 distributions are presented in Balkwill, 1992. The ratio criterion of Σt^2 values to the number of degrees of freedom (df), r , decreases slowly as the number of degrees of freedom increases (Pouliot, 1991). For one sample case ($n_1 = 40$, $n_2 = 16$) the r value for $p < .05$ for 100 df was 1.29, while for 56 df the $p < .05$ r value was 1.37. For greater numbers of df, the tables would provide a slightly conservative estimate. The df in this study ranged from 58 to 231, so for most cases the p values would be conservative.

The p values were calculated under the assumption that the n_1 and n_2 didn't vary with time. Calculating the distributions with either of these varying would require Monte Carlo simulation, and was not attempted. Instead, for each run, the mean value of n_i was calculated and rounded downwards to determine the appropriate n value for each run.

5.0 Results

The SPV response for each run was calculated using the algorithms described in chapter 4. The vertical SPV data was not analyzed, as the experiment was designed to isolate horizontal vestibular responses, although several runs were randomly chosen and manually inspected for evidence of vertical nystagmus. No incidence of significant vertical nystagmus were noted.

5.1 Calibration

The corneo-retinal potential is known to vary slowly over time, and is very sensitive to light level (Gonshor and Malcolm, 1971). Changes in the light level were large for the calibrations on the SL-1 mission. While runs were performed in total darkness, calibrations were performed in normal interior ambient light conditions. This could have the effect of changing the EOG potentials for the calibrations relative to the runs, and induced a drift in the EOG potential that sometimes seemed visible on the calibration EOG traces.

Since this analysis was performed primarily on SPV, as opposed to position, the act of differentiation would scale the SPV, so, while the absolute magnitude of the SPV may have changed slightly between calibration and test run, the relative magnitudes over the length of a run would be unchanged and thus the shape of the SPV curves wouldn't be affected, only their magnitude. From Gonshor and Malcolm, it was noted that EOG potential decreased for ten minutes when white lights were switched to red for dark adaptation, and then increased for a further ten minutes. Based upon the calibration factors that were calculated for each subject, and the knowledge that each calibration was separated by at least two runs, and therefore more than four minutes, we expect that the magnitude of change in the EOG potentials over the course of a single run would be small, on the order of 10% or less for most cases, while variations from run to run

would be accounted for through the linear interpolation of run calibration factors between calculated calibrations. Second, from the same research (Gonshor and Malcolm, 1971) we would expect that, had the lights remained off for the calibrations (to prevent EOG potential from changing due to the light) we would expect to see a decrease from the first to second calibrations, and an increase from the second to the third. This pattern only emerged twice out of 32 cases. A drop from the first to second calibration, or a rise from the second to third only occurred in six of the remaining 60 half cases. This is likely to be a result of the EOG potential responding to the room lights being turned on for the calibrations following dark adaptation. Calculated calibration factors are shown in tables A.1a through A.1d in appendix A.

One unfortunate result, was the consistently low EOG potential of subject A. This was reflected in the high calibration factors, between two to six times higher than the other three subjects on average. This meant that the resolution on eye position was similarly, $\frac{1}{2}$ to $\frac{1}{6}$ of that of the other subjects. An associated problem was that the signal to noise ratio was similarly reduced by a factor of two to six. As a result of this, the noise in the EOG signal, electro-magnetic and biological and nature, was too high to permit satisfactory analysis of subject A. Therefore subject A was arbitrarily omitted from further analysis.

In previous analysis of this data set (Kulbaski, 1988), subject A was analyzed. However, the quality of individual runs for this subject had less bearing in that analysis, due to all analyses being conducted on ensemble averaged runs, both within and between subjects. Assuming that the noise on subject A is random with zero mean, averaging the runs should reduce the RMS magnitude of the noise on the averaged run. It should be noted however, that in Kulbaski (1988) none of subject A's responses analyzed separately from the other subjects proved statistically significant. Finally, in his report, Kulbaski states

that subject A, "... has the noisiest EOG signals, ...", and visual scanning of Kulbaski's plots confirms this.

5.2 Rejected Runs

Due to previously mentioned artifacts and conditions, several of the runs were eliminated from further analysis using the rules defined in chapter 4. Tables 5.1a through 5.1d show the status of all of the runs on a subject by subject basis. In many cases, only half of a run would be omitted, either the per-rotatory or post-rotatory section only. In particular, this was prevalent for the post flight BDCs. This is because the subjects were fatigued, and instructed to relax during the per-rotatory sessions, and concentrate during the post-rotatory sessions. This resulted in few good per-rotatory runs post flight, but improved quality on the post-rotatory portions.

Run	F-90	F-60	F-30	F-11	F-10	R+1	R+2	R+4
2	12	12	12	12	12	12	12	12
3	12	12	12	12	12	12	12	12
4	--	--	12	--	--	--	--	--
5	12	12	12	12	12	12	12	12
6	12	12	--	12	12	12	12	12
10	--	12	--	--	--	--	--	--

Table 5.1a, Run rejection status for subject A. Empty boxes indicate runs kept in entirety, a "1" indicates omission of per-rotatory segment, a "2" indicates omission of a post-rotatory segment, dashes indicate runs not performed or calibrations.

Run	F-90	F-60	F-30	F-11	F-10	R+1	R+2	R+4
2				12	--	1	1	12
3		2		1	1	1	1	
4		--		--	1	--	--	--
5	1	--		1	--		1	1
6	--		--		1	1	1	12
7	--	2	--	--	1	--	--	--
11	--	2	--	--	--	--	--	--

Table 5.1b, Run rejection status for subject B. Empty boxes indicate runs kept in entirety, a "1" indicates omission of per-rotatory segment, a "2" indicates omission of a post-rotatory segment, dashes indicate runs not performed or calibrations.

Run	F-90	F-60	F-30	F-11	F-10	R+1	R+2	R+4
2	2		1	--	1	1	1	12
3			1	2		1	1	
4	--	--			--	--	--	--
5						1	1	1
6			--			12	1	12
10	--		--	--	--	--	--	--

Table 5.1c, Run rejection status for subject C. Empty boxes indicate runs kept in entirety, a "1" indicates omission of per-rotatory segment, a "2" indicates omission of a post-rotatory segment, dashes indicate runs not performed or calibrations.

Run	F-90	F-60	F-30	F-11	F-10	R+1	R+2	R+4
2		1	1	--		1	1	1
3		1				1	1	1
4	--	--	1		--	--	--	1
5	1	--	--		1	1	1	1
6	1	1	--			1	1	1
7	--	1	--	--	--	--	--	--
13	--	1	--	--	--	--	--	--
14	--	1	--	--	--	--	--	--

Table 5.1d, Run rejection status for subject D. Empty boxes indicate runs kept in entirety, a "1" indicates omission of per-rotatory segment, a "2" indicates omission of a post-rotatory segment, dashes indicate runs not performed or calibrations.

5.3 Individual Model Fitting

Two of the three models discussed in section 2.6, the simple exponential and the three parameter model, were fitted to the data separately for each subjects per and post-rotatory runs. The first model that was fitted to the individual run data was the simple exponential model. The optimal model parameters K_1 and T , for each run for each subject were calculated. The three parameter model was fit to the individual run data. The optimal model parameters K , h_0 , and g_0 for each run and each subject were calculated. The calculated model parameters for both models are tabulated in appendix A by subject and by per or post rotatory segment for all runs that were individually analyzed. Subject B's

responses are shown in tables A.2.1 and A.2.2, subject C's responses are shown in tables A.3.1 and A.3.2, and subject D's model responses are shown in tables A.4.1 and A.4.2.

5.3.1 Assessment of Model Gain Results

It is noticeable that the average first order exponential model fit gains of all three subjects are higher than the expected values. All three subjects showed mean preflight gains of between 0.65 and 0.9, while 0.6 is considered to be approximately the norm for humans with "stare straight ahead" instructions. Several methods were used to test for why this occurred. First, calibration factors were recomputed on a random sample of 8 calibration runs across subjects B, C, and D to test for faulty calibration calculations. The average difference between the old and new calculated calibration factors was found to be 1.2%, which is too small to account for the differences observed. A second possible source of error was the calibration target set-up. If the measurement of eye to target distance was wrong, (e.g. if measurements had been improperly made from the headrest instead of the eye), calibration factors would be affected. Lab notebooks from the experimenters do not show any evidence of such a mistake. A third possible source of this discrepancy is in the run rejection criterion, in particular rule number 4, rejecting runs with less than 25 degrees per second peak SPV. This could lead to elimination of runs with lower gains and thus bias the average of the remainder upward. This rule alone was only used in $7/69$ rejected run segments, however an additional $7/69$ run segments had peak SPV below 25 degrees per second, and violated another rule as well. The remainder of the rejected runs did not show a lower mean when preflight and post flight rejected runs were averaged together. However, the average gain of only the preflight rejected runs, had average gain of 0.54.

An other source of increased gain relative to Kulbaski, 1988, is the method of model computation. Kulbaski chose to do a log-linear fit to the data to obtain the gains and time

constants. For this thesis, the model was fit to the first order exponential without first taking the log. Log-linear fits were computed herein during the outlier removal algorithm. Approximately twenty cases per subject were examined for differences between the gains found by this log-linear fit and the first order exponential model. Cases examined included per and post rotatory runs in both directions, but did not include dumping runs. This study found that the first order exponential gain for subject B was an average of 0.115 higher than for the log-linear gain. Similarly subjects C and D had simple exponential gains that were 0.074 and 0.100 higher than their log-linear gains respectively. The reasons for this seems to be that the 1OE model overestimates the SPV in the first two to four seconds of a run, and the log-linear fit weights the later SPV points more than the 1OE model. Since the model fit routine did not fit the first two seconds of data, the extension of the model fit over this region quite often predicted higher and sharper initial peaks in the data. This did not seem to affect the three parameter model fits, because the velocity storage terms allowed the model to fit a more rounded initial peak to the data.

Finally, the outlier removal process could also have contributed to increasing the gain. Any dropouts occurring early in the data would tend to force the model fit to pick a lower gain because dropouts are regions of low SPV. Removal of dropouts by the outlier detection algorithm, *stat_prep2*, would give higher estimates for the gain fitted to the remainder of the data.

This combination of effects from the rejected runs, and model fitting procedure, could conceivably account for the observed upward bias in the gain in the preflight runs.

5.3.2 Three Parameter Model Directional Asymmetry Analysis

Directional asymmetries were noted in several D-1 and SLS-1 subjects (Oman and Weigl, 1989, Balkwill, 1992) therefore following initial model fits to the individual runs, the model parameters of the three parameter model were examined to determine if any significant directional asymmetry existed. Per rotatory responses in each direction were compared to each other, as were post rotatory head up responses. Dumping responses were not analyzed as the dumping occurred only for the t=5 to t=10 seconds after chair stop, preventing fitting of a model over the whole post-rotatory section. The small time duration of the dumping pitch head movement precluded individual analysis of dumping model parameters. Results of directional asymmetry are noted in table 5.2. The model parameters were compared using the students t test with the assumption of unequal variances for each direction. The only potential directional asymmetry found was for subject C, for whom there were two model parameters out of the set of six, that showed a probability of $p < .05$ for directional asymmetry. The per-rotatory g_0 and post-rotatory h_0 were found to be significantly different. However, the other four parameters, including post-rotatory g_0 and per-rotatory h_0 , were not found to be statistically significantly asymmetrical. For any random distribution of 18 parameters such as these, we would expect one of them to be significant simply due to random effects. It therefore seemed unlikely that a significant directional asymmetry existed in these subjects.

Subject	Section	N_{ccw}	N_{cw}	prob(K)	prob(g_0)	prob(h_0)
B	per	7	6	.329	.757	.711
	post	4	3	.991	.403	.466
C	per	10	8	.128	.622	.001
	post	7	5	.775	.025	.757
D	per	4	4	.800	.859	.126
	post	6	6	.854	.133	.177

Table 5.2, Summary of directional asymmetry t-test results on three parameter individual model fit parameters.

In his analysis, Kulbaski tested for differences in the directional responses of these subjects using a χ^2 test on direction for both the preflight head up and dumping runs. He

also found that there was no significant directional asymmetries in this subject population.

5.3.3 Normalization of Data

In order to remove any possible variation due to differences between subjects, between per and post rotatory sections, and any (undetected) directional asymmetries, each subjects model fit parameters were normalized. In each case, the normalization was done with respect to the mean of all per or post rotatory preflight parameters for a particular subject and particular stimulus direction. This implied that the effects of space flight would have a similar effect on subjects responses (model parameters) regardless of run segment or direction. This allowed the data sets to be combined for analysis, reducing several small data sets into fewer larger data sets that would improve the ability to differentiate changes in the model parameters. A similar approach was recently used by Oman and Calkins (1993) in analyzing the IML-1 MVI data. The preflight clockwise and counter clockwise mean values used in the normalization are shown at the bottom of tables A.2.1 through A.4.2 in appendix A.

A side effect of this normalization process is that it sets the preflight baselines all to a value of 1.0. Differences between preflight and post flight then become the difference between the post flight normalized means and 1.0.

5.3.4 Comparison of Preflight and Post flight Responses

For comparison between preflight and post flight responses, the data was divided into two categories, preflight (F-90 to F-10), and return (R+1, R+2, and R+4). (Analysis of data was also repeated after separating R+4 into a separate category denoted recover. This was to check whether subjects had begun to re-adapt to the 1-G environment, moderating the changes relative to preflight by test day R+4. This had the trade off of

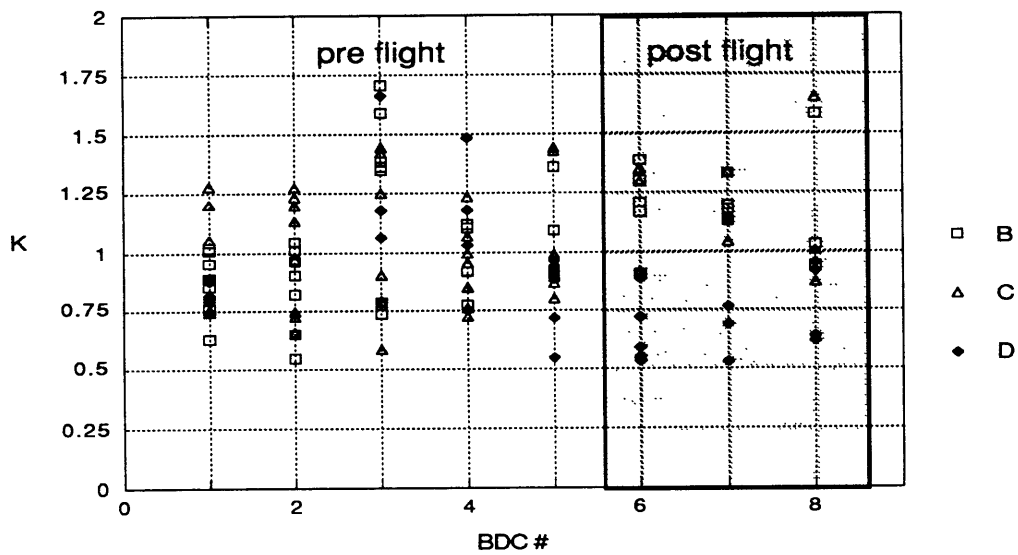


Figure 5.1a, Normalized Three Parameter Model gain, K , for all subjects, both CW and CCW, per and post rotatory.

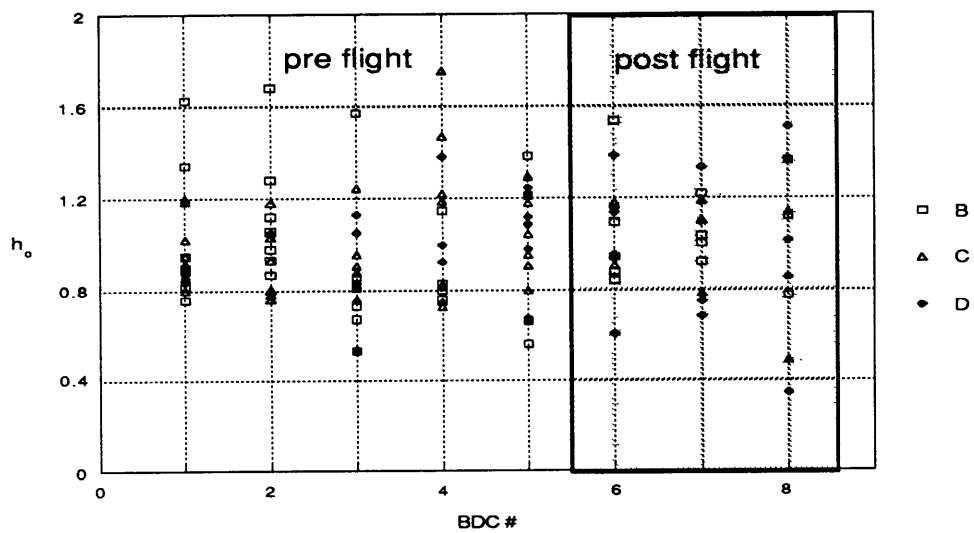


Figure 5.1b, Normalized Three Parameter Model h_0 , for all subjects, both CW and CCW, per and post rotatory.

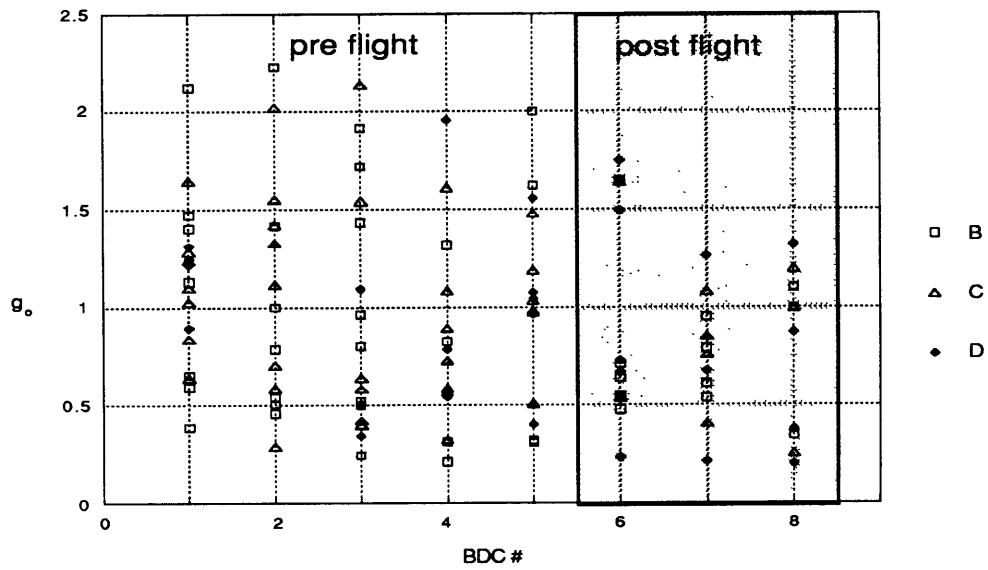


Figure 5.1c, Normalized Three Parameter Model g_0 , for all subjects, both CW and CCW, per and post rotatory.

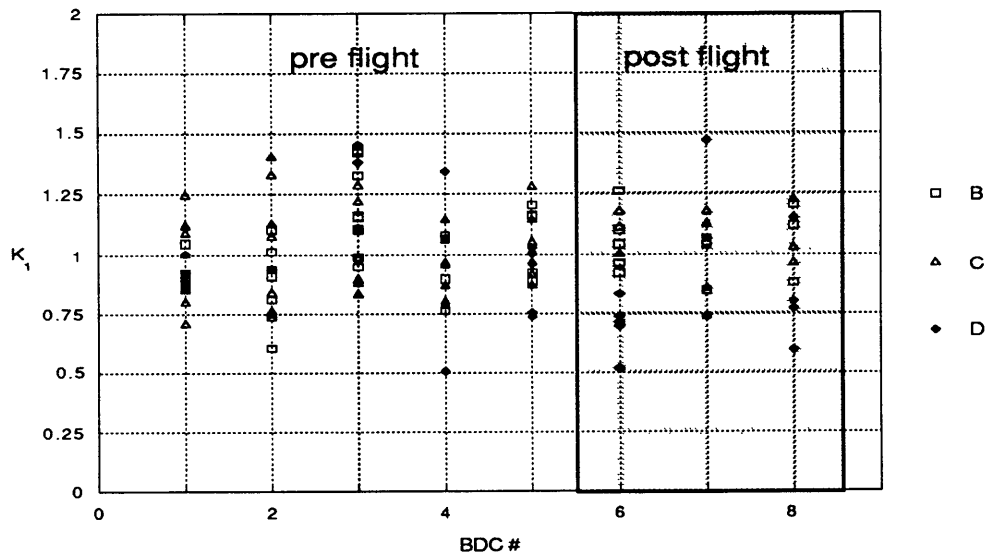


Figure 5.2a, Normalized first order model gain, K , for all subjects, both directions, per and post rotatory.

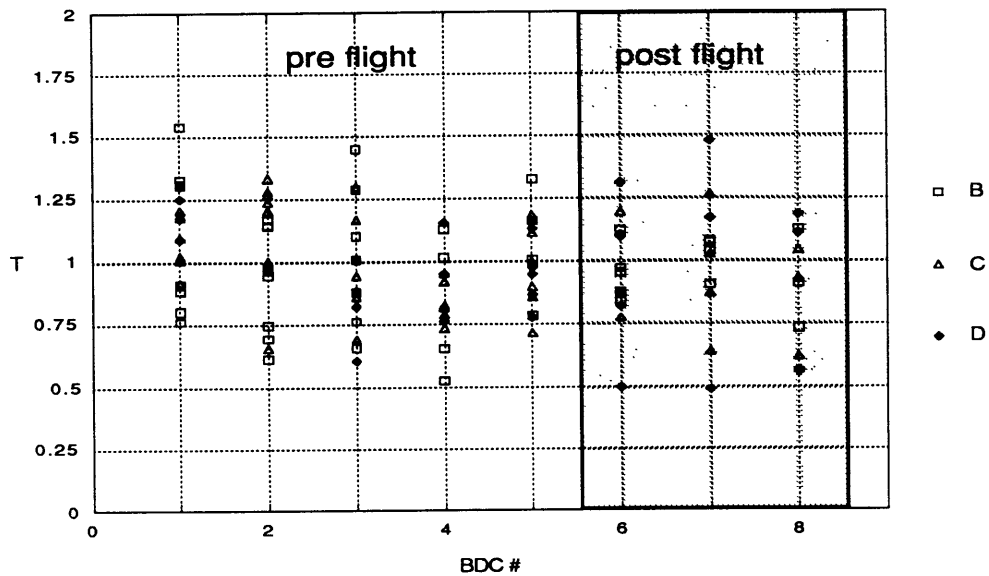


Figure 5.2b, Normalized first order model time constant, T, for all subjects, both directions, per and post rotatory.

reducing the sample size of the return portion, and having a small sample size in the recovery portion. As a result, no additional factors showed as significant, and therefore only the two gravity level (preflight and return) analysis was presented here.) Plots of three parameter model parameters for all subjects in both CW and CCW directions of both per and post-rotatory normalized data are shown in figures 5.1a through 5.1c.

Individual three parameter model fits did not show any clear trends for the changes in model parameters post flight. The mean gains of the three parameter model fits increased for subjects B and C, but decreased for subject D. The leak rate time constant of velocity storage, h_0 , showed little change in any subject. The trend in indirect pathway gain, g_0 , was towards a decrease in all three subjects, but this parameter had the most variation of the three parameters. Also, there was a trend to reduced spread in the model parameters

post flight in h_0 and g_0 . Three parameter model mean parameters, and variance, for all subjects are shown in table 5.3.

For the first order exponential model gain, there was no distinct trend across the three subjects. Subjects B and C each showed slight post flight increases in gain, while subject D showed a decreased gain post-flight. Due to the small number of samples, none of the changes had statistical significance. The first order exponential time constant showed a consistent trend among the three subjects. In each subject, the first order exponential time constants were seen to decrease post-flight. None of the subjects showed evidence of recovery by day R+4. Table 5.4 is also included to show the variances and means for the fits to the first order model for all three subjects.

In order to compare the post flight response to the preflight baselines, two tests were applied to the normalized data; the students t test with unequal variances (Microsoft Excel, version 4.0), and fully factorial multiple ANOVA (Systat, version 5.2). For the students t test, the return portion was compared to the preflight baseline, and the two-tail t test was used because subject D exhibited changes in model parameters in different directions from subjects B and C. The ANOVA was performed separately on each subject for the same reason, using direction of rotation, and preflight versus post flight as factors (2x2 ANOVAs on each subject). T-test results for both models are shown in table 5.5.

Examining tables 5.3, 5.4 and 5.5 shows that there is a diversity in the three subjects responses to micro gravity. Subjects B and C showed similar responses, while subject D showed changes in model parameters in the opposite directions. In particular, while subject B showed a significant increase in three parameter model gain post flight, and

Subject			K	ho	go	# samples
B	Pre Flight	mean	1	1	1	30
		variance	0.079	0.096	0.390	
	Return	mean	1.203	1.112	0.797	12
		variance	0.035	0.078	0.139	
C	Pre Flight	mean	1	1	1	35
		variance	0.062	0.059	0.227	
	Return	mean	1.175	1.021	0.826	10
		variance	0.056	0.062	0.173	
D	Pre Flight	mean	1	1	1	16
		variance	0.076	0.035	0.83	
	Return	mean	0.699	0.975	0.817	12
		variance	0.076	0.121	0.281	

Table 5.3, All subjects three parameter model mean normalized model parameters for all subjects, CW and CCW for both per and post-rotatory segments.

Subject			K	T	# samples
B	Pre Flight	mean	1	1	25
		variance	0.037	0.072	
	Return	mean	1.045	0.977	9
		variance	0.016	0.016	
C	Pre Flight	mean	1	1	35
		variance	0.033	0.035	
	Return	mean	1.084	0.927	10
		variance	0.013	0.046	
D	Pre Flight	mean	1	1	15
		variance	0.060	0.038	
	Return	mean	0.813	0.950	12
		variance	0.066	0.120	

Table 5.4, All subjects first order model mean normalized model parameters for all subjects, CW and CCW for both per and post-rotatory segments.

subject C showed an trend to increase in gain, subject D showed a significant *decrease* in gain. None of the subjects showed any significant change in the leak rate time constant, h_0 . The indirect pathway gain, g_0 , showed no significant change, but had a decreasing trend for B, C, and D. The lack of significance may be due to the high variability in this parameter. First order exponential model gain showed an increasing trend for B and C and decreased for D, where subjects C and D were both significant at the $p < 0.10$ level. The apparent time constant had a decreasing trend for all three without significance.

The 2x2 ANOVA results showed significance in the preflight versus post flight factor for the three parameter model gains as well for subject B ($F = 5.76$, $df = 1, 38$, $p = .021$), subject C ($F = 4.24$, $df = 1, 41$, $p = .046$) and subject D ($F = 5.52$, $df = 1, 22$, $p = .011$). However, the first order model fit gains, which were almost significant ($p < 0.10$) for the t-tests for subjects B and C did not register flight condition as a significant factor. The 3P and 1OE ANOVAs also suggested the possibility of a directional asymmetry in subject C, however the small sample size of post flight cw responses precluded any significance.

Subject		3P Model			1OE Model	
		K	h_0	g_0	K	T
B	return	0.010	0.266	0.203	0.377	0.711
C	return	0.061	0.808	0.276	0.092	0.350
D	return	0.001	0.827	0.338	0.064	0.662

Table 5.5, All subjects two tailed t-test probabilities assuming unequal variances for all model parameters. Statistically significant results are presented in bold text.

5.3.5 Evaluation of s^k Model

Since the s^k model has not been applied to human horizontal angular VOR response data previously, this model was studied and compared with existing models in order to assess

the relative strengths and weaknesses of each in their ability to describe the data. Each of the models possesses a physiological or mathematical basis which suggests that it is capable of modeling the VOR, however, the s^k model will only be compared to the three parameter model. Justification for this choice stems from the fact that this model is the closest mathematically to the s^k model. The significant difference between them lies in the replacement of the adaptation time constant with the s^k operator.

5.3.5.1 Comparison of s^k and Three Parameter Models

Mathematically, the two models are identical with the exception of the adaptation time constant of the three parameter model being replaced by the s^k operator in the s^k model, both of which are meant to capture adaptation. This has the effect of changing the model from a third order linear model, to a fractional order linear model through the replacement of one pole with the s^k term. This change has a bearing on the subsequent time series responses of the two models. These were studied two ways, first by fitting synthetic data generated by one model to the other model. Second, by comparing each model's fit to actual data.

5.3.5.2 Comparison Using Synthetic Data

Several comparisons between the two models were made using each model to generate data for the other model to fit. For the generation of data, model parameters were chosen that were similar to parameters of fits to real data. The fits were conducted on only a sixty second portion of data, representing either per-rotatory or post-rotatory data in order to simulate the manner in which real data was fit. One example of such synthetic fits are included in figure 5.3. For figure 5.3, the three parameter model response to a velocity pulse input was used to calculate the synthetic data. This was then fit by the s^k model using the model fitting routines described in chapter 4. The model parameters from this fit (First Fit) were then used to generate synthetic data which was in turn fit by

the three parameter model (Second Fit). Both models were run with the cupula time constants fixed at 6 seconds in order to reduce the computational intensity of the models and aid convergence by reducing the number of degrees of freedom.

From the fit of the s^k model to the three parameter model synthetic data, it can be seen that the two models are fairly close to each other, and similar in shape. The indirect pathway gain of the s^k model fit is 13% greater than that used by the three parameter

Initial Synthetic	First Fit		Second fit	
K = .7		G = .948		K = .69
Ta = 80	MSE = 3.717	k = .301	MSE = .0002	Ta = 80
Tc = 6	105 iterations	Tc = 6	78 iteration	Tc = 6
go = .120		go = .136		go = .121
1/ho = 32		1/ho = 22.1		1/ho = 31.74

Table 5.6, Synthetic data generation parameters and model fit parameters from figure 5.1.

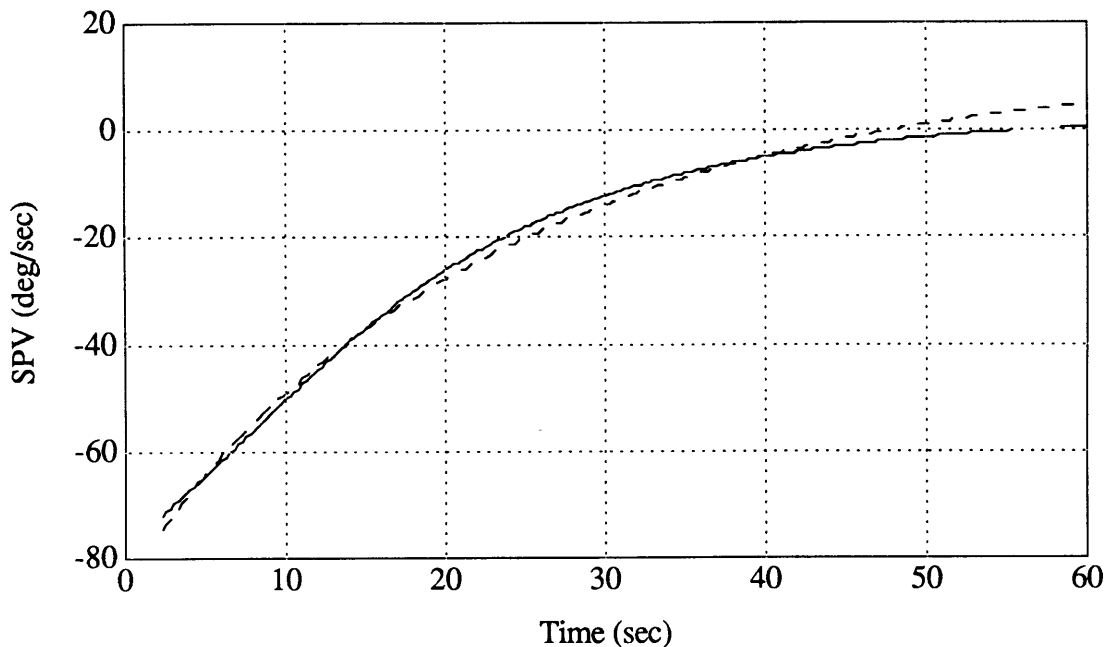


Figure 5.3, Comparison of s^k and three parameter models. Dashed line is three parameter model synthetic data, solid line is s^k fit.

model used to generate the data, while the leak rate time constants, h_0 , differ by 32%. In both cases, the model fits are equally physiologically reasonable to the values used to generate the data. The gain terms, K and G cannot be easily compared. This is because the gamma function gain changes with the time constant that it is being convolved with, and with k . Therefore, while the transfer function associated with K has unity gain, that associated with G does not, and therefore they cannot be directly compared.

5.3.5.3 Fitting Both Models to Real Data

As a second method to compare the models, each model was fit to several sets of individual run data. The results of each model fit to one such post-rotatory head erect run are shown in figure 5.4. Model fit parameters for both models for this run are tabulated in table 5.7.

From figure 5.4, there is little difference to be seen between the two models. The indirect pathway gains found by each model differ by 4% while the h_0 was found to differ by 14% between the two models. Again it should be noted that both models converged on physiologically reasonable solutions. Additional insight may be gained through analysis of the residuals between the two models, and between each model and the data. These are presented in figure 5.5.

Model	MSE	# iter.					
s^k	20.41	134	$G = 1.262$	$T_1 = 6$	$k = .287$	$g_0 = .138$	$1/h_0 = 23.04$
three par.	15.70	80	$K = .818$	$T_c = 6$	$T_a = 80$	$g_0 = .143$	$1/h_0 = 20.15$

Table 5.7, Model fit parameters for s^k and three parameter models to C203 post rotatory data.

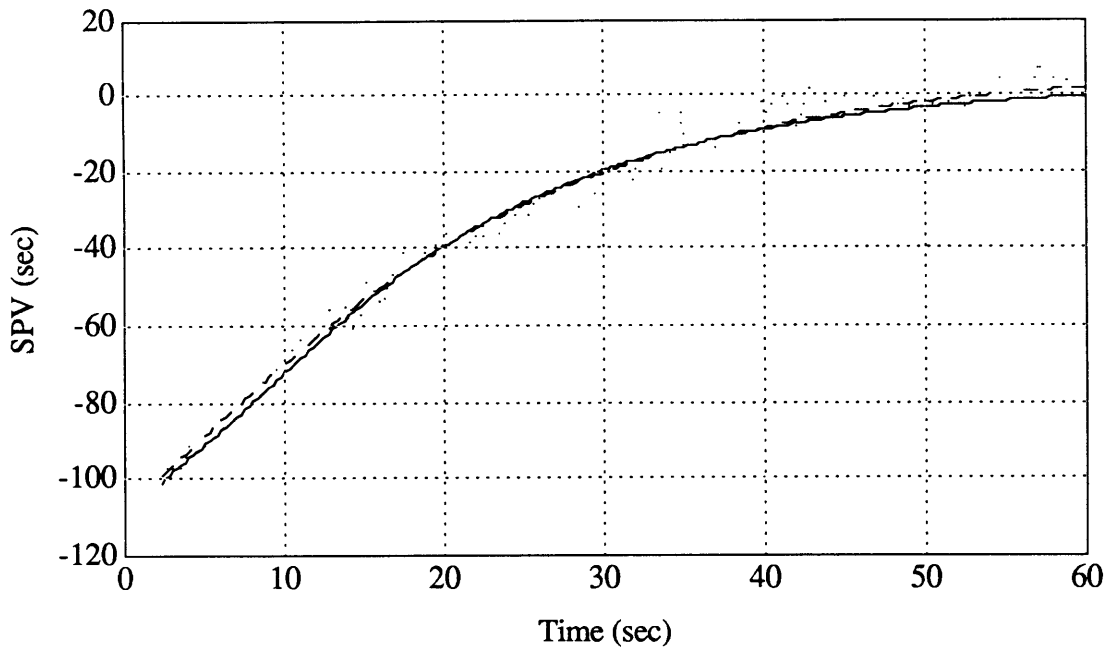


Figure 5.4, s^k (dashed line) and three parameter (solid line) model fits to the C203 post rotatory data (dotted line).

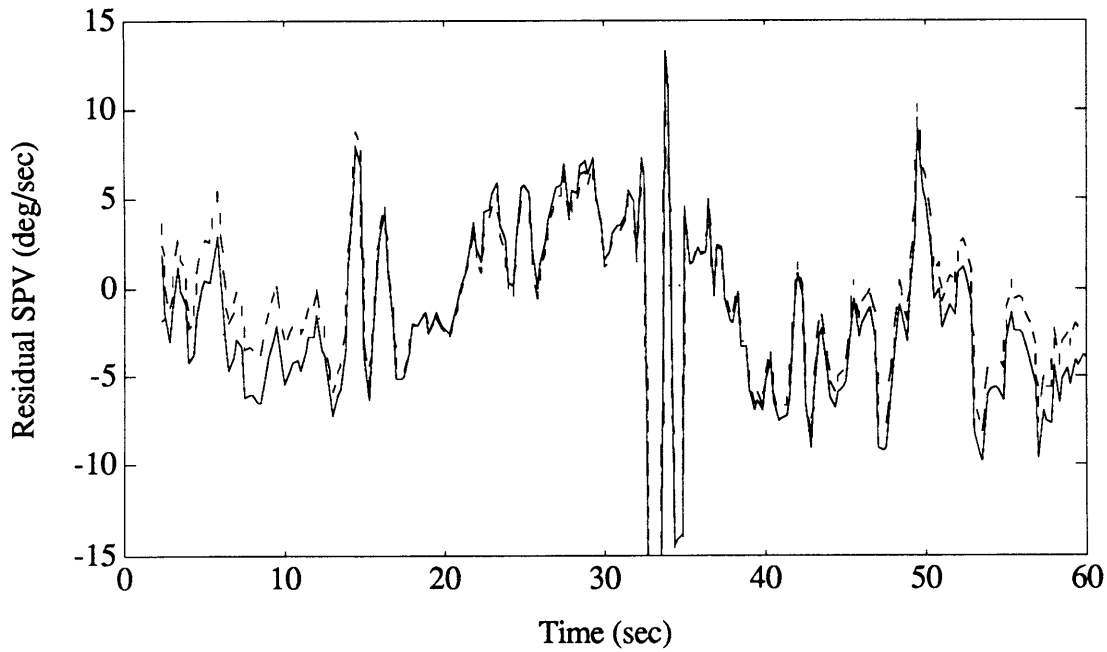


Figure 5.5, Residuals of C203 post-rotatory model fits between s^k model and data (dashed line), between three parameter model and data (solid line) and between models (dotted line).

The residuals pictured in figure 5.5 are fairly characteristic of the pattern for these models run on good (low noise) data. From this figure it can be seen, that while neither model fits the curve perfectly, the residuals of the data around each model fit are comparable in magnitude. In particular, it is impossible to differentiate between the two models as to which is a better fit to the data given that the noise (residual) between the data and either curve is greater than the difference between the two models.

The s^k model was run on 67 individual run segments including all three subjects preflight and post flight, per and post rotatory, to examine the quality of the fits over many runs. The results of these fits are included in Appendix A as tables A6 through A8. Throughout this data set, the quality of the runs was measured visually by the operator, and by the MSE of the model fits. In 56% of the test cases, the s^k model had a higher MSE, while it was lower in the remaining 46%. Comparison of the MSE using a paired-t test showed no significant difference between the errors in the two models. However, there were several cases of the s^k model choosing a fit that was at the limit of one or more of the constraints, or failing to converge on a solution. This happened for 4 of 67 test segments (either per or post-rotatory). Over the same data set, the three parameter model never failed. While fits at model constraints did not seem to affect the quality of the s^k fits, it would make the analysis much more difficult, as the s^k model had chosen a parameter at the constraint, or beyond, if the constraints are relaxed, that are either physiologically unreasonable, or may represent other parameters that have not yet been correctly identified. This was likely due to the extra degree of freedom in this model (C, k, g_0, h_0) versus the three parameter model (K, g_0, h_0).

The s^k model may require a longer data set in order to achieve good, unconstrained model fits. The s^k term is used to replace the adaptation time constant in the three parameter

model, which is believed to be quite long, on the order of 80 seconds. The three parameter model has proven in the past to be unable to fit this long time constant with only sixty second windows of data (Balkwill, 1992), and thus for this rotation protocol the adaptation time constant was fixed at 80 seconds for analysis to aid model convergence. This additional degree of freedom in the s^k model slows convergence, and adds an additional sink for the variance in the data. Reducing the degrees of freedom in the s^k model would aid convergence, but in order to fix the adaptation term, k , a reasonable value would be needed. Lack of previous experience with the model precludes this constraint. A possible improvement may be gained through fitting to the entire 120 seconds of per and post-rotatory response at once, rather than fitting the halves separately. This would provide increased data to aid in the fit of the adaptation operator. Due to the small number of individual runs with both per and post-rotatory responses of sufficient quality for individual model fitting, this was not attempted.

A brief statistical analysis of the s^k model fits was conducted on a subset of data from subjects B and D. None of the four s^k model variables showed any significant changes post flight versus preflight when tested using the student's t test for unequal variance. This was possibly due to having too many degrees of freedom, or data samples that were too short. On the basis of this result it was felt justified not to fit the remainder of the data set to this model. Also, based on this analysis of the s^k data with four degrees of freedom, it was not possible to confirm the changes seen by Correia (increasing G and k) in his s^k canal afferent model, with this corresponding s^k VOR model.

5.3.6 Miscellaneous

It was felt to be possible, that over the course of a single BDC session, the subjects may exhibit adaptation as a result of experiencing the four or more vestibular stimuli. To minimize this, stimulus directions were alternated during testing. To examine whether

any adaptation had in fact taken place, the parameters from the individual run's simple exponential model fits were examined for trends from the first stimulus to the last stimulus on any given day by plotting the parameters along the order of runs, and watching for trends. Examination of all three subjects showed no distinct trends in any of the parameters throughout the course of the BDCs.

The residuals of the individual runs around the three parameter model fit were studied for the appearance of trends that might signify unmodeled dynamics. No trends in the residuals found along time in the runs, and in every case, the mean of the residual was less than one standard deviation away from zero. The frequency content of the residuals was concentrated in the region from 0.25 to 1.0 Hz. This was to be expected as the 4 Hz sampling rate (following decimation) would eliminate noise above 2 Hz, and the OS filtering effectively smoothed the data above 1 rad/sec.

An alternate method for dealing with the slow chair acceleration to full speed due to manual control of the chair command was implemented. The three parameter model was fit to all per-rotatory runs using the tachometer signal decimated to 4 Hz. This model fit was performed on all per-rotatory preflight run segments from two seconds before chair start up to chair stop, including the acceleration portion of the chair motion that was not fit using the normal approach. The parameters calculated by these model fits were compared to the normal method parameters using a paired-t test (Excel 4.0). None of the model parameters for any subject were found to be significantly different at the $p < 0.05$ level.

5.4 Analysis of Dumping Runs

The parameters from the dumping runs simple exponential log-linear fits are included in tables A5a through A5c in appendix A. For this analysis, a fit was considered to be bad,

if the log-linear slope was found to be positive. This is because for all SPV curves after chair stop, the SPV should decay, while a positive slope indicates that SPV is growing. In general, the log-linear fit did not give consistent results for the time region before the dump. This is likely due to the existence of residuals from the chair stop as well as having

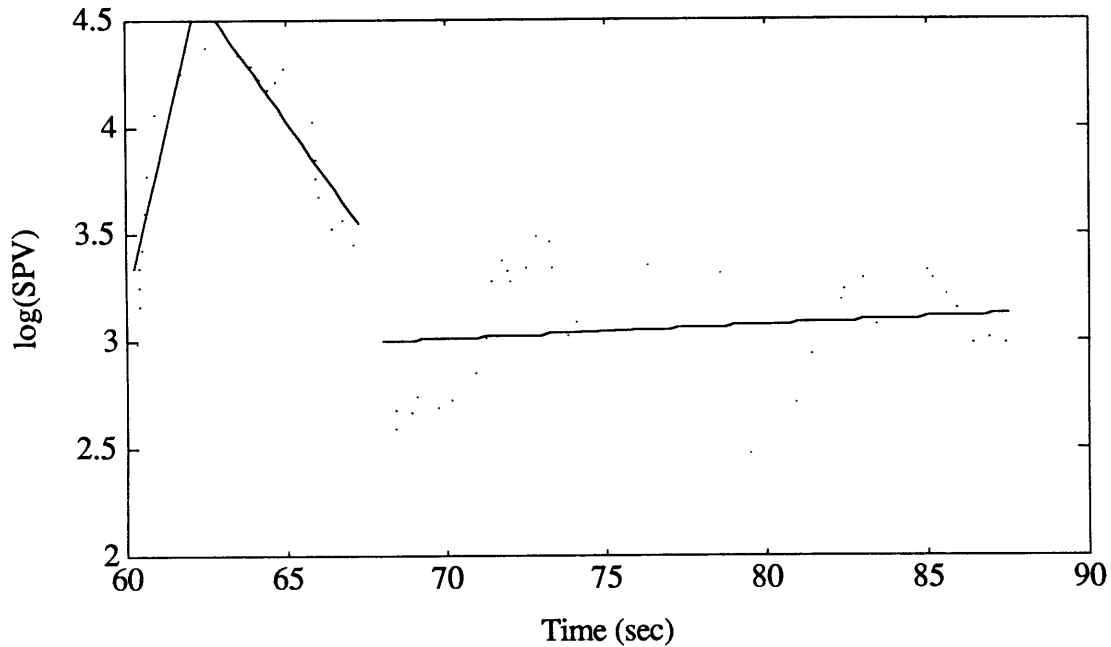


Figure 5.6, C304 log-linear fits to before dumping region, dumping region, and after dumping regions (first, second and third straight line segments from left, respectively).

little data on which to base the fits. An example of a badly fit dumping run is shown in figure 5.6. An example of a dumping run which was well fit by the model is shown in figure 5.7.

In figure 5.6, the characteristic problem of increasing SPV before the dump is initiated is shown. This occurred in 28 out of 34 tested cases. In figure 5.6, a positive slope on the after dumping region is also shown. This occurred in 2 out of 34 cases. Occurrences of positive slope in the dumping region was in 1 out of 34 cases. This case was not processed further. Figure 5.7 shows a run typical of the responses for the dumping and after dumping regions for the fits that were retained. For a single run, C506, the subject

neglected to push the button to indicate that the dumping head movement was performed. For this subject, the time of head down was assumed to occur at the nominal point of 5 seconds following chair stop.

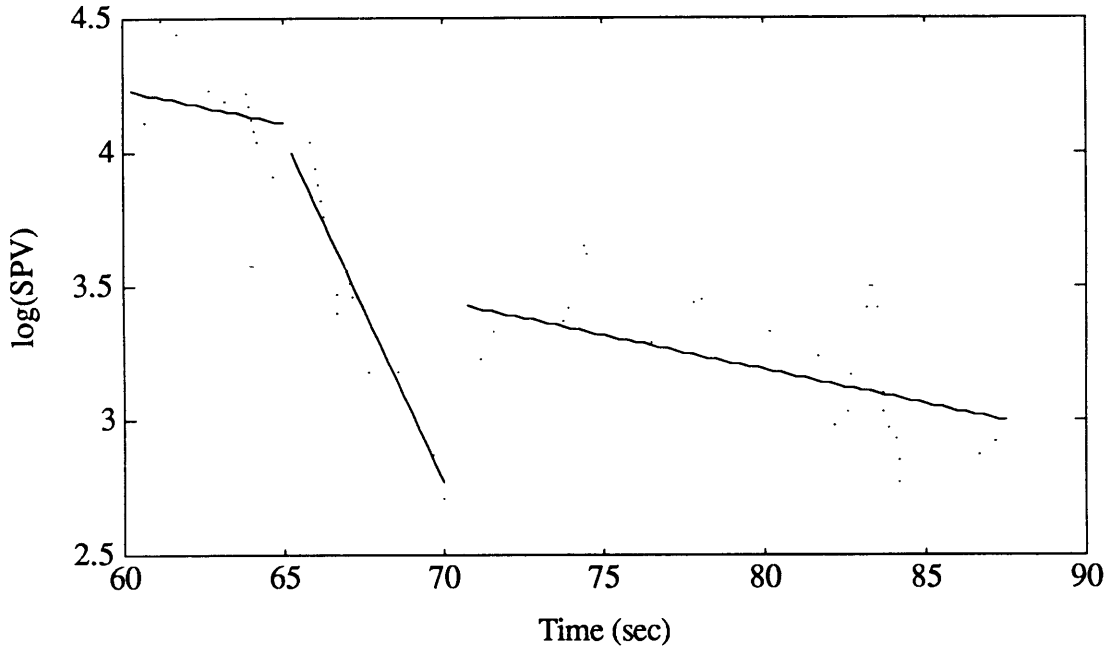


Figure 5.7, C205 log-linear fits to pre-dumping region, dumping region, and post-dumping regions (first, second and third straight line segments from left, respectively).

The pre flight and post flight mean dumping model slopes for subjects B, C, and D are shown in figures 5.8a through 5.8c respectively.

From the three figures, it can be seen that for all three subjects after dumping, and for subject C before dumping, that the slopes of the log(SPv) decreases following exposure to micro gravity. This is equivalent to a shortening of the time constant over these regions where dumping has not occurred.

On the dumping portion of the runs, subject B's slope decreases following exposure to micro gravity, while subjects C and D show increases in the slope corresponding to a

lengthening of the dumping time constants. There is a distinct trend present for dumping and non-dumping time constants to approach each other post flight. To test this the preflight versus post flight changes were tested for significance using the students-t test

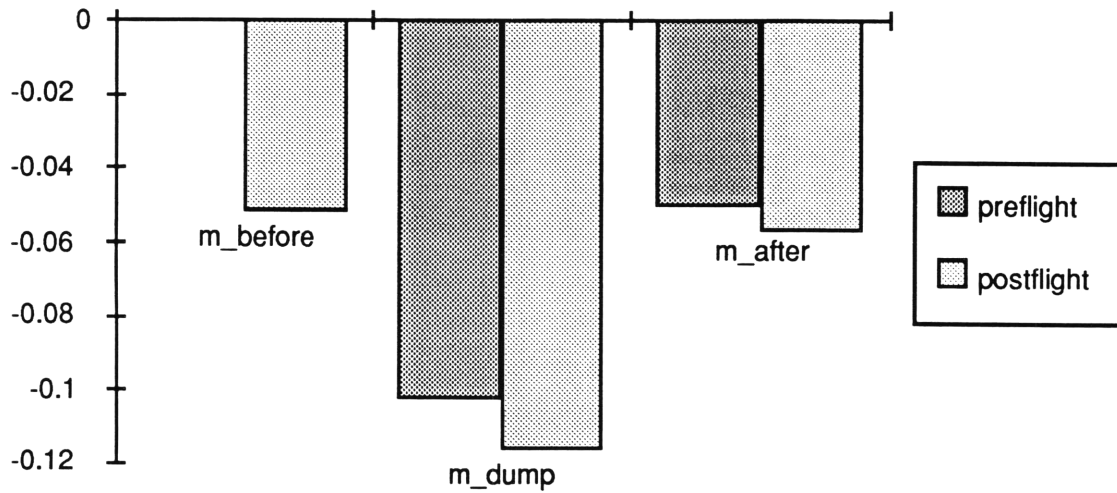


Figure 5.8a, Subject B, mean dumping model slopes.

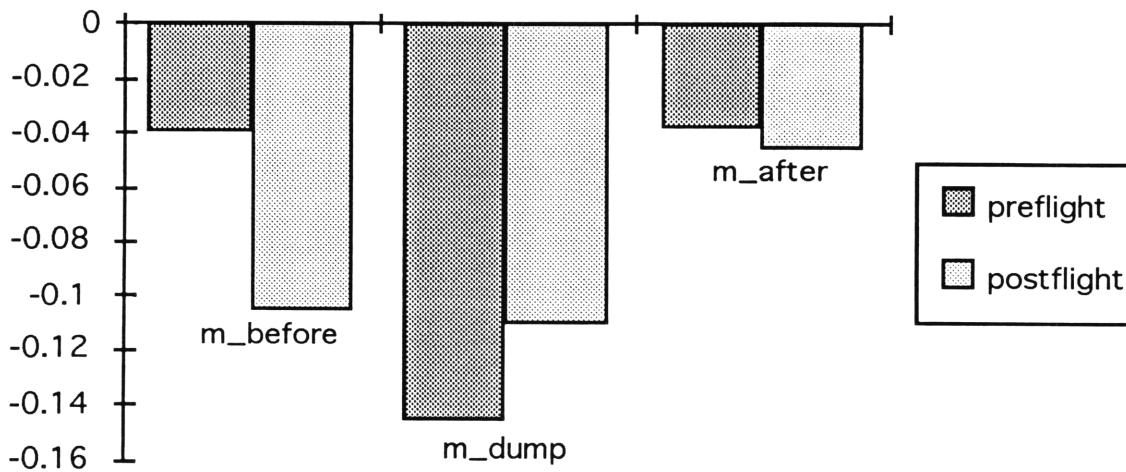


Figure 5.8b, Subject C, mean dumping model slopes.

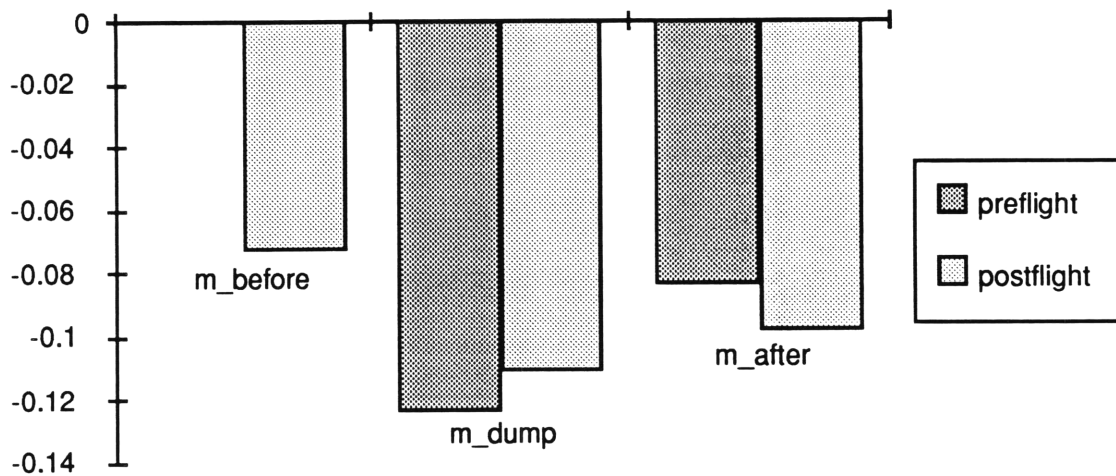


Figure 5.8c, Subject D, mean dumping model slopes.

assuming unequal variance. Due to the small numbers of runs, only subject's B and C could be tested for preflight versus post flight changes in dumping and after dumping slopes. While both B and C showed a decrease in the dumping slope post flight, B was not significant, while C was significant at the $p < 0.025$ level.

In order to provide a larger sample size to test for significance, the slopes were normalized with respect to preflight mean values in each direction, and the normalized values for all three subjects were grouped together. Analyzed this way, the grouped data showed no significant changes preflight versus return or recovery. The dumping slope showed no change, while the after dumping slope increased (time constant decreased) on return, but not with significance.

The dumping runs were not ensemble averaged and then fit with the model as was done with the per-rotatory and head-erect runs. This was a result of the dumping head movement occurring at different points in time for each run. This caused a time shift in the between runs data. Removing the time shift would introduce a magnitude shift, since

the magnitude was time dependent. This made it too difficult to average the dumping runs together, and thus, the data was only fit individually.

5.5 Analysis of Ensemble Averaged Responses

The SPV data was ensemble averaged, as described in section 4.10, and model parameters were fit to the ensemble averaged responses. The ensemble averaging process makes several assumptions about the nature of the VOR: First, that the VOR dynamics are stationary and therefore there is no variation in model parameters. Second, that the measured response contains additive zero mean noise. Third, that all dropouts and other non-zero mean artifacts have been successfully removed. Finally, if averaging across directions, that no directional asymmetries exist. If any of these assumptions were violated, the average of the individual run model fits will not be equal to the ensemble average model fits.

Some additional runs were included in the ensemble averages that could not be fit as individual runs. These consisted primarily of either runs that showed the characteristic SPV decay profile but were too noisy to fit as individual runs, and runs that were fit as individual runs, but had fits that reached one or more of the model constraints. The additional run segments included in the ensemble averages were;

Post-Rotatory:	B203	C102	D105
	B211	C606	D106
			D405
			D406

Model fits were performed separately on the per and post rotatory sections, and separately on the pre and post flight sections. The ensemble averaged pre-flight and post-flight head up PRN curves are shown in figures 5.9 through 5.11. Due to having too few good runs (2 for subject B, 1 for subject C, 0 for subject D), there was no post-flight per-

rotatory ensemble averages, therefore preflight per-rotatory runs will not be presented either.

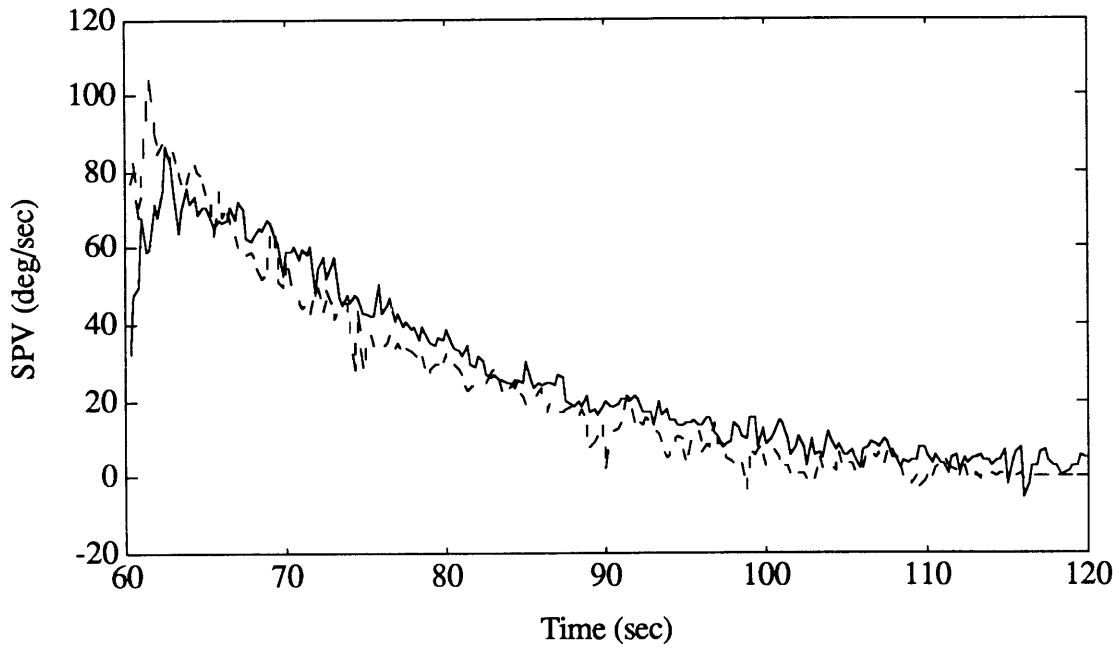


Figure 5.9, subject B ensemble averaged PRN response preflight (solid) versus post flight (dashed).

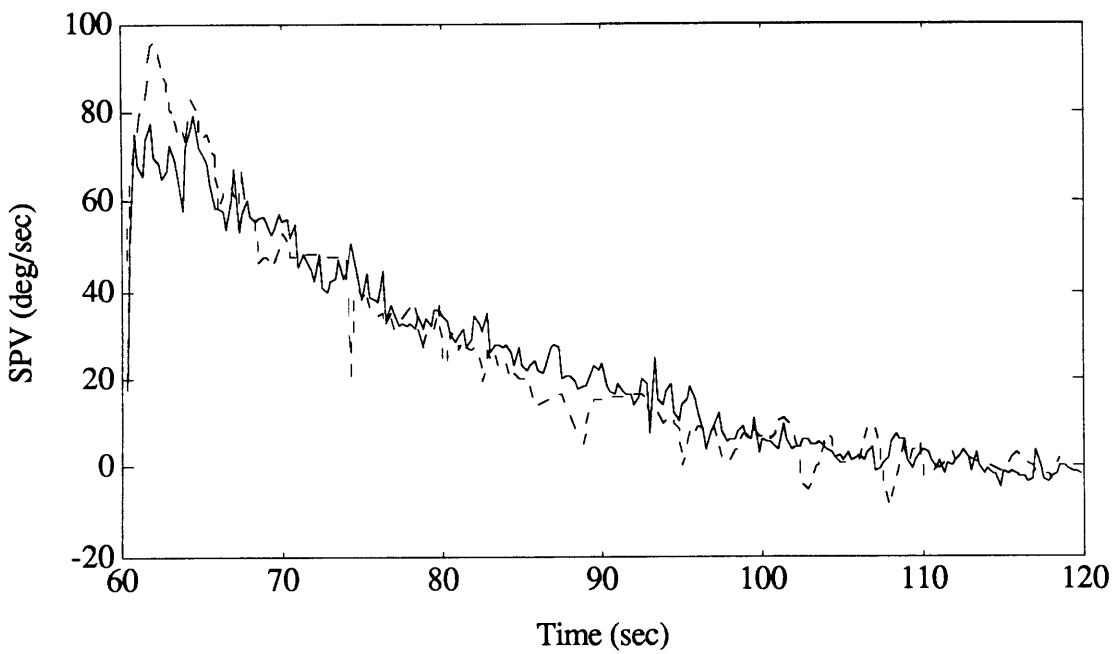


Figure 5.10, subject C ensemble averaged PRN response preflight (solid) versus post flight (dashed).

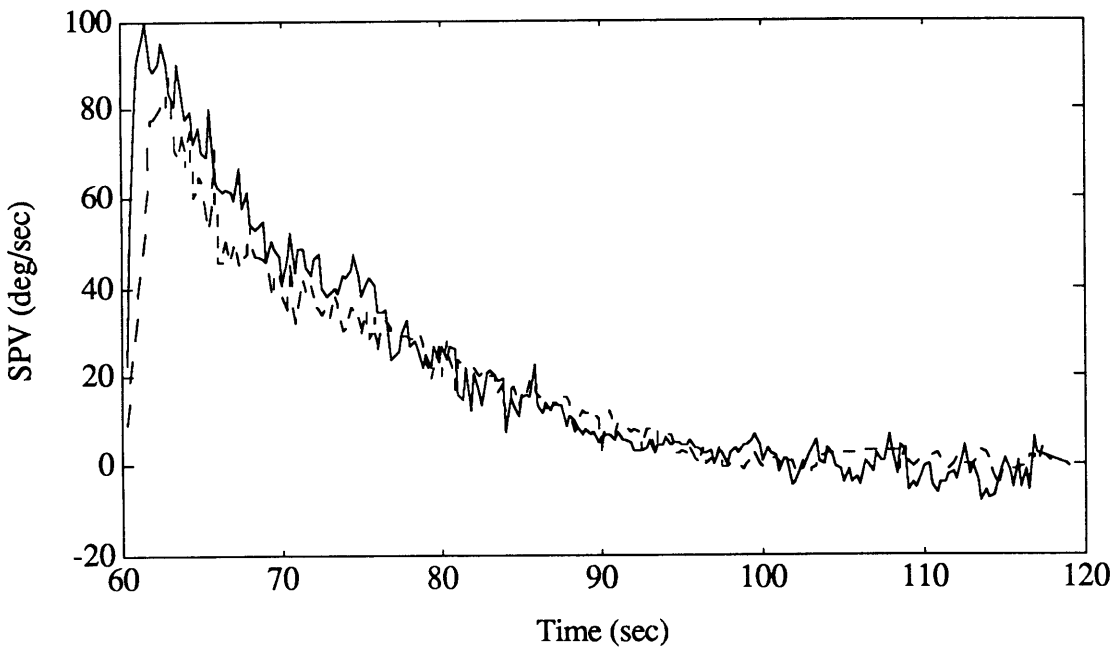


Figure 5.11, subject D ensemble averaged PRN response preflight (solid) versus post flight (dashed).

In figures 5.9 through 5.11, the increase in the post flight peak SPV can be easily seen for subjects B and C. For both these subjects, and for subject D as well, the region from $t=60$ to $t=65$ seconds is visibly different post flight. This consistent with the individual run analysis finding that gain may have increased post flight for subjects B and C.

Comparison of the ensemble averaged runs with Kulbaski's curves by subject, was carried out visually. In subject B, the increase in post flight peak SPV response seen here in figure 5.9 was not evident in Kulbaski's figure. The post flight peak SPV increase in subject C and decrease in subject D were visible however. More detailed visual analysis was not possible, as Kulbaski did not plot the preflight and post flight head up curves together. Visual comparison of Balkwill, 1992, ensemble averaged per rotatory and head up post rotatory curves showed evidence of higher peak SPV post flight in 5 cases. Seven cases showed little or no change in the peak SPV post flight, while 4 cases showed decreases post flight peak SPV.

The three parameter model was fit to the ensemble averaged data for each subject, and the results are presented in table 5.8. As with the individual run model fits, in the changes in the ensemble model fit parameters, subjects B and C are qualitatively similar, while subject D is qualitatively different. Post flight three parameter model gains increased for both subjects B and C by 29% and 35% respectively, while it decreased for subject D by 16%. The parameter h_0 showed a 9% increase in subject B, no change in subject C and a 15% decrease in subject D.

			3P Model		1OE	Model
Subject	pre/post flight	K	$1/h_0$	g_0	K	T
B	pre	0.615	0.042	0.152	0.877	17.57
	post	0.795	0.046	0.094	0.902	14.28
C	pre	0.566	0.046	0.155	0.781	16.59
	post	0.765	0.046	0.097	0.953	13.37
D	pre	0.760	0.064	0.107	0.957	11.34
	post	0.641	0.054	0.103	0.824	11.98

Table 5.8, Ensemble averaged model fit parameters for each subject.

Finally, the indirect pathway gain, g_0 , showed a 38% decrease in subject B, 37% decrease in subject C, and a 4% decrease in subject D.

As might be expected, the parameters of the ensemble averaged fits were not identical to the average of the parameters of the individual fits. While parameters for subjects B and C were generally close, subject D showed a greater difference. However, for all three subjects, the same trends preflight versus post flight were present.

The Σt^2 test was performed on each pair of preflight and post flight ensemble averaged SPV curves to determine if they were significantly different. The Σt^2 test was run twice on each subject. The first test was conducted on only $t = 2$ seconds to $t=20$ seconds after chair stop. This region was chosen because it was expected that chair stop transients in the first two seconds of data might affect the results, and that the greatest differences

between the curves were expected in the early to middle time range since both signals asymptotically decay to zero. The second test was run over t=2 seconds to t=60 seconds following chair stop, which was the full extent of the data, using the same method as Balkwill, 1992. Results are presented in table 5.9.

From table 5.9, it can be seen that all three subjects individually showed significantly different ensemble averaged SPV curves post flight relative to preflight. The reduced Σt^2 value of subject B ($n_1=7, n_2=5, df=231,72$) relative to C ($n_1=9, n_2=4, df=181,58$) and D ($n_1=8, n_2=6, df=204,72$) over t=62 to t=82 seconds is likely a result of subject B having a higher variance over this region.

Subject	time	Σt^2	p
B	62 - 82	96	>.100
	62 - 120	516	<.001
C	62 - 82	209	<.001
	62 - 120	863	<.001
D	62 - 82	180	<.010
	62 - 120	408	<.001

Table 5.9, Σt^2 results for pre and post flight head up ensemble averaged SPV curves.

To determine the regions of the curves which contributed the most to the Σt^2 totals, paired t tests were conducted along the length of the curves to look for individual points that were significantly different between the two curves. On this analysis, subject B showed no $p<.95$ significant points. Subject C had 11 significant points lying mostly at the beginning and end of the 58 seconds of data. Subject D had 25 significant points all lying between 15 and 30 seconds after chair stop.

As a final evaluation of the s^k model, the ensemble averaged data was fit with the s_k model. Results of the fits are presented in table 5.10.

Subject	pre/post flight	G	k	h_0	g_0
B	pre	0.832	0.248	0.039	0.141
	post	1.192	0.371	0.039	0.148
C	pre	1.183	0.363	0.040	0.153
	post	0.953	0.247	0.051	0.126
D	pre	0.814	0.146	0.075	0.099
	post	0.919	0.208	0.071	0.107

Table 5.10, s^k model fit parameters to ensemble averaged data.

For the fits presented in table 5.10, the cupula long time constant, τ_1 , was fixed at 6 seconds to speed convergence. From the results shown in table 5.10, it is hard to draw any conclusions about what model parameters have changed as a response to micro gravity. Gain, G, increases for subjects B and D, but decreases for C. Similarly, the adaptation parameter k also increases for B and D but decreases for C. The leak rate time constant $1/h_0$, doesn't change for B, decreases for C, and increases slightly for subject D. Finally, the indirect pathway gain, g_0 , which decreased for all subjects post flight with the three parameter model, increased slightly for B and D, and decreased for C. With this model, the pairing in direction of responses seen in the other two models, namely B with C, has been replaced by a pairing of B with D for three out of four parameters.

The s^k model was then run again, with the g_0 and h_0 parameters frozen to the values chosen by a model fit to the preflight data with all four parameters free (Table 5.10). This was to test Correia's Hypothesis that all post flight changes would be confined to the G and k parameters in afferent recordings. In particular, he hypothesized that the k parameter increases post flight (Correia et al, 1992). Results of this two parameter s^k model fit are shown in Table 5.11. For these 'two parameter' s^k fits, the quality of the model fits was seen to degrade as measured by the MSE of the fits. This indicated that freezing the g_0 and h_0 parameters forced a fit that confirmed the Correia hypothesis by removing the CNS parameters that could have accounted for the post flight changes.

From table 5.11, we see that all three subjects show an increase in the gain term, C. This is largest for subjects B (+28%) and C (+37%), and smallest for subject D (+8%). The adaptation parameter k, increases for subjects B (+35%) and subject C(+27%), while it decreases for subject D (-15%). Thus here we again see the split in responses that was observed with the other two models, between subjects B and C, and subject D. From Landolt and Correia, 1980, he found that the larger the value of k, the more adaptation that a unit exhibited. Similarly with this work, subjects B and C tended to show the anticipated change directions, and these subjects also had the larger values of k.

Subject	pre/post flight	G	k
B	pre	0.838	0.249
	post	1.080	0.338
C	pre	1.159	0.357
	post	1.846	0.453
D	pre	0.854	0.156
	post	0.919	0.133

Table 5.11, Two parameter s^k model fits to ensemble averaged data.

6.0 New Software and Hardware

In the process of processing and analyzing the SL-1 data, several areas for improvement over previous missions were noted. These generally fell into three categories; procedural changes, hardware changes and software changes. Procedural changes resulting from experience on the SL-1 mission were incorporated into the 1991, SLS-1 Space Lab mission, and shall not be discussed here (Balkwill, 1992). Similarly, many of the hardware changes that resulted from the SL-1 mission were also incorporated on the SLS-1 mission (Balkwill, 1992), however, since that flight several changes in the hardware have occurred. Finally, new methods have been developed in the rotating chair control and data acquisition since the SLS-1 mission that bear mention here. All of the changes noted below will be incorporated on the upcoming SLS-2 Space Lab mission.

6.1 Data Analysis Scripts

Significant amounts of new code were written in association with this thesis project, to develop them for future Space Lab missions such as the upcoming SLS-2 mission. The software was developed in two languages, Think C, and MatLab. Functionally, the software can be put into two groups; First, a series of scripts implementing new algorithms to analyze BDC data. Second, a series of scripts referred to as batch analysis, which were developed to automate and speed the BDC data analysis process to allow rapid, on-site data processing and preliminary analysis on future missions.

6.1.1 New Algorithms

There are several new MatLab scripts utilizing new algorithms for this analysis. These are presented in appendix C. These scripts are, *dec_30_new*, *decimate_mean*, *mean_model_err*, *model_err_exp*, *model_err_sk* and *t_chisq*.

dec_30_new is used to decimate the 120 Hz files down to 4 Hz, in order to reduce the number of data points that will subsequently be fit with models to a computationally reasonable number. The algorithm computed the output to be a boxcar average of the good (i.e. not marked as outliers by *stat_prep*) data points in each 1/4 second window. A first order polynomial was fit to the good points over the window, and the variance of the points was calculated about this line for each window. The variances for each window were sorted into three regions of equal numbers of points, based on the value of the variance. All points in each region were then set to be equal to the mean value of the region. This was done to remove variance outliers that would cause problems with the model fits. Weights were then calculated for each point as being the number of good contributing points divided by the modified variance estimate.

dec_mean used the weighting factors generated in *dec_30_new* to generate a weighted average of several runs that had the same stimulus and gravity conditions. The ensemble averaged run at any point in time was calculated as a simple weighted average of all contributing runs at the same point in time. Variance for this estimate was calculated as;

$$error = \sum_{j=1}^I w_j * (\bar{x}_j - \hat{x}_j)^2 * \frac{(n_i - 1)}{n_i}$$

where n is the number of runs being averaged. The $\frac{n_i}{(n_i - 1)}$ factor was included to account for the lost degree of freedom. The variance then had outliers removed using the same method as *dec_30_new* . A weight was calculated for each point in time of the averaged runs as the number of runs divided by the variance.

mean_model_err performed model fits on the ensemble averaged runs in a manner with one significant change relative to the individual run model fits. The calculation of the

error function for the individual model fits was chosen to be a simple sum of the squared differences between the data and the model at each point in time. For the mean runs, the error function was weighted, and therefore calculated according to;

$$error = \sum_{j=1}^t w_j * (\bar{x}_j - \hat{x}_j)^2$$

where \bar{x}_j = ensemble averaged data at time j

\hat{x}_j = model estimate at time j

w_j = ensemble weight at time j

This provided the statistical maximum likelihood estimate of the model to fit the data. It was chosen not to use weighted error for the individual model fits in order to maintain uniformity with earlier studies.

model_err_exp, does a model fit on individual data using the first order exponential model described in chapter 2.

model_err_sk does a model fit on individual data using the s^k velocity storage model described in chapter 2.

t_chisq did χ^2 fits to the ensemble averaged curves using the formula described in chapter 4, and did $p < .05$ students t test at each point in time along the curves.

6.1.2 Batch Analysis Scripts

The batch analysis scripts were written to bring together and automate the various analysis scripts under a single controlling script. For this purpose, the algorithms used in the existing analysis scripts were not changed, however information transfer and file handling was changed. Another goal was to increase the speed of analysis. This was done three ways. First, the number of intermediate data steps that were saved to, or read

from disk was reduced by retaining the data in memory and automatically performing the next analysis step without saving the intermediate form of the data. Second, several scripts that were computationally slow in MatLab were rewritten as MatLab external C files for faster computation. Third, some aspects of data analysis that were previously performed as stand alone C files, were rewritten as mex files to allow all analysis to be performed through the MatLab user interface.

batch_analyse was written as the top level user interface script. It prompts the user for decisions on what sort of data analysis is to be done, and calls the appropriate subroutines to perform the analysis. It is set up for performing the analysis on a single BDC session for one subject each time it is run, from data conversion through to model fitting any of the three models.

mexchair_convert completes the first step in processing, converting the data from binary to MatLab format. If the user responds positively to *batch_analyse*'s query to convert the data, *mexchair_convert* is called, given the data path, subject name and BDC #, and it converts all the files in the named folder with the correct names to MatLab format.

cal_from_file collects calibration information from previous calibrations to be applied to the current data set, while *cal_factor_gen* is used to call the NysA calibration script to perform calibrations if they haven't been done previously. *calibrate_calc* is then called by either of these routines in order to interpolate or extrapolate around the calibration runs to generate calibration factors (cal factors) for each of the runs.

multiple_AATM is used to create the batch file for AATM processing of the runs. It uses a mex file called *batch_save* to create a file of data paths, run names, and the

associated calibration factors on the hard disk. A mex file version of AATM, called *mexAATM4* is invoked. This version does AATM processing on all files named in the file generated by batch save.

CODES is used to create a matrix of data path and file name information for all of the runs, excluding calibrations.

stat_prep and *tachan* are called to perform tachometer signal analysis and statistical outlier removal and decimation on the runs. These scripts are not functionally changed from Balkwill, 1992.

model_select queries the user as to which model they would like to fit to the data. After all runs have been fit with a model, the user is given the option of fitting another model to the data.

mex_gamma is a MatLab external file used to calculate the partial gamma function for the s^k model. The code was written as a mex file in order to speed computation, which was very slow in MatLab due to the iterative nature of the computation.

6.2 EOG Amplification

During the D-1 and SLS-1 missions, the same EOG amplification set up was used (see section 3.1). The main disadvantage with this amplifier, was that it required manual adjustments of the DC offset in order to maintain the output signals within the ± 10 volt input range on the A/D board. To remedy this, a new amplifier set up was obtained consisting of a Denver Research Institute (DRI) EOG signal conditioner with nominal gain of 1000 and cut-off frequency of 200 Hz, followed by two parallel OP27GN8 op amps in non-inverting, nominal gain of 4 configuration. The DRI amplifier was a two

channel, light weight, miniaturized, battery operated low power electronic system designed to amplify EOG potentials. It is equipped with an automatic level restoring circuit which continuously monitors the output voltage and adjusts the DC bias whenever this voltage exceeds 96% of the maximum allowable output of ± 2.5 volts (DRI, 1984). The DRI signal conditioner is identical to the flight unit used on D-1, SLS-1 and the upcoming SLS-2 missions. The DRI amplifier was mounted in a interface box on the back of the rotating chair, while the booster amplifier is connected between the chair base plate, and the analog filter box.

6.3 LabView Data Acquisition and Chair Control

During the SL-1 mission, data was acquired using an FM tape instrumentation recorder (see section 3.1) and data was subsequently digitized off line. For SLS-1, a program called Labtech Notebook was used to sample the data in real time. This program was found to be inefficient due to limitations in the names under which data could be saved and because it was relatively unreliable. To replace these methods, a new data acquisition system was implemented by modifying existing Labview software to perform rotating chair data acquisition needs.

During the SL-1 mission, the rotating chair command voltage was controlled by manually turning a potentiometer. This had been automated for the SLS-1 mission, using a combined analog/digital circuit to create a timed command with an exponential ramp up, followed by an automatically timed period of rotation and another exponential ramp down to stop. The timer however was unable to consistently hold identically long runs, allowing 59.5 to 61.3 second run lengths. Also, as the controller and data acquisition were separate, the data acquisition had to be manually triggered. In order to correct for these problems, chair control was moved to within the same LabView shell as is used for data acquisition. This allowed for identically long runs with identical

profiles for the stimulus, eliminating the need for separate data acquisition triggering, and consolidating all data acquisition and control in a single place.

A user's manual for the LabView routines is included in appendix B.

7.0 Conclusions

Several significant findings were noted in the analysis of the SL-1 data set. The major conclusions resulting from this investigation are of two sorts, conclusions on the changes in the behavior of the VOR, and conclusions on the efficacy of the engineering innovations relative to the previous analyses (Kulbaski, 1988, Balkwill, 1992). These two categories will be discussed separately;

7.1 Trends in Data and Interpretation

General trends were:

1. Strength of space motion sickness is directly related to adaptation
2. Post flight responses are different than preflight
3. Gain increases post flight
4. Indirect pathway gain probably decreases post flight
5. 1OE time constant probably shortens slightly post flight
6. Dumping time constants do not change post flight

One important note that is significant in the interpretation of the results, is the subjectively reported strength of space motion sickness observed by the subjects while on orbit (Oman et al, 1984, Oman and Shubentsov, 1992). Subject B was reported as the crew member with the strongest symptoms, subject C experienced moderate symptoms and subject D was asymptomatic. Examination of the data has shown a correspondence in the responses to space flight in each of the three subjects. Subjects B and C showed changes in all model parameters in the same direction, while subject D generally showed changes in the opposite direction. Possibly this indicates a different manner of adapting to micro gravity that can be related to the severity of SMS symptoms. Both sickness level and VOR changes are presumably caused by sensory conflict, which might in turn

be the result of changes in end-organ characteristics. Perhaps those subjects with the strongest symptoms have the strongest sensory conflict and VOR changes in the micro gravity environment, while subjects with milder symptoms have less sensory conflict driving their VOR changes. The difference in VOR responses between subjects B and C, and subject D, but not the correlation with symptoms, was noted by Kulbaski in his earlier analysis of this data set.

We may postulate that the physiological phenomena causing a post flight increase in gain also caused sensory conflict and SMS in flight. But why would a decrease in VOR gain not also be associated with SMS? An explanation is as follows; Higher than average VOR gain (B, C) is very seldom encountered in the natural world. Thus the presence of high VOR gain would represent an unusual condition that the CNS would be forced to adapt to, and the associated oscillopsia could cause SMS according to the sensory conflict theory of motion sickness. In contrast, reduced VOR gain is commonly encountered in normal experience. Common events, such as reduced alertness, can cause a drop in VOR gain (Collins, 1962), and thus the CNS would be accustomed to dealing with drops in gain. Therefore no motion sickness and no (or different) adaptation would result.

While subjects B and C change in a different direction from subject D, the comparison of the preflight versus post flight ensemble averaged responses show clearly that some form of VOR change is occurring in all three subjects. Σt^2 analysis of the ensemble averaged runs showed that all three subjects were significantly different post flight relative to preflight for head up post rotatory nystagmus runs when tested over $t = 62$ to 120 seconds. Subjects C and D were also significantly different over the $t = 62$ to 82 seconds regions. Previous analysis of this data set by Kulbaski showed significant difference in the post flight responses of subjects B and D only, by comparing the Σt^2 statistic to the χ^2

distribution over $t = 60$ to 80 seconds. Ensemble averaged model parameters and averaged individual model fit parameters also showed significant changes which are discussed below.

The mean apparent time constants of subjects B and C were each found to decrease post flight 19% relative to preflight values, while subject D increased their time constant by 6%. This is similar to Kulbaski's findings in direction, however he found slightly larger time constant changes for all subjects post flight.

	B		C		D	
	K	T	K	T	K	T
pre	0.877	17.57	0.781	16.59	0.957	11.34
post	0.902	14.28	0.953	13.37	0.824	11.98

Table 7.1, Apparent time constants for ensemble averaged runs as found previously (Kulbaski, 1988).

	B		C		D	
	K	T	K	T	K	T
pre	0.520	13.90	0.580	16.70	0.780	11.10
post	0.580	7.10	0.750	11.20	0.590	13.90

Table 7.2, Apparent time constants for ensemble averaged runs as found in this study .

Ensemble average SPV is quite different between 60-65 seconds, suggesting that VOR gain has changed. Both subjects B and C showed a gain increase post flight in the gain of the three parameter model fit, significant at the $p < 0.01$ for B and $p < 0.10$ for subject C. Also, both subjects showed smaller gain increases in the simple first order model gains, with subject C being significant at the $p < 0.10$ level. Ensemble averaged post flight first order model gains for subjects B and C increase 3% and 22% respectively, while subject D's gain drops 14%. These changes are in the same directions as was previously calculated for this data set (Kulbaski, 1988), however, the values of the gains found in this study averaged 41% higher than those found by Kulbaski. The most likely causes of this are; First, that Kulbaski included all runs in his analysis, whereas case selection was much more stringent in this study. In particular, as discussed in chapter 5, the rejection

of runs based on the rules of section 4.6 had removed many low gain runs from this analysis, thereby increasing the gains calculated here relative to Kulbaski, who included all runs. Second, the comparison of the model fitting methods, (i.e. fitting in the time domain as opposed to log linear fits) from section 5.3.1, showed that an average increase in model gain of approximately 10-15% would be found due to the different model fitting method used for the first order exponential models alone. Finally, Balkwill's *stat_prep* algorithm (section 4.5) filtered out dropouts which might have been more frequent post flight due to fatigue, thereby lowering the post flight gains calculated by Kulbaski.

In all three subjects, the 3P model mean post flight indirect pathway gains of the individual runs were seen to trend downwards, although none with significance. In subjects B and C, the indirect pathway gain of the ensemble averaged model fits was also seen to decrease post flight, while subject D showed only a marginal decrease (-4%). Thus while statistical significance was not achieved, due to the high variability of this parameter. The behavior of the model fits may indicate that the CNS is adapting the indirect pathway gain to compensate for the exposure to micro gravity.

The suggestion of a shortening of the simple exponential time constant post flight is shown by all three subjects individual model run results. All three subjects trend downwards, although none of them achieved statistical significance. Also, the ensemble averaged model fits for both of subjects B and C showed post flight decreases in the first order model time constant. A third indication for the change in the apparent time constant comes from the dumping study. The after dumping time constant showed a downwards trend for all three subjects, without statistical significance.

This shortening of the apparent time constant can be tied to the reduction in the indirect pathway gain. Since the velocity storage mechanism is used to prolong SPV responses to

vestibular cues, when the gain on the velocity storage is reduced, the contribution to the SPV signal from the velocity storage mechanism will drop, while the direct pathway contribution will be unchanged. This will have the effect of shortening the apparent time constant of the response, and thus the two changes are related (Arakawa et al, 1990).

A possible justification for decrease in indirect pathway gain and the shortening of the apparent time constant is as follows. When the subject is exposed to micro gravity, the GIF environment is changed. Similar to the case of tilt suppression (dumping), the CNS recognizes that the world environment has changed and does not trust its assessment of body motion. Thus it suppresses the velocity storage information in a similar manner as occurs when the dumping maneuver is performed. In the models, this is reflected in a decrease in the indirect pathway gain for the three parameter model, and a decrease in the apparent time constant for the first order model. Different time constants result for whole body tilt induced suppression (0.4 of head up time constant), as compared to dumping (0.6 of head up time constant) , and parabolic flight (0.7 of head up 1-G time constant)(Oman and Balkwill, 1993). The time dimension of all these changes is instantaneous. However, the effects on head erect and dumping responses measured post flight on SL-1 were long lasting. It seems as if humans return from 0-G already partially 'dumped' by their adaptation to micro gravity, and that there is a residual effect lasting several days.

From the analysis of dumping runs, it seems likely that the post flight dumping constant is not changed by exposure to micro gravity. The post flight dumping time constant increases for B, decreases for C significantly, and decreases for D. While C is significant, the unusual split in the results (B versus C and D) relative to trends in the other parameters, in addition to the limited amount of data caused by the brief five second

dumping duration, makes it seem unlikely that this one significant number represents a trend of dumping slope changing post flight.

7.2 Engineering Innovations

7. New data filtering methods are superior to previous methods.
8. Analysis of individual runs permits statistical evaluation of changes seen in model parameters.
9. New data acquisition and control software will provide improved data quality.
10. Near real time data processing allows faster processing and on-site analysis.
11. s^k model needs further investigation.
12. Quantitative analysis provided new insight in fitting models to VOR data.

As one measure of the effectiveness of the new data filtering methods, the results of the Σt^2 tests of subjects B, C, and D were compared to Kulbaski's calculation of the same value. In each case, the Σt^2 statistic for this thesis was higher than for Kulbaski's analysis of the data. This measure reflects on the improved filtering and outlier removal methods which has reduced the noise and thus the variance of the ensemble fits, and thereby increased the value of the Σt^2 statistic.

Another measure of the improvements in the new analysis methods is the discovery of significant changes in the post flight gains of the subjects. Kulbaski (1988) noted changes in mean gain values but concluded that there was no significant gain change post flight in contradiction to this study. While it could be claimed that the run rejection rules used (section 4.6) influenced the present finding, they could not have caused it: Rules for the exclusion of data were developed on the basis of maintaining high data quality and were used with the intent of preventing artifacts from contaminating the good data. The runs that were excluded had generally lower gains preflight than the kept runs, while the

post flight rejected runs had generally higher gains. Thus, the rules for run rejection will have reduced the likelihood of finding a significant gain increase, not aided it.

Despite the improved filtering methods individual run data from one subject, A, could not be satisfactorily analyzed. This subject was noted to have significant noise problems in Kulbaski (1988) and did not provide any statistically significant results in that analysis when analyzed individually. Kulbaski's analysis of this subject was confined to ensemble averaged responses.

New statistical methods developed to perform the ensemble averaging process took advantage of improvements in computing capability to give more statistical power to those data points with the best data, and arguably provided better estimates of the true means of the populations.

Another improvement over Kulbaski's analysis is the ability to analyze the runs individually. This has allowed the estimation of model parameters and assessment of the statistical significance of changes seen. Analysis of individual runs has also provided a measurement of the variability in the data. This has implications for clinical testing where often very few trials are taken. Due to the high variability seen in this data set, it seems possible that conclusions based on small sample populations may be misleading.

In association with this thesis, a new data analysis and experiment control software package was developed, *DAM/DQM.L-mod6*. This new software has reduced operator workload for conducting baseline data collection sessions. Also, with the addition of the integrated chair control, velocity and duration of stimuli provided to the subject has become consistent and repeatable, simplifying data analysis requirements.

The new *batch_analysis* software developed as a part of this thesis has become an almost fully automated, self-contained pipeline for data analysis within the MatLab user interface. Operator input has been minimized, and external programs have been rewritten for use from within MatLab. This has greatly increased the speed of the data processing procedure, allowing near real time processing of data. Combined with the new acquisition and control system, the new software allows all individual runs of a full BDC session data set for an individual to be analyzed in under an hour (using the first order exponential model), compared to several days required in the past. This met one of the goals of this thesis by allowing rapid on site data processing and preliminary analysis on future missions.

Another contribution of this thesis, is the development of the s^k VOR model. This model provides an alternate mathematical formulation of what is happening in the canal afferent neurons as subjects are stimulated, and provides another method to measure changes in human VOR responses.

As a result of there yet being no definitive way to differentiate between the three parameter model and the s^k model on the basis of the quality of the model fits, and considering that the s^k model would be both more difficult to analyze both within this data set, and for comparisons to previous data (SLS-1), it was decided to use this model for data analysis only in a limited manner. The s^k model was limited in its effectiveness by two elements. First, the additional degree of freedom in the model added another parameter for preflight versus post flight variations to be assigned to, and thus reduced visible changes in any of the model parameters. Second, the k term can be represented by an apparent adaptation time constant that is longer than the duration of this data set. Use of this model would be better suited to a data sets with longer runs. Additional experience may allow one or more of the model constraints to be fixed to aid

convergence. h_0 seems to be a likely prospect to be fixed. In both models the h_0 represents the same physiological trait, and this is not expected to change preflight versus post flight based on experience with the three parameter model. Also, in the test segments, the two models chose values for this parameter which were similar.

Quantitative comparison of the s^k and three parameter models, and with the first order exponential model has provided additional insight into the requirements of model fitting as related to the number of free parameters. Both the three parameter model, and four parameter s^k model were capable of generating very good fits to the data. Neither subjective visual analysis, or comparison of the MSEs was capable of discerning any advantage to the quality of either model's fits. However, the additional degree of freedom of the s^k model provided an additional parameter for the model fit procedure to use to fit the data. This led to smaller changes and higher variance in all parameters which directly affected the ability of the statistical analysis to determine changes. As a contrast, with the ensemble averaged data, the s^k model was also fit with only two free parameters (velocity storage parameters were frozen to preflight values) when fitting post flight curves. While this confined the change in the curves to only two parameter, and thus made parameter changes easier to see, it caused a small but noticeable drop in the quality of the model fits. In a similar manner, fits of the two parameter simple exponential model also had lower quality of fit than either the three parameter or s^k models. In short, it is very important to be careful when choosing a model, or freezing parameters within a model, to consider carefully the effects on quality of fit and ability to discern changes.

In general, the results of this study agree well with those found in previous space shuttle mission studies. The significance of some of the results has decreased relative to

previous analysis of this data, while other aspects have become more significant. This is a result of the new, more stringent methods of data filtering.

7.3 Suggestions for Future Work

Additional study of the behavior of EOG potentials with respect to changing light intensities is needed. Calibration methods for future Space Lab missions involve allowing eyes to dark adapt before runs begin, and performing all calibrations with filtered red light. Examining the time effects of these lighting conditions on EOG potential is necessary.

Further improvements to the automated analysis system could also be implemented. Significant amounts of time could be saved by eliminating the need to convert data from binary format to MatLab format. Also, while sampling data at low rates (e.g. 120 Hz), the CPU is not doing any useful work. Rewriting the data acquisition system to operate on an interrupt status would allow the implementation of the digital OS filters including AATM in real time and reduce the number of analysis steps required. A further improvement could be realized by writing the data acquisition software as a MatLab mex file, which would allow all acquisition and analysis functions to take place through one user interface.

Additional experimentation with the s^k model seems warranted. Applying this model to other data sets that have longer trials would be better suited to this model. Fixing the h_0 term could also be attempted to aid convergence, and then retesting the model on this data set. Finally, it would be interesting to examine if there was any difference in the k values of subject D relative to B and C in light of that subjects different responses to space flight.

References

- Aarakawa, G. Oman, C. Wall, C. M.** Modelling of Spaceflight Effects Upon 1-g Postrotatory VOR. presented at the Barany Conference, Tokyo, 1990.
- Balkwill, M.D.** Changes in Human Horizontal Angular VOR after the Spacelab SLS-1 Mission. S.M. Thesis, Massachusetts Institute of Technology, Cambridge, MA, 1992.
- Barr, C. Schultheis, L. Robinson, D.** Voluntary, non-visual control of the Human Vestibulo-ocular Reflex. *Acta Otolaryng.* (Stockholm) 81:365-375, 1976.
- Benson, A.J.** Post-rotational Sensation and Nystagmus as Indicants of Semicircular Canal Function. In: Third Symposium on the Role of the Vestibular Organs in Space Exploration, NASA SP-152. pp. 421-432, 1967.
- Collins, W.** Effects of Mental Set Upon Vestibular Nystagmus. *J. Exp. Psychol.* 63:191, 1962.
- Correia, M.J. Perachio, A.A. Dickman, J.D. Kozlovskaya, I.B. Sirota, M.G. Yakushin, S.B. Beloozerova, I.N.** Changes in Monkey Horizontal Semicircular Canal Afferent Responses Following Space Flight. *Supp. to the J. of Appl. Physiol.*, August, 1992.
- Churchill, S. ed., et al.** Introduction to Space Life Science.
- Denver Research Institute** EOG Signal Conditioner; Operating, Maintenance and handling Manual. DRI purchase Order #SC-Aa361965. 1984.
- DiDonato, A.R.** Personal Correspondence to Manning J. Correia, 28 Sept, 1978.
- Dizio, P. Lackner, J.R.** The effects of gravito-inertial force level and head movements on post-rotational nystagmus and illusory after rotation. *Exp. Brain Research*, 70:485-495, 1988.
- Engelken, E.J. Stevens, K.W.** A New Approach to the Analysis of Nystagmus: An Application for Order Statistic Filters. *Aviation, Space, and Environmental Medicine*, 61 (9):859-864, 1990.
- Engelken, E.J. Stevens, K.W. Enderle, J.D.** Optimization of an Adaptive Nonlinear Filter for the Analysis of Nystagmus. *Rocky Mountain Bioengineering Symposium*, 1991.
- Fernandez, C. Goldberg, J.M.** Physiology of Peripheral Neurons Innervating otolith organs of the Squirrel Monkey. I. Response to Static Tilts and to long Duration Centrifugal Force. *J. of Neurophysiology*. 39:970-984, 1976.
- Ferry, J.D.** Viscoelastic Properties of Polymers. John Wiley and Sons. New York, 1980.
- Fetter, M. Tweed, D. Hermann, W. Wohland-Braun B. Koenig, E.** The Influence of head Position and Head Reorientation on the Axis of Eye Rotation and the Vestibular Time Constant During Post-Rotatory Nystagmus. In Progress, 1992.

Gonshor, A. Malcolm, R. Effect of Changes in Illumination Level on Electro-oculography(EOG). *Aerospace Medicine*, 42(2):138-140, 1971.

Grace, A. Optimisation Toolbox, for use with MatLab, User's Guide. The MathWorks Inc., South Natick, MA, 1990.

Gross, B Mathematical Structure of the Theories of Viscoelasticity. Hermann & Co., Paris, 1953.

Heinonen, P Nuevo, Y. FIR-Median Hybrid Filters with predictive FIR Substructures. *IEEE Transactions on Acoustics, Speech, and Signal Processing*. 36(6):892-899, 1988.

Komatsuzaki, A. Harris, H.E. Alpert, J. Cohen, B. Horizontal Nystagmus of Rhesus Monkeys. *Acta Otolaryng*. 67:535-551, 1969.

Kulbaski, M.J. Effects of Weightlessness on the vestibulo-Ocular Reflex in the crew of Spacelab 1. B.S. Thesis, Massachusetts Institute of Technology, Cambridge, MA, 1986.

Landolt, J.P. Correia, M.J. Neurodynamic Response of Anterior Semicircular Canal Afferents in the Pigeon. *J. of Neurophysiology*. 43(6):1746-1769, 1980.

Laurence Urdang Associates, Ltd. The Bantam Medical Dictionary. Bantam Books, New York, NY, 1982.

Massoumnia, M.A. Detection of Fast Phase of Nystagmus using Digital Filtering. S.M. Thesis, Massachusetts Institute of Technology, Cambridge, MA, 1983.

Merfeld, D.M. Spatial Orientation in the Squirrel Monkey: An Experimental and Theoretical Investigation. Ph.D. Thesis, Massachusetts Institute of Technology, Cambridge, MA, 1990.

Oldham, K.B. Spanier, J. The Fractional Calculus. Academic Press, New York, 1974.

Oman, C.M., Lichtenberg, B.K. Money, K.E. Space motion sickness monitoring experiment: Spacelab 1. NATO-AGARD Aerospace Medical Panel Symposium on Motion Sickness: Mechanisms, Prediction, Prevention and Treatment, Conference Proceedings No. 372, pp 35/1-35/21, 1984.

Oman, C.M. Weigl, H.J. Postflight vestibulo-ocular reflex changes in Space Shuttle/Spacelab D-1 crew, abstract 21, Aerospace Medical Association 60th Annual Scientific Meeting, Washington, D.C., May 7-11, 1989.

Oman, C.M. Shubentsov, I. Space sickness symptom severity correlates with average head acceleration, *Mechanisms and Control of Emesis*, eds., Bianchi, A.L., Grelot, L., Miller, A.D., & King, G.L., Colloque INSERM/John Libbey Eurotext Ltd. 233:185-194, 1992.

Oman, C.M. Balkwill, M.D. Horizontal Angular VOR, Nystagmus Dumping, and Sensation Duration in SpaceLab SLS-1 Crewmembers. Barany Society Meeting, Prague, 1992.

Oman, C.M. Calkins, D.S. Effect of Orbital Flight on the Human Horizontal Vestibulo-Ocular Reflex Response to 120 deg/sec Step Stimuli. Final Report, Microgravity Vestibular Investigations, pp.33-54, April 1993.

Pouliot, C.F. Summary of the Sigma T-squared Simulation. Massachusetts Institute of Technology, Man-Vehicle Laboratory internal report, 1991.

Raphan, Th. Matsuo, V. and Cohen B. Velocity Storage in the Vestibulo-Ocular Reflex Arc (VOR). *Experimental Brain Research*, 35; 229-248, 1979.

Robinson, D.A. Vestibular and Optokinetic Symbiosis: an example of explaining by modelling. In: *Control of Gaze by Brain Stem Neurons. (Developments in Neuroscience, Vol 1)* Baker, R and Berthoz, A., eds. Amsterdam: Elsevier-North Holland Biomedical Press, pp. 49-58, 1977.

Robinson, D.A. Ocular Motor Control Signals. In: *Basic Mechanisms of Ocular Motility and Their Clinical Implications.* G. Lennerstrand and P. Bach-y-Rita, eds. Pergamon Press, Oxford. pp.337-334, 1975.

Robinson, D.A. Models of oculomotor organization. In: *The Control of Eye Movements.* Bach-y-Rita, P., Collins, C.C., Hyde, J.E. eds. New York: Academic Press, pp.519-538, 1971.

Rosner, B. *Fundamentals of Biostatistics.* Second Edition. PWS Publishers, Boston, MA, 1986.

Stearns, S.D. Hush, D.R. *Digital Signal Analysis.* Prentice-Hall Inc., Englewood Cliffs, N.J., 1990.

Thorson, J. Biederman-Thorson, M. Distributed Relaxation Processes in Sensory Adaptation. *Science* 183:161-172, 1974.

Van de Vegte, J. *Feedback Control Systems.* Second Edition. Prentice Hall, Englewood Cliffs, N.J.. 1990.

Wilson, V.J. and G. Melvill Jones. *Mammalian Vestibular Physiology.* Plenum Press, New York, NY, 1979.

Appendix A

Data

Run	F-90	F-60	F-30	F-11	F-10	R+1	R+2	R+4
1	.5288	.6785	.2651	.3420	.3885	.3896	.2533	.2433
4	.4888	()	--	--	--	--	.5504	--
6	--	--	()	--	--	()	--	--
10	(.3020)	--	--	--	(.6425)	.4003	.6167	.4455
11	--	.5405	--	--	--	--	--	--
12	--	--	--	.4676	--	--	--	--

Table A.1a, Horizontal calibration factors for subject A in degrees of eye movement per measured A/D unit. Calibration factors in brackets were considered unreliable and were not used for interpolation. Dashes indicate that the run was not a calibration run.

Run	F-90	F-60	F-30	F-11	F-10	R+1	R+2	R+4
1	.0839	.0666	.0618	.0994	.1014	.0473	.0442	.0391
2	--	--	--	--	.1090	--	--	--
4	--	--	--	--	--	.0510	.0513	--
5	--	.1052	--	--	.1352	--	--	.0749
6	--	--	.1718	--	--	--	--	--
9	.1058	--	--	--	--	--	--	--
10	--	--	--	--	--	--	--	--
11	--	--	--	.1038	.1177	--	--	--
12	--	.1065	--	.0857	--	--	--	--

Table A.1b, Horizontal calibration factors for subject B in degrees of eye movement per measured A/D unit. Dashes indicate that the run was not a calibration run.

Run	F-90	F-60	F-30	F-11	F-10	R+1	R+2	R+4
1	.1234	.1521	.0982	.0685	.0844	.1297	.1216	.1171
4	.1825	.1210	--	--	.1177	.1421	.1422	.1680
6	--	--	.1587	--	--	--	--	--
7	--	--	--	.2227	--	--	--	--
10	--	.0980	--	--	--	.1457	.1515	.1719
11	.1379	--	--	--	.0950	--	--	--

Table A.1c, Horizontal calibration factors for subject C in degrees of eye movement per measured A/D unit. Dashes indicate that the run was not a calibration run.

Run	F-90	F-60	F-30	F-11	F-10	R+1	R+2	R+4
1	.2105	.1430	.0920	.0946	.0893	.1098	.0669	.1078
4	.1941	--	--	.3745	.0990	.2654	.0882	.1026
5	--	.0614	.1589	--	--	--	--	--
10	.3115	--	--	.2199	--	.1153	.1269	--
11	--	--	--	--	.1123	--	--	--
15	--	.0793	--	--	--	--	--	--

Table A.1d, Horizontal calibration factors for subject D in degrees of eye movement per measured A/D unit. Dashes indicate that the run was not a calibration run.

Run	K ₃	h _o	g _o	K ₁	T
102	0.690	0.0522	0.170	0.94	13.05
103	0.609	0.0239	0.152	0.7	20.98
104	0.820	0.0287	0.072	0.8	11.83
202	0.850	0.0278	0.122	0.91	16.86
203	0.375	0.0532	0.298	0.69	15.53
206	0.821	0.0298	0.095	0.84	13.97
207	0.563	0.0335	0.072	0.56	11.19
211	0.446	0.0405	0.068	0.46	9.88
302	0.598	0.0274	0.208	0.85	21.33
303	0.952	0.0212	0.129	1.01	20.71
304	1.097	0.0265	0.061	1.04	11.26
305	1.091	0.0230	0.107	1.09	17.72
406	0.770	0.0261	0.110	0.81	16.35
605	0.954	0.0298	0.095	0.96	14.12
802	0.709	0.0355	0.134	0.85	14.65
ccw means	0.687	0.0316	0.134	0.76	16.05
cw means	0.813	0.0321	0.121	0.90	14.72

Table A2.1, Subject B per-rotatory model fit parameters

Run	K	h _o	g _o	K	T
102	0.541	0.0323	0.170	0.70	24.34
103	0.461	0.0540	0.191	0.73	16.37
104	0.679	0.0373	0.076	0.69	14.40
105	0.747	0.0355	0.035	0.72	9.43
202	0.645	0.0441	0.164	0.89	18.48
206	0.686	0.0385	0.053	0.65	11.86
302	0.554	0.0618	0.222	0.93	15.95
303	0.575	0.0213	0.129	0.84	15.86
304	0.974	0.0335	0.061	0.89	13.92
305	1.250	0.0326	0.022	1.20	8.13
403	0.655	0.0451	0.153	0.87	17.84
405	0.788	0.0315	0.037	0.72	10.37
406	0.568	0.0305	0.019	0.64	6.50
503	0.646	0.0477	0.188	0.97	18.34
504	0.669	0.0556	0.180	0.98	16.36
506	0.970	0.0220	0.036	0.74	12.41
507	0.799	0.0266	0.029	0.75	12.40
601	0.930	0.0331	0.055	0.84	13.28
602	0.663	0.0618	0.148	0.93	13.82
604	0.864	0.0346	0.064	0.74	15.08
605	0.857	0.0440	0.058	0.81	12.00
701	0.843	0.0395	0.092	0.84	16.43
702	0.829	0.0490	0.086	0.89	13.33
704	0.856	0.0362	0.071	0.68	16.99
705	0.975	0.0416	0.048	0.90	11.20
802	0.689	0.0548	0.099	0.74	13.89
804	1.130	0.0306	0.040	0.97	11.60
ccw means	0.724	0.0366	0.086	0.84	12.15
cw means	0.714	0.0394	0.116	0.81	15.79

Table A2.2, subject B post-rotatory model fit parameters.

Run	K	h _o	g _o	K	T
102	0.756	0.0400	0.136	0.90	14.23
103	1.071	0.0240	0.093	1.03	15.79
105	0.572	0.0430	0.203	0.83	15.63
106	0.730	0.0210	0.071	0.65	14.17
202	0.536	0.0340	0.138	0.63	15.60
203	0.585	0.0310	0.224	0.86	20.54
205	0.916	0.0320	0.087	0.93	12.78
206	0.645	0.0270	0.158	0.77	19.73
304	1.020	0.0320	0.072	1.01	11.47
305	1.285	0.0230	0.071	1.18	13.27
403	0.753	0.0320	0.099	0.89	12.66
404	0.520	0.0620	0.134	0.66	10.72
405	0.947	0.0190	0.063	0.80	14.21
406	0.714	0.0500	0.09	0.79	10.24
503	1.271	0.0250	0.056	1.18	11.04
505	0.705	0.0440	0.128	0.84	12.89
506	0.710	0.0340	0.164	0.89	17.15
803	0.773	0.0360	0.133	0.95	14.41
ccw means	0.889	0.0262	0.111	0.92	15.39
cw means	0.717	0.0421	0.1235	0.82	12.95

Table A3.1, subject C per rotatory model fit parameters

Run	K	h_o	g_o	K	T
103	0.922	0.0430	0.095	0.99	15.23
105	0.499	0.0460	0.146	0.63	17.73
106	0.535	0.0570	0.119	0.63	14.20
202	0.795	0.0360	0.156	1.00	21.79
203	0.818	0.0500	0.143	1.06	16.40
205	0.642	0.0310	0.069	0.52	17.66
206	0.889	0.0370	0.027	0.85	8.50
302	0.524	0.0370	0.181	0.70	22.85
303	0.419	0.0590	0.197	0.71	15.06
304	0.829	0.0208	0.047	0.59	16.64
305	0.651	0.0429	0.039	0.70	8.94
404	0.502	0.0680	0.189	0.82	13.61
405	0.888	0.0390	0.03	0.77	9.53
406	0.632	0.0290	0.069	0.56	16.76
502	0.573	0.0500	0.14	0.75	15.82
503	0.712	0.0430	0.09	0.73	15.30
505	0.955	0.0310	0.06	0.82	15.09
506	0.641	0.0560	0.091	0.69	12.95
602	0.895	0.0370	0.063	0.84	13.65
603	0.661	0.0560	0.151	0.88	15.43
605	0.857	0.0350	0.063	0.71	15.34
702	0.753	0.0460	0.1	0.80	15.39
703	0.75	0.0524	0.1	0.89	13.31
705	0.813	0.0373	0.07	0.68	16.34
706	0.885	0.0427	0.048	0.84	11.30
803	0.723	0.0540	0.092	0.76	13.52
805	1.093	0.0190	0.03	0.88	10.93
ccw means	0.719	0.0474	0.092	0.79	12.90
cw means	0.661	0.0388	0.117	0.71	17.55

Table A3.2, subject C post rotatory model fits

Run	K	h_o	g_o	K	T
102	0.527	0.0390	0.189	0.77	15.77
103	0.661	0.0290	0.134	0.75	17.01
303	1.252	0.0280	0.076	1.20	12.82
402	0.985	0.0430	0.119	1.13	12.79
502	0.477	0.0580	0.146	0.62	11.66
503	0.688	0.0410	0.157	0.87	14.80
506	0.414	0.0380	0.233	0.66	17.59
ccw means	0.754	0.0340	0.150	0.87	15.55
cw means	0.663	0.0470	0.151	0.84	13.41

Table A4.1, subject D per-rotatory model fit parameters

Run	K	h_o	g_o	K	T
102	0.688	0.0490	0.128	0.84	16.00
103	0.808	0.0440	0.085	0.82	14.59
302	0.897	0.0590	0.107	1.07	12.88
303	1.071	0.0590	0.024	1.19	6.78
402	0.994	0.0560	0.053	1.04	9.78
403	0.935	0.0722	0.136	0.41	12.93
502	0.792	0.0610	0.102	0.93	12.50
503	0.852	0.0510	0.075	0.84	12.90
506	0.874	0.0350	0.028	0.82	8.72
602	0.465	0.0650	0.170	0.69	14.03
603	0.536	0.0490	0.104	0.60	14.70
605	0.607	0.0780	0.023	0.67	6.35
606	0.484	0.0316	0.047	0.42	12.37
702	0.747	0.0640	0.071	0.81	10.53
703	0.625	0.0390	0.088	0.60	16.54
705	0.644	0.0750	0.021	0.71	6.26
706	0.481	0.0355	0.047	1.20	13.11
802	0.771	0.0480	0.085	0.77	14.22
803	0.864	0.0530	0.092	0.94	13.27
805	0.521	0.0850	0.037	0.58	7.17
806	0.581	0.0180	0.014	0.63	6.34
ccw means	0.908	0.0522	0.070	0.82	11.18
cw means	0.843	0.0563	0.098	0.97	12.79

Table A4.2, subject D post-rotatory model fit parameters

Run	m pre	b pre	RMS pre	m dump	b dump	RMS dump	m post	b post	RMS post
104	0.207	3.511	0.18	-0.089	4.632	0.05	-0.008	3.436	0.11
105	0.283	3.402	0.21	-0.196	4.959	0.25	-0.041	3.522	0.13
206	0.193	3.594	0.30	-0.122	4.617	0.10	-0.053	3.811	0.21
211	0.268	1.811	0.13	-0.216	3.997	0.35	-0.085	2.817	0.57
304	1.451	2.841	0.41	-0.041	4.635	0.01	-0.063	4.481	0.16
305	0.047	4.308	0.55	0.051	2.926	0.23	-0.033	3.681	0.13
405	0.56	3.24	0.28	-0.08	4.436	0.06	-0.103	4.486	0.21
406	0.038	3.823	0.27	-0.003	2.986	0.20	-0.035	2.763	0.62
506	0.113	4.172	0.14	-0.076	4.44	0.40	-0.034	3.66	0.26
604	-0.092	4.557	0.21	-0.02	3.903	0.08	-0.059	4.428	0.12
605	-0.011	4.336	0.28	-0.159	5.01	0.09	-0.044	4.11	0.18
704	0.132	4.067	0.37	-0.061	4.351	0.22	-0.055	4.366	0.21
705	1.288	3.331	0.27	-0.157	5.062	0.09	-0.051	4.112	0.26
804	0.141	3.993	0.22	-0.184	5.319	0.07	-0.075	4.545	0.42
mean	-0.052	4.447	0.25	-0.128	5.304	0.17	-0.053	3.874	0.26
pre flight				-0.103	4.338	0.17	-0.050	3.628	0.27
post flight	-0.052	4.447	0.25	-0.116	4.789	0.11	-0.057	4.312	0.24

Table A5a, Dumping log-linear model fits for subject B.

Run	m pre	b pre	RMS pre	m dump	b dump	RMS dump	m post	b post	RMS post
105	0.131	3.76	0.19	-0.097	4.511	0.12	-0.041	4.166	0.13
106	0.463	3.122	0.19	-0.076	4.372	0.07	-0.042	3.98	0.14
205	-0.025	4.229	0.27	-0.258	5.349	0.14	-0.007	3.417	0.15
206	1.208	3.019	0.13	-0.054	4.436	0.07	-0.053	3.727	0.32
304	0.631	3.181	0.27	-0.215	5.098	0.18	0.004	2.967	0.31
305	0.044	3.94	0.16	-0.296	5.337	0.27	-0.057	3.656	0.34
405	0.104	4.075	0.29	-0.195	4.895	0.31	-0.054	3.865	0.20
406	7.802	-9.272	6.65	-0.153	4.648	0.21	-0.005	3.32	0.23
505	0.141	3.858	0.32	-0.043	4.171	0.10	-0.021	3.835	0.12
506	-0.056	4.412	0.07	-0.07	4.146	0.05	-0.059	4.247	0.13
605	-0.105	4.6	0.23	-0.041	4.034	0.12	-0.047	4.249	0.10
705	0.134	4.049	0.35	-0.062	4.38	0.20	-0.023	3.797	0.14
805	0.099	3.963	0.22	-0.228	5.482	0.10	-0.068	4.234	0.21
mean	-0.062	4.413	0.19	-0.138	4.681	0.15	-0.040	4.227	0.2
pre flight	-0.040	4.320	0.17	-0.146	4.696	0.15	-0.038	3.801	0.20
post flight	-0.105	4.6	0.23	-0.110	4.632	0.14	-0.046	4.090	0.15

Table A5b, Dumping log-linear model fits for subject C.

Run	m pre	b pre	RMS pre	m dump	b dump	RMS dump	m post	b post	RMS post
506	0.149	3.726	0.24	-0.124	4.524	0.11	-0.084	4.113	0.26
605	4.266	-14.35	7.13	-0.001	3.031	0.20	-0.059	2.963	0.32
606	0.135	3.171	0.47	-0.028	3.363	0.13	-0.075	3.68	0.17
705	0.803	2.258	0.11	-0.261	4.895	0.11	-0.307	6.537	3.92
706	0.253	3.081	0.64	-0.195	4.651	0.19	-0.046	3.378	0.23
805	2.871	-11.93	6.25	-0.155	4.364	0.15	-0.007	2.402	0.14
806	-0.073	3.616	0.48	-0.029	2.767	0.09	0.012	1.453	0.23
mean	-0.073	3.616	0.48	-0.113	3.942	0.14	-0.080	3.503	0.75
pre flight		3.726	0.24	-0.124	4.524	0.11	-0.084	4.113	0.26
post flight	-0.073	3.616	0.48	-0.111	3.845	0.15	-0.098	3.791	0.96

Table A.5c, Dumping log-linear model fits for subject D.

Run	C	k	g ₀	h ₀
102	0.844	0.301	0.159	0.026
103	1.595	0.552	0.176	0.022
202	1.214	0.343	0.152	0.034
302	1.169	0.236	0.126	0.056
303	1.295	0.348	0.140	0.044
403	1.118	0.318	0.148	0.037
503	0.983	0.192	0.133	0.049
504	1.137	0.231	0.129	0.052
preflight mean	1.169	0.316	0.145	0.040

Table A.6a, Per rotatory s^k model fit parameters for subject B.

Run	C	k	g _o	h _o
102	1.67	0.33	0.12	0.064
103	1.72	0.59	0.19	0.014
104	1.11	0.28	0.11	0.068
202	1.12	0.27	0.14	0.048
203	1.45	0.39	0.14	0.052
206	2.51	0.69	0.19	0.016
207	0.86	0.37	0.12	0.058
211	1.11	0.40	0.10	0.082
302	0.79	0.08	0.12	0.058
303	0.73	0.09	0.13	0.048
304	0.84	0.07	0.08	0.094
305	1.53	0.37	0.15	0.031
406	1.45	0.49	0.17	0.027
605	0.87	0.18	0.12	0.060
802	1.39	0.34	0.13	0.053
preflight mean	1.269	0.340	0.137	0.050

Table A.6b, Post rotatory s^k model fit parameters for subject B.

Run	C	k	g _o	h _o
202	0.857	0.167	0.140	0.039
203	1.262	0.287	0.138	0.043
103	0.734	0.098	0.110	0.063
302	0.660	0.189	0.143	0.037
303	1.276	0.470	0.162	0.034
502	0.948	0.314	0.141	0.042
503	1.217	0.456	0.153	0.028
preflight mean	0.993	0.283	0.141	0.041

Table A.7a, Per rotatory s^k model fit parameters for subject C.

Run	C	k	g _o	h _o
102	1.446	0.334	0.130	0.055
103	0.195	0.027	0.000	0.400
105	1.369	0.304	0.130	0.057
106	1.065	0.479	0.152	0.025
202	1.002	0.368	0.143	0.043
203	0.858	0.032	0.109	0.072
205	1.013	0.139	0.093	0.084
206	1.056	0.315	0.150	0.037
304	1.789	0.493	0.145	0.036
305	0.884	0.046	0.086	0.086
403	1.174	0.546	0.220	0.061
404	1.630	0.501	0.133	0.056
405	1.029	0.416	0.143	0.026
406	1.623	0.494	0.135	0.050
503	1.376	0.380	0.131	0.042
505	1.480	0.352	0.124	0.060
506	1.135	0.229	0.128	0.056
preflight mean	1.184	0.321	0.127	0.073

Table A.7b, Post rotatory s^k model fit parameters for subject C.

Run	C	k	g _o	h _o
102	1.296	0.353	0.143	0.049
103	1.900	0.596	0.182	0.019
302	0.927	0.439	0.110	0.076
303	0.926	0.128	0.103	0.069
303	0.926	0.128	0.103	0.069
402	1.647	0.310	0.121	0.061
402	1.647	0.310	0.121	0.061
502	1.443	0.477	0.135	0.053
503	1.507	0.360	0.136	0.051
506	0.804	0.194	0.125	0.059
preflight mean	1.302	0.329	0.128	0.057

Table A.8a, Per rotatory s^k model fit parameters for subject D.

Run	C	k	g _o	h _o
102	0.811	0.200	0.126	0.052
103	0.694	0.005	0.081	0.093
302	1.386	0.342	0.132	0.047
303	1.240	0.420	0.113	0.055
402	1.685	0.477	0.136	0.042
502	0.942	0.098	0.086	0.090
503	1.939	0.571	0.157	0.025
602	0.795	0.189	0.111	0.069
603	0.661	0.288	0.132	0.044
702	1.125	0.384	0.125	0.053
703	1.205	0.512	0.161	0.021
802	0.793	0.276	0.128	0.044
803	0.828	0.187	0.114	0.060
preflight mean	1.242	0.302	0.119	0.058

Table A.8b, Post rotatory s^k model fit parameters for subject D.

Appendix B

Labview Routines

User's Manual

B.1 Introduction

This appendix is meant as a quick introduction to the use of the LabView routines that are used with rotating chair data acquisition. Since the creation of these routines, they have been customized for use on other experiments beyond the rotating chair, including the MVL Link trainer, linear sled, and other rotating chair usages. This manual will not cover the specifics of these other versions since the operation of these other versions is similar.

This manual is written for persons that have some rudimentary knowledge of the operation of LabView Software. If you are unfamiliar with the use of LabView, refer to the LabView user's manual tutorial.

B.2 History

The LabView routines used for chair data acquisition had their genesis in a set of routines originally written in the MVL in 1991 by Nicolas Groleau, who was then working on the Principal Investigator in a Box (PI) project. The PI project performed control, data acquisition and analysis on an experiment utilizing a rotating dome. Originally, the LabView routines were used to acquire the raw data, perform some analyses to determine statistical data parameters, and save the data to a file. In some cases, this package was also used to provide a steady output voltage that would be used to drive the rotating dome at constant velocity for a set length of time.

Starting in early 1992, these LabView routines, then named *DAM/DQM.L*, were provided to the staff of the rotating chair project, for modification to replace the existing rotating chair data acquisition system. Improvements that would be gained by the change to LabView included automatic triggering, control over data filenames, simultaneous data acquisition and chair control, and real-time data display.

Beginning with the original *DAM/DQM.L* , the software was customized for use with the rotating chair over the following 15 months. As it changed, the name received the extension '-mod#', in order to identify significantly changed versions as it evolved. The current version of the software in use for the rotating chair is *DAM/DQM.L-mod6* . The majority of changes that have taken place through the evolution of *DAM/DQM.L* were made in the higher, organizational level of the original program. The low level functions including A/D board drivers have remained generally unchanged. Many of the changes were actually removal of portions of the original program that were not relevant to the rotating chair usage, in order to speed up the processing time. As a result of this path of creation, there are many remnants of the original rotating dome software, both in structures, and in names, still present in the latest version.

B.3 Before Using *DAM/DQM.L-mod6*

The front panel of the *DAM/DQM.L-mod6* routine is shown in figure B.1. The chart regions on left hand side are the frames for plotting of real time data. The numeric indicators on the right hand side of the screen represent the controls and states of the software. The color convention used for controls and indicators is as follows;

red	-->	controls
blue	-->	indicators
green	-->	indicators (older versions)

Before beginning data collection, it is necessary to make sure that all controls are at the desired position. The controls appear in two groupings at the top and bottom of the right hand side of the window. In general, the controls at the top will need to be changed for each subject, and each BDC. The controls at the bottom generally will only need to be altered whenever the program is moved to a different machine.

Other indicators and controls are present off screen. These represent vestiges of the original dome program ability to relay data from file. They are disabled, but the ability to replay data is latent within the program.

B.3.1 Controls

- Subject Code:** Mounted at the top of the screen, the Subject Code control sets the name under which all subject data files will be saved. It must be set for each subject. It is changed by clicking the cursor within the window and typing the subject name or code.
- BDC#:** This refers to the number of the Baseline Data Collection and should be set at each session. It is changed by clicking the cursor on the arrow heads on the bottom of the control.
- # of runs:** This controls the total number of runs and calibrations to be performed before the program shuts itself off. It should be set appropriately each time the program is run.
- save path:** This controls where the run folder is created.
- Slot #:** This indicates which slot the Macadidos A/D board is in.
- Cal:** This sets the duration (in seconds) of calibration runs.
- secs:** This sets the duration (in seconds) of regular data acquisition runs.
- freq:** This sets the data sampling frequency (in hertz).
- Chair Type:** This defines the which chair is going to be used. There are three regular settings,
- passive - indicates that no output mode will be used, three channels of data will be taken
 - BDCF - normal baseline data collection mode, with chair output corresponding to a step function passed through a low pass filter of time constant 0.17 seconds.

other - latent modes that have not been defined

write: Sets data file save type to either binary or ASCII. Binary save is default due to faster save time.

B.3.2 Indicators

run folder name: indicates the name of the folder that data will be saved into.

RUN #: Shows the number of the current run or calibration in the series.

motor output: The chart border contains the real-time display of the voltage sent to the motor servo controller.

A/D inputs: This chart border contains the real-time display of the data being acquired for all three input channels.

B.3.3 File and Run Name Conventions

DAM/DQM.L-mod6 will open a folder following the path information given in the save path, with a name following the convention;

Subject Code BDC# - time - day

The subject code and BDC# are taken from the front panel controls, while the time and day are read from the computer's clock.

Each individual run will have three files saved within this folder using the following notation;

*Subject Code BDC# RUN# .HEOG
.VEOG
.TAC*

where the subject code and BDC# are the same as defined on the front panel controls, and the RUN# is defined by the indicator of the same name, and has a value between 01 and 99. The suffixes .HEOG, .VEOG, and .TAC refer to the signals saved on channels 6, 4, and 2 respectively, which are defined to be the horizontal eog, vertical eog and

tachometer signals. These files can be converted to matlab format using a variety of conversion programs including `mexchair_convert`, which is described in appendix C.

B.4 Running *DAM/DQM.L-mod6*

Once all front panel controls are set to the proper values, the program can be initiated. This is done by clicking on the single arrow at the top left of the screen(not shown in the figures). At the beginning of a BDC session, the computer will present a dialog box containing the name of the run folder as defined by the front panel controls. If the subject code or BDC# is incorrect, you may abort by clicking on the Reset button and then change the appropriate control before restarting. If the name is correct, click on the Continue button. For all subsequent runs within a BDC session, the process will be identical for each run.

The computer will present another dialog box with the choices of Run or Cal, corresponding to whether a run or a calibration will take place. If run is chosen, you will then be presented with another dialog box asking for the direction of the run, right or left. The default values alternate according to the nominal run profiles chosen for the SLS-2 mission. Following the choice of direction, there will be an approximately 15 second delay as the computer develops the output array and initializes the A/D board. The background of the motor output, and A/D input charts will be re-drawn in white. The motor command output and A/D input traces will appear in their respective charts, and will be drawn across the screen. At approximately halfway through the run, the data will reach the right edge of the chart, and data plotting will continue from the left hand edge, erasing the earlier points. Data collection will stop after a period of time equal to secs plus two seconds has elapsed. A dialog box will appear asking whether or not to save the data. If NO is pressed, the previous run will not be incremented to the run counter. If

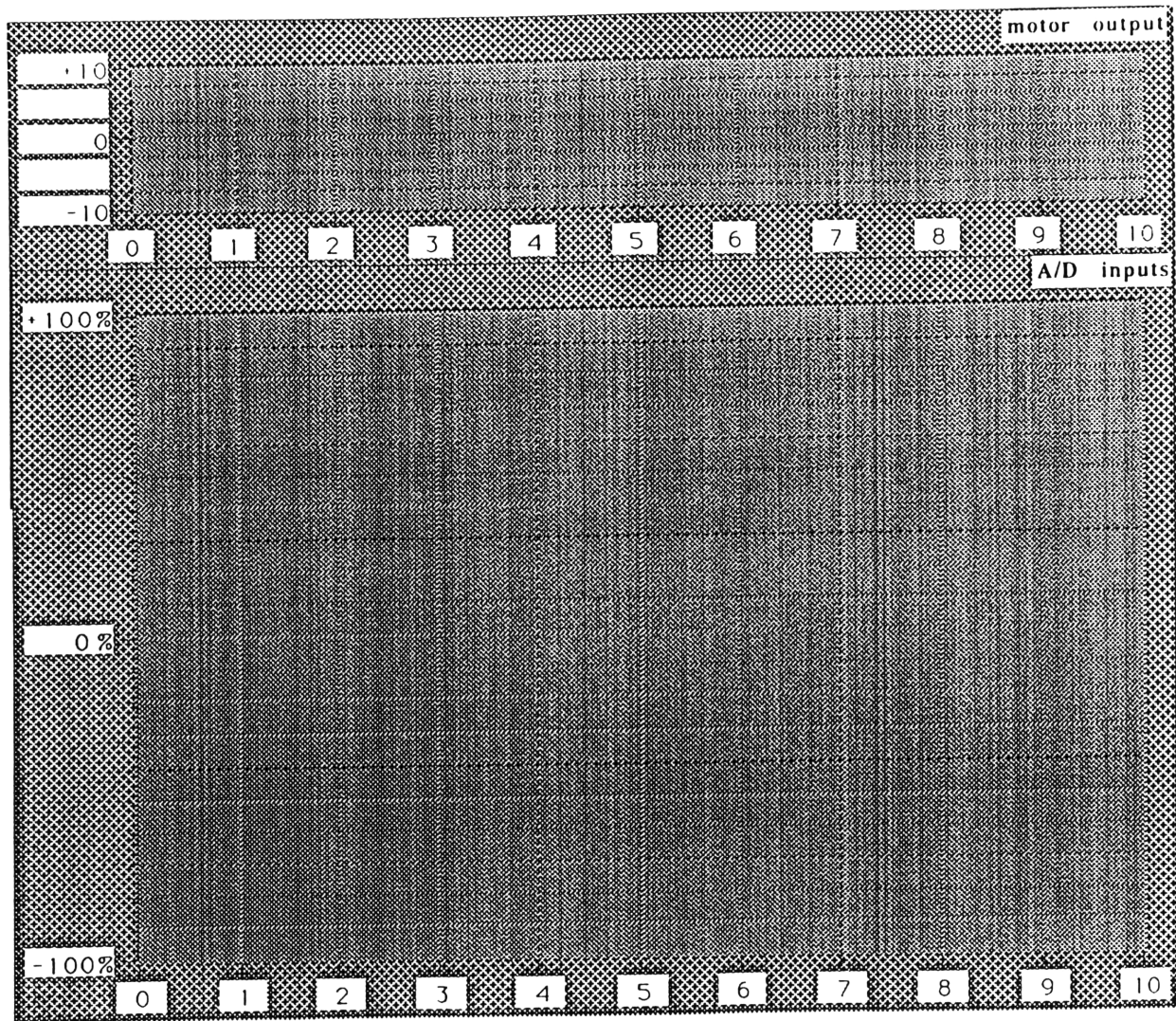
yes is pressed, the data will be saved and the run counter will be incremented by one. If this was not the last run, it will return to the run/cal dialog box.

If cal is chosen from the run/cal dialog box, the run/cal panel will appear in the middle of the screen. This panel is shown in figure B.2. There are two controls on this panel, the motor voltage slider, and the done switch. At this point, the operator has direct control over the output channel 1, driving the rotating chair. By moving the slider left or right, the chair will be driven accordingly so that it can be lined up to external calibration targets. The slider appears spring loaded, so that releasing the mouse button will trigger an immediate stop, and is limited to ± 1 volt (approximately ± 50 °/sec). Once the chair is properly aligned, the done switch should be clicked. At this point the run/cal panel disappears, and data collection begins for the calibration run. Data collection lasts according to the number of seconds defined by the cal control on the front panel, and wraps over the display area twice, as with regular data collection. During the calibration run, motor voltage is held to 0 volts. At the end of data collection, a dialog box will appear asking whether or not to save the data. If NO is pressed, the previous run will not be incremented to the run counter. If yes is pressed, the data will be saved and the run counter will be incremented by one. If this was not the last run, it will return to the run/cal dialog box.

After the last run has been completed, the program will automatically terminate.

References:

LabVIEW 2 User Manual, January 1990 edition. National Instruments Corporation Part Number 320244-01.



Rot. Chair BDC

Subject Code BDC #

of runs

save path

run folder name

RUN #

slot #

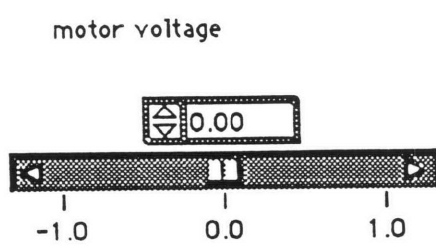
Cal

secs

freq

Chair type WRITE

Figure B1, DAM/DQM L-mode front panel



YES

Figure B2, run/cal front panel

Appendix C

MatLab External C Codes

mex_gamma.c
mexchair_convert.c
batch_fact_save.c

```

/* mex_gamma.c */
/* Created by T. Liefeld February, 1993 */
/* Calculates the complete and incomplete gamma functions for sk modelling */
/* Complete gamma function taken from Numerical recipes in C, pages 167-174 */
/* Returns the gamma function multiplied by an exponential with the same time */
/* series corresponding to the fractional derivative of an exponential */
/* to invoke from MatLab, use the following protocol; */
/*          mex_gamma( a , x ); */
/* where x can be a array */

#include <stdio.h>
#include <stdlib.h>
#include <string.h>
#include <unix.h>
#include <fcntl.h>
#include <math.h>

#include <cmex.h>

#define ITMAX 100
#define EPS 2.5e-5

double hcal, vcal,sigma;

#define A_IN    prhs[0]
#define X_IN    prhs[1]
#define N_IN    prhs[2]
#define G_OUT   plhs[0]

user_fcn( nlhs, plhs, nrhs, prhs )
INT      nlhs, nrhs;
Matrix   *plhs[], *prhs[];
{
    int m;
    long int p,i;
    char data_path[40];
    short double *a,*x,*ret_val,*num,gammln();
    short double gammp(),r,y,GG,sum,n,R,Rold;

/* get the data path from the MatLab pointer */

    a = A_IN->pr;
    x = X_IN->pr;
    num = N_IN->pr;

    G_OUT = create_matrix(1,*num,REAL);
    ret_val = G_OUT->pr;

    for (i=0;i<=(*num-1);i++){

        y=fabs(*(x+i));
        GG = exp(-1*y)/exp(gammln(1+*a));
    }
}

```

```

        sum = 0;
        n=1;
        R=1*y;
        sum=sum+*a*R/(n+*a);
        while((R/(n+*a))>fabs(EPS*(sum-1))){
            n=n+1;
            Rold=R;
            R=y/n*Rold;
            sum=sum+*a*R/(n+*a);
        }
        ret_val[i] = GG*sum;
    }
}

```

```

short double gammmp(a,x)
short double a,x;
/* returns the incomplete gamma functionP(a,x) */
{
    short double gamser,gammcf,gln;
    void gser(),gcf();

    if (a<0.0) a=a*(-1);
    if (x<(a+1.0)){
        gser(&gamser,a,x,&gln);
        return gamser;
    } else{
        gcf(&gammcf,a,x,&gln);
        return 1.0-gammcf;
    }
}

```

```

void gser(gamser,a,x,gln)
short double a,x,*gamser,*gln;
{
    int n;
    short double sum,del,ap;
    short double gammln();

    *gln = gammln(a);

    ap = a;
    del = sum=1.0/a;
    for (n=1;n<=ITMAX;n++){
        ap+= 1.0;
        del *= x/ap;
        sum +=del;
        if (fabs(del) < fabs(sum)*EPS) {
            *gamser = sum*exp(-x+a*log(x)-(*gln));
            return;
        }
    }
}

```

```

    return;
}

short double gammln(xx)
short double(xx);
/* returns ln(GAMMA(xx)) for xx>0.0. */
{
    double x,tmp,ser;
    static double cof[6]={ 76.18009173,-86.50532033,24.01409822,-
1.231739516,.0120858003e-2,-0.536382e-5};
    int j;

    x=xx-1.0;
    tmp = x+5.5;
    tmp -= (x+.5)*log(tmp);
    ser = 1.0;
    for (j=0;j<=5;j++){
        x+= 1.0;
        ser += cof[j]/x;
    }
    return -tmp+log(2.50662827465*ser);
}

void gcf(gammcf,a,x,gln)
short double a,x,*gammcf,*gln;
{
    int n;
    short double gold = 0.0,g,fac=1.0,b1=1.0;
    short double b0 = 0.0,anf,ana,an,a1,a0=1.0;
    short double gammln();

    *gln = gammln(a);
    a1=x;
    for (n=1;n<=ITMAX;n++){
        an = (short double) n;
        ana = an-a;
        a0 = (a1+a0*ana)*fac;
        b0=(b1+b0*ana)*fac;
        anf = an*fac;
        a1=x*a0+anf*a1;
        b1=x*b0+anf*b1;
        if (a1){
            fac = 1.0/a1;
            g=b1*fac;
            if (fabs((g-gold)/g)<EPS){
                *gammcf = exp(-x+a*log(x)-(*gln))*g;
                return;
            }
            gold = g;
        }
    }
}

```

```

/* Written by Ted Liefeld, February 1993. */
/* batch_fact_save is a MatLab mex file that takes a data path and run code from */
/* MatLab, along with horizontal and vertical calibration factors and writes these */
/* to a file called 'batch_factors' which can then be used as a batch file for AATM */
/* processing. A version of AATM that specifically looks for this batch file has */
/* been written as a mex file and renamed mexaatm4 */

/* to invoke from MatLab, use the following protocol; */
/* batch_fact_save('run_name',hcal,vcal) */
/* where run_name includes both path and file information, hcal is the horizontal */
/* calibration factor, and vcal is the vertical calibration factor. */

#include <stdio.h>
#include <stdlib.h>
#include <string.h>
#include <unix.h>
#include <fcntl.h>
#include <cmex.h>

#define out_filename "batch_factors"
#define F_IN prhs[0]
#define CH_IN prhs[1]
#define CV_IN prhs[2]

double hcal, vcal, velA;

user_fcn( nlhs, plhs, nrhs, prhs )
INT nlhs, nrhs;
Matrix *plhs[], *prhs[];
{
    int create_output_file(), get_file_parameters(),m,out_handle;
    void write_matlab_header();
    void save_vel_data(), save_os_data();
    long int p;
    char data_path[40];
    short double *c1,*c2;
    FILE *file_ptr;

/* get the data path from the MatLab pointer */
    p = (F_IN->n);
    for(m=0; m<p; m++){
        data_path[m] = (char)*(F_IN->pr+m);
    }
    data_path[m] = '\0';
    c1 = CH_IN->pr;
    c2 = CV_IN->pr;

/* write the data to file */
    file_ptr=fopen(out_filename,"a+");
    fprintf( file_ptr, "%s\r",data_path);
    fprintf(file_ptr, "%6.4f\r",*c1);
    fprintf(file_ptr, "%6.4f\r", *c2);
    fclose(file_ptr);
}

```

```

/* mexchair_convert.c          */
/* Originally written D. Balkwill 1991 */
/* Modified by T. Liefeld, 03/93      */

/* Originally written as a stand alone application (Balkwill, 1992), this version has */
/* been re written to be used as a mex file with altered file names, and the expanded */
/* ability to handle up to 99 files */

/* to invoke from MatLab, use the following protocol; */
/*          mexchair_convert('path:subject BDC',num_runs) */
/* where path is the file path to the data, subject BDC is the subject is letter code and */
/* BDC is the BDC number, eg/ data_path:A1, for subject A, BDC #1 */

/* Only the main body of the program is included, as the rest of the program and */
/* subroutines are unchanged */

#include <stdio.h>
#include <stdlib.h>
#include <fcntl.h>
#include <unix.h>
#include <string.h>
#include <cmex.h>

#define FALSE 0
#define TRUE 1

#define MAX_LINE_LENGTH 81

#define BLOCK_SIZE 16384
#define BAD_TYPE 0
#define DOUBLE_TYPE 1
#define FLOAT_TYPE 2
#define LONG_TYPE 3
#define SHORT_TYPE 4

#define MATLAB_DOUBLE 1000
#define MATLAB_FLOAT 1010
#define MATLAB_LONG 1020
#define MATLAB_SHORT 1030

#define TORSIONAL_VAR "tor" /* channel 1 */
#define HORIZONTAL_VAR "hor" /* channel 2 */
#define VERTICAL_VAR "ver" /* channel 3 */
#define ACCELERATION_VAR "acc" /* channel 4 */

/*char *matvar_names[] = {
    TORSIONAL_VAR, HORIZONTAL_VAR, VERTICAL_VAR,
    ACCELERATION_VAR
};*/

char run_code[MAX_LINE_LENGTH];
char out_code[MAX_LINE_LENGTH];
char temp[MAX_LINE_LENGTH];
char temp2[MAX_LINE_LENGTH];

```

```

char in_filename[MAX_LINE_LENGTH];
int in_fnamelen;
int in_handle;
FILE *in_fptr;
char *in_buffer;
int in_bytes;

char out_filename[MAX_LINE_LENGTH];

int out_handle;
FILE *out_fptr;
char *out_buffer;
int out_bytes;
int out_name_len;
char inter_filename[MAX_LINE_LENGTH];
int inter_handle;
FILE *inter_fptr;

typedef struct {
    long type;
    long mrows;
    long ncols;
    long imagf;
    long namlen;
} Fmatrix;

Fmatrix F_out;
long mrows = 0L;
long ncols = 0L;

int sample_size[5] = { 0, 10, 4, 4, 2 };
int in_size, out_size;
int in_type, out_type;
int num_channels;
long total_bytes;

int save_intermediate = FALSE;

int zz;

#define ALLOCATE_BUFFER(BUF) \
{ \
(BUF) = malloc(BLOCK_SIZE); \
if (!(BUF)) { \
mex_printf("Out of memory on buffer allocation.\n"); \
goto done; \
} \
}

#define READ_BUFFER() \
in_bytes = read(in_handle,in_buffer,BLOCK_SIZE);

#define WRITE_BUFFER(NUM) \
write(out_handle,out_buffer,NUM);

```



```

#define WRITE_INTER(NUM) \
write(inter_handle,out_buffer,NUM);

char in_line[MAX_LINE_LENGTH];
char matlab_name[MAX_LINE_LENGTH];

#define F_IN    prhs[0]
#define CH_IN   prhs[1]
#define CV_IN   prhs[2]

user_fcn( nlhs, plhs, nrhs, prhs )
INT      nlhs, nrhs;
Matrix   *plhs[], *prhs[];
{
    int open_input_file(), create_output_file(), create_inter_file(), get_file_parameters();
    int num_run,m;
    long calculate_num_samples();
    void write_matlab_header(), transfer_data();
    int i,ll,i1,i2;
    long int p;
    char data_path[40];
    short double *num;

    ALLOCATE_BUFFER(in_buffer)
    ALLOCATE_BUFFER(out_buffer)

    /* get the data path from the MatLab pointer */
    p = (F_IN->n);
    for(m=0; m<p; m++){
        data_path[m] = (char)*(F_IN->pr+m);
    }
    data_path[m] = '\0';
    num = CH_IN->pr;

    strcpy(run_code,data_path);

    ll = strlen(run_code);
    out_name_len = ll;
    strcpy(temp,run_code);
    strcpy(temp2,run_code);

    for (i=0; i < (10);i++) {
        if ((out_filename[i] >= 'a') && (out_filename[i] <= 'z'))
            out_filename[i] += 'A' - 'a';
    }

    zz = 1;

    while (zz < 5) {
        zz = zz + 1;

        for (i = 1; i <= *num; i++) {

```

```

i2 = i%10;
i1 = i/10;
        run_code[l1+1] = '0' + i2;
        run_code[l1] = '0' + i1;

        strcpy(temp,run_code);
        strcpy(temp2,run_code);

if (zz == 2) {
    strcat(temp, ".HEOG");
    strcat(temp2, ".eogh");
}
else
if (zz == 3) {
    strcat(temp, ".VEOG");
    strcat(temp2, ".eogv");
}
else
if (zz == 4) {
    strcat(temp, ".TAC");
    strcat(temp2, ".tach");
}
else
if (zz == 5) {
    strcat(temp, ".POS");
    strcat(temp2, ".pot");
}

        strcpy(in_filename,temp);
        strcpy(out_filename,temp2);
        strcpy(matlab_name,in_filename);

if (open_input_file() {
    if (create_output_file() {
        if (get_file_parameters(i) {
            mrows = calculate_num_samples();
            write_matlab_header();
            transfer_data();
        }
    }
}
strcpy(temp,run_code);
save_intermediate = FALSE;
}
}
}
done:

```

```
if (in_handle > 0)
    close(in_handle);
if (out_handle > 0)
    close(out_handle);
if (inter_handle > 0)
    close(inter_handle);
}
```

Appendix D

Batch Analysis Scripts

batch_analyse
cal_from_file
cal_factor_gen
calibration_calc
multiple_AATM
CODES
model_select

Appendix D notes:

This collection of scripts comprises the new material added to the automated analysis of Space Lab data originally developed by Balkwill (1992). The primary additions here are in file and data handling, not in the generation of new algorithms (with the exception of the sk modelling routines). Other routines that are called from within *batch_analyse*, such as *stat_prep* and *tachan* that are not listed here, are not functionally changed from the scripts presented in Balkwill, 1992.

Figure D1, that follows is a flow chart of the main components of the batch analysis system showing the interconnectivity and order of use of the separate scripts. In the figure, shaded ovals represent mex files, and lightly shaded round cornered squares represent other MatLab scripts called by *batch_analysis*.

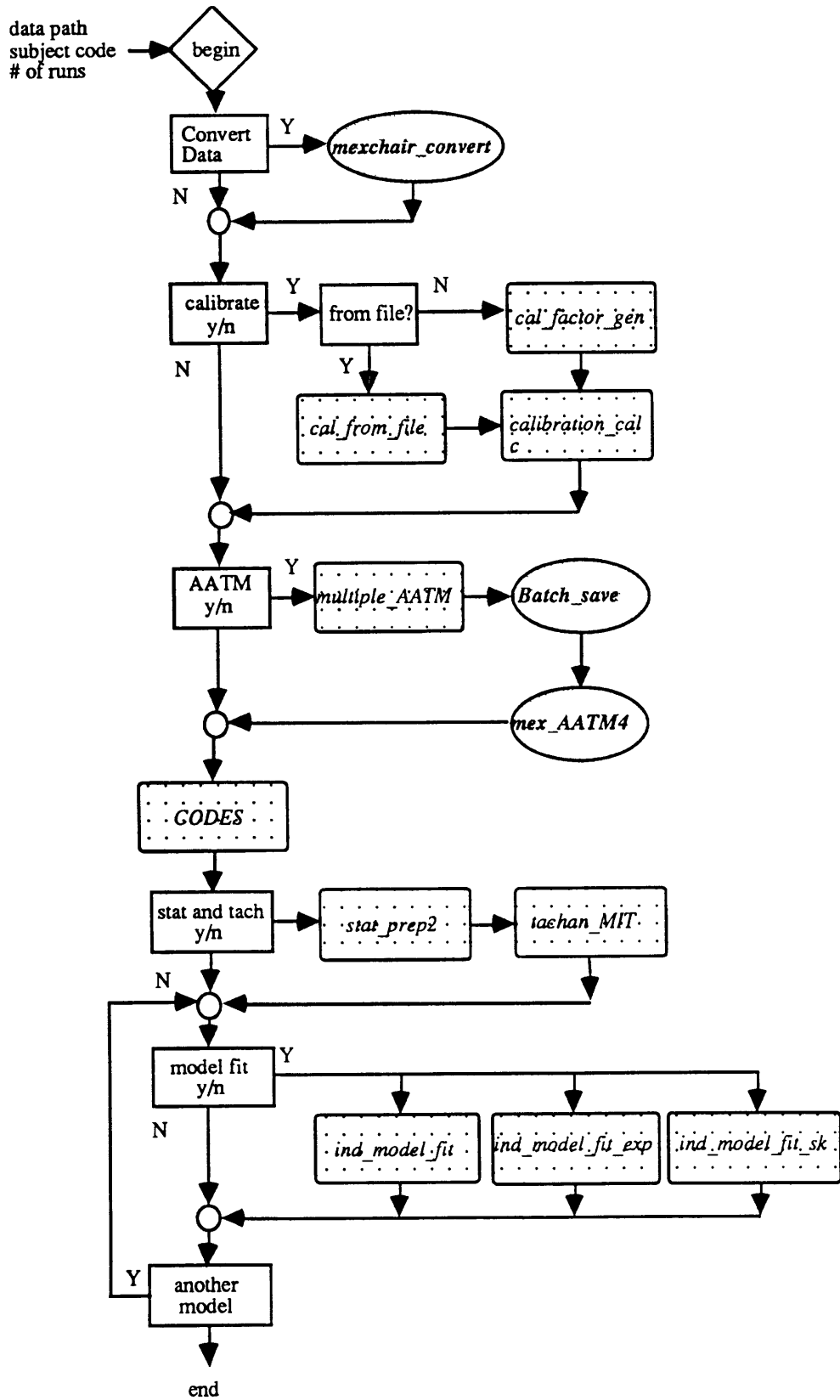


Figure D1, *batch_analysis* flow chart (explanation of symbols in text)

```

%*****
% batch_analyse
%*****
% written by T. Liefeld throughout spring 93
% given a folder of runs from a BDC, this functions as a
% superscript that will prompt the user for all analysis
% from data collection through to model fitting.

data_path = input('Enter Data Path >> ','s');
sub_code = input('Enter Subject Code >> ','s');
number = input('Enter Number of Runs >> ');

convert = input('Convert the data to MatLab format? >>','s');
if ((convert == 'y') | (convert == 'Y'))
    code = [data_path,sub_code];
    mexchair_convert(code,number);
end

q1 = input(' Do you want to do a calibration? >> ','s');
if ((q1=='y') | (q1=='Y'))
    q = input('Calibration factors from file or new? (f/n) >> ','s');
    if ((q == 'f') | (q == 'F'))
        cal_from_file
    end
    if ((q == 'n') | (q == 'N'))
        cal_factor_gen
    end
end;

q2 = input(' Do you want to perform AATM? >> ','s');
if ((q2 == 'y') | (q2 == 'Y'))
    multiple_AATM;
end;

% create the run_code matrix, codes
CODES
number = number-n_cals;

q3 = input(' Do you want to perform Tachan and Stat_Prep >> ','s');
if ((q3=='y') | (q3=='Y'))

    for i = 1:number
        run_code = codes(i,:);
        fprintf(['\nRun code = ',run_code,'\n']);

        % perform statistical analysis on tach and SPV
        tachan_batch;
        stat_prep_batch;
    end
end

q4 = input(' Would you like to fit a Model? >>','s');
while ((q4=='y') or (q4=='Y'))
    model_select;
end

```

```

    q4 = input(' Would you like to fit another Model? >>');
end;

```

```

%*****
% cal_from_file
%*****
% written by T. Liefeld, 22/4/93
% Takes previously generated calibrations from a file
% specified by the user and generates the vector of
% calibration factors for use with mexAATM4

```

```

filename = input(' Enter the data path and name of the file containing the calibration
factors','s');

```

```

load filename
calibration_calc
clear_filename

```

```

%*****
% cal_factor_gen
%*****
% calls calibrate for a number of runs and generates the cal factors
% for the PRN and dumping runs

```

```

chdir HardDisk:SIMULINK:NysA_V2:scripts:

```

```

run = ones(1,number);
n_cals = input('How many cal?');
dim = input('Enter # of dimensions (1/2) >> ');

```

```

if (n_cals >= 0)
    fprintf('\n Enter the run number for the cal in order')
    fprintf('\n from lowest to highest')
    for i=1:n_cals
        calnum(i) = input('cal # >> ');
        run(calnum(i)) = 0;
        if (calnum(i) < 10)
            n = num2str(calnum(i));
            cal_code = [data_path,sub_code,'0',n]

            calibrate
            hcal(i) = scale 1;
            if (dim == 2)
                vcal(i) = scale2;
            end
            g(i) = input('Was this cal good enough to use? >>','s');
        else
            if (calnum(i)>=10)
                n = num2str((calnum(i)));
                cal_code = [data_path,sub_code,n]
            end
        end
    end
end

```



```

        calibrate
        hcal(i) = scale1;
        if (dim == 2)
            vcal(i) = scale2;
        end
        g(i) = input('Was this cal good enough to use? >>', 's');
    end
end
end
end

```

```

% calculate calibration factors for the runs
% based only on the good calibrations
for i = 1:n_cals
    if ((g(i) == 'y') | (g(i) == 'Y'));
        g_cal(i) = calnum(i);
        calh(i) = hcal(i);
        if (dim == 2)
            calv(i) = vcal(i);
        end
    end
end
end

```

```

q = input('Would you like to save measured cal values? >>', 's');
if ((q == 'y') | (q == 'Y'))
    save_name = input('Save File Name : ', 's');
    save_name = [data_path, save_name];
    if (dim == 2)
        save save_name data_path sub_code number dim g_cal hcal vcal
    else
        save save_name data_path sub_code number dim g_cal hcal
    end
end

```

calibration_calc

```

%*****
% calibration_calc
%*****
% written by T. Liefeld, 22/4/93
% interpolates or extrapolates as necessary to generate the
% calibration factors for runs, given the number of runs,
% the position of the calibration runs in the series, and the
% calibration factors

```

```

if (length(g_cal) == 0)
    fprintf(' No good calcs?')
elseif (length(g_cal) == 1)
    for i = 1:number
        hor_cal(i) = hcal(1);
        if (dim == 2)

```

```

        ver_cal(i) = vcal(1);
    end
end
elseif (length(g_cal) >1)
    for i = 1:number
        for j = 1:(length(g_cal)-1)
            if (i < g_cal(1)) % runs before first cal, extrapolate
                delta = g_cal(1) - i;
                del2 = g_cal(2) - g_cal(1);
                hor_cal(i) = hcal(1) - (hcal(2) - hcal(1)) * delta / del2;
                if (dim == 2)
                    ver_cal(i) = vcal(1) - (vcal(2) - vcal(1)) * delta / del2;
                end
            end
            if (i == g_cal(1)) % first cal run
                hor_cal(i) = hcal(1);
                if (dim == 2)
                    ver_cal(i) = vcal(1);
                end
            end
            if ((g_cal(j) < i) & (i < g_cal(j+1))) % interpolate between
                delta = i - g_cal(j);
                del2 = g_cal(j+1) - g_cal(j);
                hor_cal(i) = hcal(j) + (hcal(j+1) - hcal(j)) * delta / del2;
                if (dim == 2)
                    ver_cal(i) = vcal(j) + (vcal(j+1) - vcal(j)) * delta / del2;
                end
            end
            if (i == g_cal(j))
                hor_cal(i) = hcal(j);
                if (dim == 2)
                    ver_cal(i) = vcal(j);
                end
            end
            if (i == g_cal(j+1))
                hor_cal(i) = hcal(j+1);
                if (dim == 2)
                    ver_cal(i) = vcal(j+1);
                end
            end
            if (i > g_cal(j+1))
                delta = i - g_cal(j+1);
                del2 = g_cal(j+1) - g_cal(j);
                hor_cal(i) = hcal(j+1) + (hcal(j+1) - hcal(j)) * delta / del2;
                if (dim == 2)
                    ver_cal(i) = vcal(j+1) - (vcal(j+1) - vcal(j)) * delta / del2;
                end
            end
        end
    end
end
end
end
end
end

```

```

%*****
% multiple_AATM
%*****
% written by T. Liefeld, 21/4/93
% prepares a batch file for AATM processing using the
% appropriate calibration factors and names, and a
% predefined batch file name, batch_factors, for use
% with mexAATM4.

% create file of ones for the vertical calibration if no vertical
% calibrations were performed
if (dim == 1)
    ver_cal = ones(1,number);
end

% remove earlier files
chdir HardDisk:SIMULINK
if (exist('batch_factors') == 2)
    delete batch_factors
end

for i = 1:number
    if ((i < 10) & (run(i) > 0))
        n = num2str(i);
        run_code = [data_path,sub_code,'0',n];
        batch_save(run_code,hor_cal(i),ver_cal(i));
    else
        if (i >=10 & (run(i) > 0))
            n = num2str(i);
            run_code = [data_path,sub_code,n];
            batch_save(run_code,hor_cal(i),ver_cal(i));
        end
    end
end
% send the EOF marker that mexAATM4 looks for
batch_save('&',0,0);

mexAATM4;

%*****
% CODES
%*****
% written by T. Liefeld, 21/4/93
% creates a matrix, called codes, containing all the run codes
% of non-calibration runs

j = 0;
for i = 1:number
    if (run(i) == 1 )

        stln = length([data_path,sub_code])+2;
        if (i < 10)

```

```

        n = [num2str(0),num2str(i)];
    else
        n = num2str(i);
    end
    codes(i-j,1:stln) = [data_path,sub_code,n];
elseif (run(i) == 0)
    j = j+1;
end
end
end

```

```

%*****
% model_select
%*****
% written by T. Liefeld, 21/4/93
% model_select allows the user to choose which models are to
% be fitted to the data being processed through batch_analyse.

fprintf('\n\n  MODEL SELECTION:\n\n')
fprintf(' 1. First Order Exponential\n');
fprintf(' 2. sk model (w/ velocity storage)\n');
fprintf(' 3. Three Parameter (w/ velocity storage)\n');
model = input(' Enter Number >>');
pr = input(' Print outputs? >>');

for i = 1:number
    run_code = codes(i,:);
    fprintf(['\nRun code = ',run_code(stln-3:stln),'\n']);

    if (model == 1)
        ind_model_fit_exp
    elseif (model == 2)
        ind_model_fit_sk2
    elseif (model == 3)
        ind_model_fit
    end
end
end

end

```

Appendix E

New Algorithm Scripts

dec_30_spv
dec_mean
mean_model_err
model_err_exp
model_err_sk
t_chisq

```

%*****
% dec30_new
%*****
% written by T. Liefeld 3/93
% in addition to decimating the SPV files, it also
% creates the decimated Tach and SPV for the model fits
% using the real tach signal, and calculates weights
% for the model fit to use calculating MSE

% set bad data to zero for summation purposes
norm_spv = norm_spv .* good_data;

l = length(good_data);

new_l = (l - 1)/30; %new sampling frequency

y = zeros(30,new_l);
g = zeros(30,new_l);
n = zeros(1,new_l);
d = zeros(1:new_l);
x = zeros(1,new_l);
z = 1:1:30;

for t=1:(new_l-1)
    for i = 1:30
        y(i,t) = norm_spv(30*t+i);
        g(i,t) = good_data(30*t+i);
    end;
    x = sum(y);
    n = sum(g);
    [a] = polyfit(z,y(:,t)',1); % linear least squares fit to each bin
    for i = 1:30 % calc variance about the linear fit
        d(t) = d(t) +((y(i,t) - (a(2)+a(1)*i)).*g(i,t)).^2;
    end;
end;

dec_good = (n>0); % good data flag

% Decimated SPV is box-car average across row, with n=number of
% good samples. Correction in denominator to prevent division
% by zero for an entire bin of bad data; dec_spv=0 in this case.
dec_spv = x ./ (n + (~dec_good));

% Variance within trace is variance of each bin around a linear
% polynomial fit to each bin. A correction in case of
% good samples in bin is <= 1; variance within=0 in this case.
within = d ./ (n - 1 + 2*(n<=1) );

% calculate weights as the number of samples divided by the variance of each
% sample.
dec_weight = n ./ within;
bad_weight = pack_true(isnan(dec_weight));
dec_weight(bad_weight) = zeros(1,max(size(bad_weight)));

```

```

zero_var = pack_true((within<=1e-7));
dec_weight(zero_var) = zeros(1,max(size(zero_var)));

% remove outliers in the weights
% sort variances into ascending order
[y,i] = sort(within);

% calculate mean variance of three equal sized regions
mean1 = mean(y(1:160));
mean2 = mean(y(161:320));
mean3 = mean(y(321:480));

% set all points in each region equal to their mean variance
var(i(1:160)) = mean1*ones(1,160);
var(i(161:320)) = mean2*ones(1,160);
var(i(321:480)) = mean3*ones(1,160);

% calculate n, for each point;
n = dec_weight .* within;

% calculate the new weighting function to be used for averaging
% of runs
weight = n./var;

plot(dec_weight,'x')
%save data, having departed from 'file_specs' by now
eval(['save ',run_code,'.dec_spv dec_spv']);
eval(['save ',run_code,'.dec_weight dec_weight']);
eval(['save ',run_code,'.within within']);

%clear dec_good dec_spv i l new_l within x out_weight zero_var dec_weight

%*****
%DecMean:
%*****

% Written 3/93 by T. Liefeld
% calculates the ensemble weighted mean of several runs
% and its variance for best estimate model fitting

num_runs = input('Number of Runs >> ');

for i = 1:num_runs
    run_code(i,:) = input('Enter Run Code: ','s');
end

stat_code = input('Enter code for stats file: ','s');

sample = 4 ;
minute_size = 60 * sample;

sum_spv = zeros(1,2*minute_size);

```

```

sum_square = zeros(1,2*minute_size);
total = zeros(1,2*minute_size);
n_tot = zeros(1,2*minute_size);

for i = 1:num_runs

    if (exist([run_code(i,:),'.dec_spv']) ~= 2)
        fprintf(['Error: cannot find data for run code ',run_code]);
    else
        eval(['load ',run_code(i,:),'.dec_spv']);
        eval(['load ',run_code(i,:),'.weight']);
        eval(['load ',run_code(i,:),'.n']);
        eval(['load ',run_code(i,:),'.parms']);

        sum_spv = sum_spv + (abs(spinv)/spinv*dec_spv .* weight);
        total = total + weight;
        d_spv(i,:) = abs(spinv)/spinv*dec_spv;
        wt(i,:) = weight;
        n_tot = n_tot + n;

    end
end

mean_spv = sum_spv ./total;

for i = 1:num_runs
    sq(i,:) = ((d_spv(i,:) - mean_spv).^2).*wt(i,:);
end
var_spv = sum(sq) ./total;
var_spv = var_spv *(num_runs/(num_runs-1));
var_spv(pack_true(isnan(var_spv))) = zeros(1:sum(isnan(var_spv)));

% do the same variance histogram method developed for the ind.
% runs and apply it here to make the weighting funtion less
% extreme in the weight calculation

% sort variances into ascending order
[y,i] = sort(var_spv);

% calculate mean variance of three equal sized regions
mean1 = mean(y(1:160));
mean2 = mean(y(161:320));
mean3 = mean(y(321:480));

% set all points in each region equal to their mean variance
var(i(1:160)) = mean1*ones(1,160);
var(i(161:320)) = mean2*ones(1,160);
var(i(321:480)) = mean3*ones(1,160);

% calculate the new weighting function to be used for averaging
% of runs
weight = num_runs*ones(1:480)./var;

sigma_sq = mean(var_spv);

```



```

eval(['save ',stat_code,'.stats mean_spv var_spv n_tot num_runs weight'])

std_spv = sqrt(var_spv);
plot(mean_spv+2*std_spv,'g')
hold on
plot(mean_spv-2*std_spv,'g')
plot(mean_spv);grid
title('Mean SPV +- two standard deviations');
xlabel('Sample Number');
ylabel('SPV (deg/sec)');
hold off

clear total mean_spv var_spv std_spv
clear stat_code run_code i num_runs sample minute_size
clear nysa_path data_path

function [f,g] = model_err(model_parms,t,u,dec_spv,good_indices,norm_parms, weight)
%*****
%mean_model_err
%*****
% Error function for model fitting. Constrained optimization
% minimizes the output of this function, which is currently set
% as the mean square error (MSE) between the SPV data and the
% model SPV data.
%
% D. Balkwill 12/9/91
% modified T. Liefeld 3/93
%
% calculate physical parameters for transfer function, and
% determine the corresponding model response
%

model_parms = model_parms .* norm_parms;
K1 = model_parms(1);
Tc = model_parms(2);
Ta = model_parms(3);
h0 = model_parms(4);
g0 = model_parms(5);

num = -[K1, (K1 * (h0 + g0)), 0, 0];
den = [1, (1/Tc + 1/Ta + h0), (1/(Ta*Tc) + h0/Tc + h0/Ta), h0/(Ta*Tc)];
y = lsim(num,den,u,t);

% ensure that y and dec_spv are both either row vectors or column vectors
[m1,n1] = size(y);
[m2,n2] = size(dec_spv);
if (m1 > n1) % y is column vector
    if (m2 < n2) % dec_spv is row vector
        y = y';
    end
else % y is row vector
    if (m2 > n2) % dec_spv is column vector

```

```

        y = y';
    end
end

%
% Only base MSE on data points at which we have valid data.
%
d = y(good_indices) - dec_spv(good_indices);
d = d .* d .* weight(good_indices);
f = sum(d) / length(d);

%fprintf('MSE = %f\n',f);

plot(t(good_indices),dec_spv(good_indices))
hold on
plot(t(good_indices),y(good_indices),'g');
hold off

%
% dummy value which 'constr' requires but is unused for our
% purposes; this must be some constant value for our purposes
%
g = -1;

return;

function [f,g] = model_err_sk(model_parms,t,u,dec_spv,good_indices,norm_parms)
%*****
%model_err_exp
%*****
% Error function for model fitting. Constrained optimization
% minimizes the output of this function, which is currently set
% as the mean square error (MSE) between the SPV data and the
% model SPV data.
%
% T. Liefeld 12/6/92

%
% calculate physical parameters for transfer function, and
% determine the corresponding model response
%
model_parms = model_parms .* norm_parms;
K = model_parms(1);
T = model_parms(2);
A = model_parms(3);

y=A*K*exp(-1*t/T);

% ensure that y and dec_spv are both either row vectors or column vectors
[m2,n2] = size(dec_spv);
[m1,n1] = size(y);
if (m1 > n1) % y is column vector

```

```

    if (m2 < n2) % dec_spv is row vector
        y = y';
    end
else % y is row vector
    if (m2 > n2) % dec_spv is column vector
        y = y';
    end
end

%
% Only base MSE on data points at which we have valid data.
%
d = y(good_indices) - dec_spv(good_indices);

f = sum(d .* d) / length(d);

plot(t(good_indices),dec_spv(good_indices))
hold on
plot(t(good_indices),y(good_indices),'g');
hold off

%
% dummy value which 'constr' requires but is unused for our
% purposes; this must be some constant value for our purposes
%
g = -1;

return;

%*****
% t_chisq
%*****
% performs a chi squared analysis comparing two ensemble averaged
% curves. Also performs 95% and 97.5% students t tests at every
% pont in time along the curves and plots only those points that
% are significant.
%
% written by T. Liefeld, 4/93

clear
clg

t975 = [ 12.706, 4.303, 3.182, 2.776, 2.571, 2.447, 2.365, 2.306, 2.262, 2.228, 2.201,
2.179, 2.160, 2.145, 2.131, 2.120, 2.110, 2.101, 2.093, 2.086, 2.080, 2.074, 2.069, 2.064,
2.060, 2.056, 2.052, 2.048, 2.045, 2.042];

t95 = [ 6.31, 2.92, 2.35, 2.13 2.02, 1.94, 1.90, 1.86, 1.83, 1.81, 1.80, 1.78, 1.77, 1.76,
1.75, 1.74, 1.73, 1.73, 1.72, 1.72, 1.72, 1.72, 1.71, 1.71, 1.71, 1.71, 1.70, 1.70, 1.70,
1.70];

% load the averaged data
eval(['data_path = input("Enter Data Path >> ","s");'])
eval(['run_code = input("Enter Run Code >> ","s");'])

```

```

eval(['load ', data_path,run_code, '.stats'])

% use only post-rotatory
meanA = mean_spv(249:320);
varA = var_spv(249:320);
nA = n_tot(249:320)/30;

clear mean_spv var_spv n_tot

eval(['run_code = input("Enter Run Code >> ","s");'])
eval(['load ', data_path,run_code, '.stats'])

% use only post-rotatory
meanB = mean_spv(249:320);
varB = var_spv(249:320);
nB = n_tot(249:320)/30;

clear mean_spv var_spv n_tot

% evaluate to find the good regions, i.e. where both curves
% have good points.

goodA1 = (~isnan(meanA));
goodA2 = (nA >0.1); % at least 10 pre-decimation points
goodA = (goodA1 .* goodA2);

goodB1 = (~isnan(meanB));
goodB2 = (nB >0.1); % at least 10 pre-decimation points
goodB = (goodB1 .* goodB2);

good = pack_true(goodA .* goodB); %both curves must be good

% redefine curves only at good points
meanA = meanA(good);
varA = varA(good);
nA = nA(good);
meanB = meanB(good);
varB = varB(good);
nB = nB(good);

% calculate the pooled variance for A and B
wons = ones(1,length(nA));
p_var = (wons./nA+wons./nB).*(((nA-1).*varA + (nB-1).*varB)./(nA+nB-2));

% calculate chi-squared value
chi = ((meanA - meanB).^2)./p_var;
chisquare = sum(chi);
n_chi = length(chi);
fprintf(' n: %f\n',n_chi);
fprintf(' chi^2: %6.2f\n',chisquare);

% calculate t values
weight = (nA + nB)./(nA .* nB); % 1/nA + 1/nB
std = (meanA-meanB)./sqrt(weight .* p_var);

```

```

df = floor(nA + nB - 2);
for i=1:length(df)
    if (df(i)<1)
        df(i) = 1;
    end
end

t=1/4:1/4:60;

% check for significance in the t-test
sig_diff_975 = pack_true(abs(std>t975(df)));
sig_diff_95 = pack_true(abs(std>t95(df)));

fprintf('\n .95 sig t-test %4.0f\n',length(sig_diff_95));
plot(t(sig_diff_95),meanA(sig_diff_95),'o',t(sig_diff_95),meanB(sig_diff_95),'x')

```